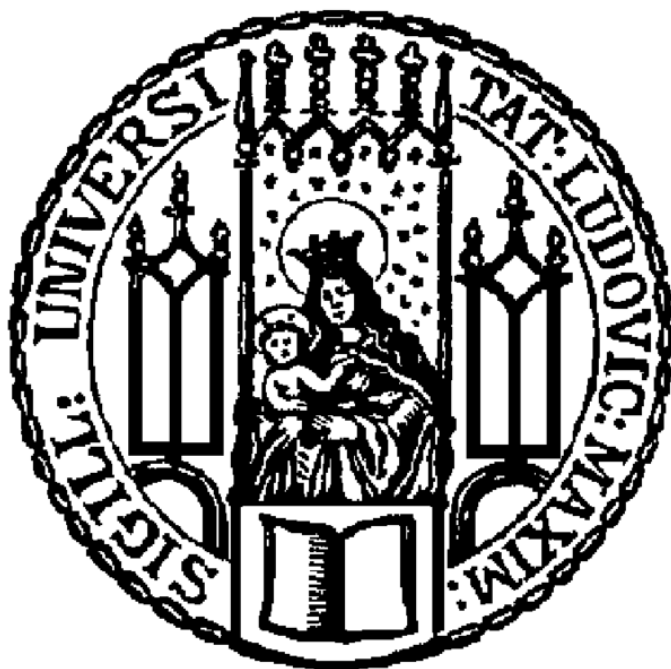


Dissertation zur Erlangung des Doktorgrades der Fakultät für Chemie und  
Pharmazie der Ludwig-Maximilians-Universität München

**Structural Analysis of Chromatin Remodeler  
by Electron Microscopy.**



Caroline Haas

aus München

2013

**Erklärung**

Diese Dissertation wurde im Sinne von § 7 der Promotionsordnung vom 28. November 2011 von Herrn Prof. Dr. Roland Beckmann betreut.

**Eidesstattliche Versicherung**

Diese Dissertation wurde selbständig, ohne unerlaubte Hilfe erarbeitet.

München, den 15.10.2013

.....

Caroline Haas

Dissertation eingereicht am 15.10.2013

1. Gutachter: Herr Prof. Dr. Roland Beckmann

2. Gutachter: Herr Prof. Dr. Karl-Peter Hopfner

Mündliche Prüfung am 22.11.2013

---

**This thesis has been prepared from March 2009 to October 2013 in the laboratory of Prof. Dr. Roland Beckmann at the Gene Center of the Ludwig-Maximilians-University of Munich (LMU).**

**Parts of this thesis have been published:**

Alessandro Tosi\*, Caroline Haas\*, Franz Herzog\*, Andrea Gilmozzi, Otto Berninghausen, Charlotte Ungewickell, Christian B. Gerhold, Kristina Lakomek, Ruedi Aebersold, Roland Beckmann and Karl-Peter Hopfner: Structure and subunit topology of the INO80 chromatin remodeler and its nucleosome complex. *Cell*, Volume 154, Issue 6, 1207-1219, 12 September 2013.

\*These authors contributed equally

**Parts of this thesis have been presented at national and international conferences:**

- Oral presentation at the SFB TR5 Meeting in Munich, Germany on the 20 October 2009.
- Poster presentation at the 3<sup>rd</sup> SFB TR5 Symposium: Chromatin Assembly and Inheritance of Functional States, 6.-8. October, 2010 in Munich, Germany.
- Poster presentation at the EMBO workshop “Chromatin structure, organization and dynamics” in Prague, Czech Republic from 9.-13. April 2011.
- Poster presentation at the Gene Center Retreat in Wildbad-Kreuth, Germany on 8.-10. June 2011.
- Oral presentation at the Chromatin Day in Munich, Germany on 25. July 2011.
- Oral presentation at the Chromatin Day in Munich, Germany on 27. July 2012.
- Poster and oral presentation at the Gene Center Retreat in Wildbad-Kreuth, Germany on 25. May 2012. => Poster prize
- Poster presentation at the Conference “Epigenetics & Chromatin: Interactions and processes” at Harvard Medical School in Boston, USA from 11.-13. March 2013.
- Poster presentation and poster prize including a talk at the EMBO Conference “Chromatin and Epigenetics” at the EMBL Heidelberg, Germany from 8.-12. May 2013.

# 1 Table of Contents

<b>1</b>	<b>TABLE OF CONTENTS</b>	<b>4</b>
<b>2</b>	<b>SUMMARY</b>	<b>7</b>
<b>3</b>	<b>INTRODUCTION</b>	<b>9</b>
<b>3.1</b>	<b>CHROMATIN IS IMPORTANT FOR ALL DNA MEDIATED PROCESSES</b>	<b>9</b>
<b>3.2</b>	<b>NUCLEOSOMES ARE THE BASIC STRUCTURAL UNIT OF CHROMATIN</b>	<b>9</b>
<b>3.3</b>	<b>CHROMATIN DYNAMICS AND REORGANIZATION</b>	<b>12</b>
3.3.1	DNA METHYLATION	12
3.3.2	HISTONE MODIFICATIONS	12
3.3.3	ATP-DEPENDENT CHROMATIN REMODELER	13
3.3.3.1	SWI/SNF family of remodeler	15
3.3.3.2	ISWI family of remodeler	16
3.3.3.3	CHD family remodeler	19
3.3.3.4	INO80 family remodeler	19
3.3.3.5	Models for chromatin remodeling mechanism	24
3.3.4	OTHER INFLUENCES ON CHROMATIN STRUCTURE	26
<b>3.4</b>	<b>STRUCTURAL INFORMATION ABOUT CHROMATIN REMODELER</b>	<b>26</b>
3.4.1	SWI/SNF FAMILY REMODELER	26
3.4.2	ISWI FAMILY REMODELER	29
3.4.3	CHD FAMILY REMODELER	31
3.4.4	INO80 FAMILY REMODELER	32
<b>3.5</b>	<b>HYBRID METHODS IN STRUCTURAL BIOLOGY</b>	<b>33</b>
<b>4</b>	<b>AIMS OF THE PROJECTS</b>	<b>35</b>
<b>4.1</b>	<b>ISWI REMODELER COMPLEXES</b>	<b>35</b>
<b>4.2</b>	<b>INO80 REMODELING COMPLEX</b>	<b>36</b>
<b>5</b>	<b>RESULTS</b>	<b>37</b>
<b>5.1</b>	<b>RECONSTITUTION OF NUCLEOSOMES</b>	<b>37</b>
<b>5.2</b>	<b>ISWI CHROMATIN REMODELER</b>	<b>39</b>
5.2.1	PURIFICATION OF <i>D.M.</i> ISWI-CONTAINING CHROMATIN REMODELER	39
5.2.2	RECONSTITUTION OF ISWI NUCLEOSOME- COMPLEXES	44
5.2.2.1	Following complex formation using electrophoretic mobility shift assay	44
5.2.2.2	Measuring binding affinities in solution using MicroScale Thermophoresis	46
5.2.2.2.1	A pre-transition state analog increased the affinity of ISWI to nucleosomes	47
5.2.2.2.2	Influence of Walker mutants on the binding affinity to nucleosomes	50
5.2.2.2.3	Indication for cooperate binding of an ISWI dimer to the nucleosome	52
5.2.2.2.4	Low in solution affinities prevent EM analysis	53
5.2.2.3	Negative staining of ISWI-nucleosome complexes	55
5.2.3	PURIFICATION OF THE NUCLEOSOME-ISWI COMPLEX	57
5.2.3.1	GraFix	57
5.2.3.2	Size exclusion chromatography	58



<b>5.3</b>	<b>INO80 CHROMATIN REMODELER</b>	<b>59</b>
5.3.1	STRUCTURAL ANALYSIS OF THE INO80 COMPLEX BY ELECTRON MICROSCOPY	59
5.3.2	A RVB1/2 DODECAMER IS LOCATED IN THE HEAD OF THE INO80 COMPLEX	63
5.3.3	MAPPING OF SUBUNIT INTERACTIONS XL-MS	65
5.3.4	THE RVB1/2 DODECAMER	66
5.3.5	THE SNF2 DOMAIN	67
5.3.6	LOCALIZATION OF NHP10-, ARP8- AND ARP5- MODULES	68
5.3.7	FUNCTIONAL ANALYSIS OF INO80 MODULES	70
5.3.8	INTERACTION OF INO80 WITH THE NUCLEOSOME	74
<b>6</b>	<b>DISCUSSION &amp; OUTLOOK</b>	<b>76</b>
<b>6.1</b>	<b>STRUCTURAL ANALYSIS OF ISWI FAMILY REMODELER</b>	<b>76</b>
<b>6.2</b>	<b>STRUCTURAL ANALYSIS OF INO80 CHROMATIN REMODELER</b>	<b>79</b>
<b>7</b>	<b>MATERIALS AND METHODS</b>	<b>86</b>
<b>7.1</b>	<b>MATERIALS</b>	<b>86</b>
7.1.1	PLASMIDS	86
7.1.2	PRIMER	87
7.1.3	YEAST STRAINS	89
<b>7.2</b>	<b>METHODS</b>	<b>90</b>
7.2.1	GENERAL METHODS IN MOLECULAR BIOLOGY	90
7.2.1.1	Polymerase chain reaction	90
7.2.1.2	Precipitation of proteins	90
7.2.1.3	SDS-polyacrylamide gel electrophoresis	91
7.2.1.4	Silver staining of SDS gels	91
7.2.1.5	Native polyacrylamide gel electrophoresis	91
7.2.1.6	Agarose gel electrophoresis	92
7.2.2	GRAFIX	92
7.2.3	GENERAL METHODS WITH <i>E. COLI</i>	93
7.2.3.1	Strains	93
7.2.3.2	Chemically competent cells	93
7.2.3.3	Media	93
7.2.3.4	Transformation	94
7.2.3.5	Isolation of plasmids and sequencing	94
7.2.4	EXPRESSION AND PURIFICATION FROM <i>E. COLI</i>	94
7.2.4.1	Purification of <i>D.m</i> His <sub>6</sub> -TEV-ISWI	95
7.2.4.2	Purification of <i>D.m</i> Acf1	96
7.2.4.2.1	Baculovirus expression system	96
7.2.4.2.2	Small scale purification	96
7.2.4.2.3	Large scale purification	97
7.2.4.3	Purification of <i>D.m.</i> CHRAC14/16	98
7.2.4.4	Purification of GST-TEV-FLAG-DID2	99
7.2.4.5	Purification of His <sub>6</sub> -Dyn2	100
7.2.5	RECONSTITUTION OF NUCLEOSOMES	100
7.2.5.1	DNA preparation	100
7.2.5.1.1	DNA large scale PEG precipitation	101
7.2.5.1.2	Digestion and purification of DNA	102
7.2.5.1.3	PCR amplification of DNA	102
7.2.5.2	<i>D.m.</i> core histones purification	103
7.2.5.3	Octamer reconstitution	104
7.2.5.4	Salt gradient dialysis for nucleosome reconstitution	105

---

7.2.6	MICROSCALE THERMOPHORESIS (MST)	106
7.2.7	GENERAL METHODS WITH YEAST	106
7.2.7.1	Gene deletion and tagging	106
7.2.7.2	Preparation of yeast genomic DNA	107
7.2.8	PURIFICATION OF ENDOGENOUS INO80 COMPLEX	108
7.2.9	CROSS-LINKING AND MASS SPECTROMETRY	108
7.2.10	BIOCHEMICAL ASSAYS	108
7.2.10.1	Electrophoretic mobility shift assay	108
7.2.10.2	Remodeling assay	109
7.2.10.3	ATPase assay	109
7.2.11	ELECTRON MICROSCOPY AND SINGLE PARTICLE ANALYSIS	109
7.2.11.1	Negative stain electron microscopy	109
7.2.11.2	Cryo electron microscopy	110
7.2.11.3	Subunit localization in INO80 with DID-tagging	110
7.2.11.4	Data Processing for INO80	111
<b>8</b>	<b><u>REFERENCES</u></b>	<b>112</b>
<b>9</b>	<b><u>APPENDIX</u></b>	<b>121</b>
<b>9.1</b>	<b>GENETIC INFORMATION</b>	<b>121</b>
9.1.1	601 POSITIONING SEQUENCES FOR NUCLEOSOMES	121
9.1.2	PART OF INO1 GENE FOR NUCLEOSOME RECONSTITUTION	121
9.1.3	INO80-FLAG2	121
9.1.4	URA3 MARKER: PROMOTER AND ORF	122
9.1.5	DID1 SEQUENCE	122
<b>10</b>	<b><u>CURRICULUM VITAE CAROLINE HAAS</u></b>	<b>123</b>
<b>11</b>	<b><u>ACKNOWLEDGEMENTS</u></b>	<b>125</b>

## 2 Summary

ATP-dependent chromatin remodeler are involved in basically all fundamental cellular processes, which require access to the DNA, such as transcription, replication or DNA repair. In the past decade the function of those remodeler has been studied intensely, however structural information, which is essential for the mechanistic understanding of the process, remained scarce. To date, the process of chromatin remodeling is not yet fully understood, hence we aimed at providing a structural basis by electron microscopy (EM) and single particle analysis to help solving this mystery.

### **ISWI chromatin remodeler**

The aim of the first presented research project was to structurally dissect the reaction catalyzed by chromatin remodeler of the *Drosophila* ISWI (Imitation Switch) family using electron microscopy, single particle analysis and three dimensional reconstruction. A main effort was to reconstruct the monomeric ISWI ATPase as well as the heterodimeric ACF complex (ATP-utilizing chromatin assembly and remodeling factor) and both remodeler in complex with their nucleosomal substrate.

Different functional states were trapped with ADP, non-hydrolyzable ATP analogs and transition state analogs in order to structurally follow the mechanism of chromatin remodeling. The formation of mono- and dimeric complexes of ISWI and ACF with DNA and nucleosomes was observed in electro mobility shift assays. Binding affinities were measured under close to native binding conditions by MicroScale Thermophoresis. The affinity of ISWI to the nucleosome was too weak to be analyzed by electron microscopy. Thus I tried to increase the affinity by introducing Walker mutations in ISWI as well as adding various ATP analogs. The transition state mimetic ADP·BeFx stabilized the complex enough for EM purposes, however recently a structure of a dimeric human ISWI homolog Snf2H on a nucleosome using those conditions was published (Racki et al., 2009). As ISWI-nucleosome complex could not be purified or enriched further, the project was ended at this stage.

### **The INO80 chromatin remodeler**

In contrast to ISWI remodeler, INO80 (Inositol requiring 80) is a large, 1.3 MDa sized, multi-subunit remodeler. INO80 is particularly versatile in the processes it is involved in and the catalyzed remodeling products, from sliding to the eviction or exchange of the H2A.Z/H2B dimer. In collaboration with Alessandro Tosi (Karl-Peter Hopfner, Gene

Center, Munich, Germany) and Franz Herzog (formerly Aebersold, ETH in Zurich, Switzerland, now Gene Center, Munich, Germany), we solved the structure and topology of the *S.cerevisiae* INO80 complex. Furthermore we analyzed the engagement of INO80 and its modules with nucleosomes and the remodeling process.

Using electron microscopy (EM), I reconstructed the 3D structure of INO80, which has an elongated embryo-like shape with head-neck-body-foot arrangement markedly different from other large chromatin remodeler, which are rather globular. The INO80 structure exhibited no obvious nucleosome binding cleft, but the flexible foot region could close thereby forming a pocket suited to engage the nucleosome.

Alessandro Tosi and Franz Herzog analyzed the subunit topology of the INO80 complex by cross-linking and mass spectrometry (XL-MS) and solved the complete interaction map of all 15 INO80 subunits with domain resolution. These data implicated a modular organization of INO80 on the Ino80 scaffold, bridged by Ies2: Rvb1/2 and Arp5/Ies6 (Arp5-module) are in close proximity to the ATPase of Ino80, Arp4/Arp8/Act1/Ies4/Taf14 (Arp8-module) are recruited via the HSA domain of Ino80, whereas Nhp10/Ies1/Ies3/Ies5 (Nhp10-module) assembled at the N-terminus of Ino80. The modular architecture could be further confirmed *in vivo* by analysis of deletion mutants and recombinant expression of sub-complexes.

The dodecameric AAA+-ATPases Rvb1/2 are located in the head of INO80 and as shown by XL-MS assemble into two hetero-hexameric rings with their flexible domain II facing each other. The neck region harbors the bi-lobed ATPase domain of Ino80 with its insertion contacting the Rvb1/2. Using DID-labeling (Flemming et al, 2010), we localized Ies2 close to the neck and the Arp5-module in the neck at the back of the Ino80 ATPase. The Nhp10 module was detected at the body, whereas the Arp8-module was found in the flexible foot region.

We could show, that apart from the Arp8-module, the Nhp10-module contributed to substrate interaction, whereas the Arp5-module and to some extent the Arp8-module were required for nucleosome sliding and proper stimulation of the ATPase activity. Finally, we analyzed INO80-nucleosome complexes by XL-MS and EM demonstrating its interaction at the concave site of INO80.

Our analysis established a first structural and functional framework for the large and flexible INO80 chromatin remodeler and thus provides the basis for understanding the remodeling and variant exchange process (Tosi et al., 2013).

### 3 Introduction

#### 3.1 *Chromatin is important for all DNA mediated processes*

Inside the nucleus, eukaryotic DNA is organized into a highly condensed structure, which is composed of nucleosomes as a basic structural unit and various associated non-histone proteins, folding up into a higher order structure termed chromatin. Compaction of DNA is not only required to fit the DNA into the dimension of a nucleus, but also to regulate and control access to the genetic information. Chromatin not only spatially organizes DNA, but also carries epigenetic information in form of DNA modifications, histone variants and a large variety of posttranslational modifications of histones within the nucleosomes. Overcoming the repressive barrier to DNA imposed by the condensed structure of chromatin is essential during all fundamental nuclear processes from DNA replication, gene expression by transcription as well as during DNA repair.

Investigating the regulation and access to DNA, its compaction and epigenetic information is therefore crucial for understanding the basis of eukaryotic life.

#### 3.2 *Nucleosomes are the basic structural unit of chromatin*

A canonical nucleosome, the standard repeating unit of chromatin consists of 147 bp of double-stranded DNA wrapped in 1.65 left-handed superhelical turns around a histone octamer comprising a (H3/H4)<sub>2</sub> tetramer and two H2A/H2B dimers (Luger et al., 1997). Association of linker histones H1 or H5 leads to further compaction of the DNA (Robinson and Rhodes, 2006).

The overall disc-like shape of nucleosomes (see Fig. 1A) is conserved between species and moreover even over all histone variants and modifications that have been crystallized so far. All four core histones are highly conserved amongst each other and across species from yeast to human. The basic histone proteins contain a characteristic, well conserved histone-fold domain with three alpha-helices inter-connected by two loops, also called helix-turn-helix:  $\alpha 1$ , L1,  $\alpha 2$ , L2,  $\alpha 3$  (see Fig. 1B). Heterodimeric interaction between histone folds (H2A/H2B or H3/H4) resembles a “handshake motif”. All histones have long, flexible N-terminal tails, which are the major sites for post-translational modifications (discussed in more detailed below).

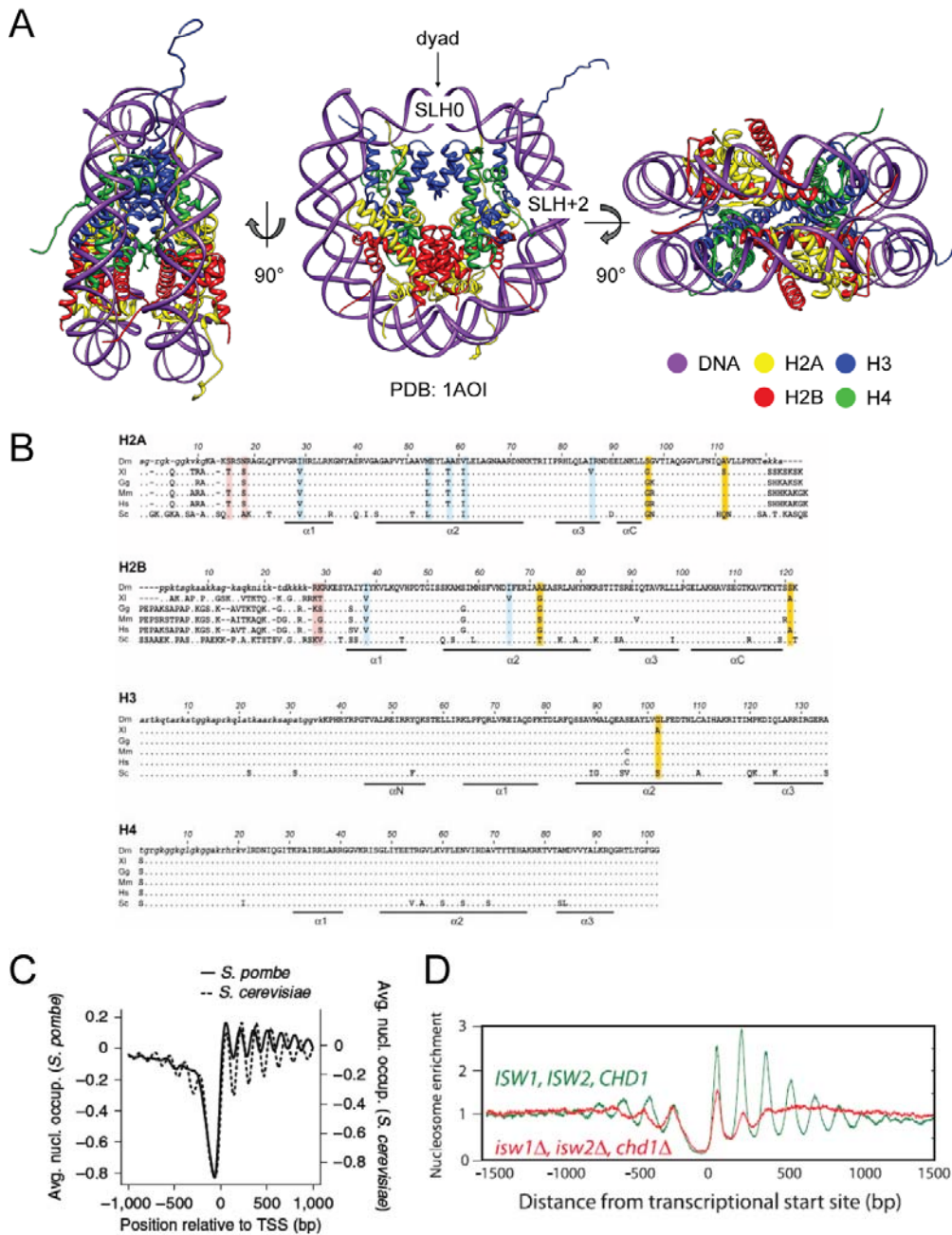


**Figure 1 Nucleosomes are the basic structural unit of chromatin.** **A)** Crystal structure of the nucleosome core particle at 2.8 Å with *Xenopus laevis* histones on α-satellite DNA (PDB code 1AOI) (Luger et al., 1997). DNA is depicted in purple, H2A H2B, H3 H4 in yellow, red, blue, and green respectively. The dyad, as well as SHL+2 region are marked. **B)** Alignment of four core histones of *Drosophila melanogaster* (*D.m.*), *Xenopus laevis* (*X.l.*), *Gallus gallus* (*G.g.*), *Mus musculus* (*M.m.*), *Homo sapiens* (*H.s.*), *Saccharomyces cerevisiae* (*S.c.*) reveals a high degree of conservation among species and shows the three main alpha-helices responsible for the histone fold (Figure adapted from (Clapier et al., 2008)). **C)** Nucleosome occupancy profiles of *S. pombe* and *S. cerevisiae* genes after TSS (transcriptional start site) alignment show a prominent upstream nucleosome free region (NFR), and regular array in the gene body, gradually decreasing from the +1 nucleosome (Figure adapted from (Lantermann et al., 2010)). **D)** Nucleosome occupancy profiles after TSS alignment in wild type and deletion of ISW1, ISW2, CHD1 underline their role in establishing a canonical nucleosome patterning (Figure adapted from (Gkikopoulos et al., 2011)).

Besides the canonical histone, various histone variants can be incorporated into nucleosomes to change their biophysical properties. Variants are most prominent in histone families H2A and H3 (Talbert and Henikoff, 2010). Histone variants have specific features and fulfill specialized roles. For example incorporation of H2A.Z (Htz1 in *S.c.*) probably renders the nucleosomes more unstable (Suto et al., 2000), controls transcription and is preferentially found at the +1 nucleosome (Albert et al., 2007; Raisner et al., 2005).

The nucleosome has a pseudo-symmetric structure with a “symmetry axis” located at the dyad where the H3/4 tetramer is located, flanked by the DNA entry and exit site. The super-helix location 0 (SHL0) is by definition on the dyad and each turn (10 bp) of DNA away on either site are called SHL+1 and SHL-1, respectively. There are 14 DNA-histone contacts, each storing approximately 1 kcal/mole (Saha et al., 2006). Those histone-DNA contacts differ significantly in their strength from the central nucleosome dyad to the entry/exit sites. DNA at the entry/exit site was shown to spontaneously unwrap, also called nucleosome breathing (Miyagi et al., 2011; Polach and Widom, 1995). There are three regions of strong contacts: one at the dyad and two  $\sim \pm 40$  bp from the dyad (Hall et al., 2009). The thermodynamically least stable contacts are at SHL $\pm 2$  (Hall et al., 2009). Nucleosomes are preferentially found at CG rich tracts, probably due to the enhanced intrinsic bending capability of the DNA (Tillo and Hughes, 2009; Valouev et al., 2011). AT-rich region on the other hand disfavor nucleosome and are thus often found in nucleosome free regions (NFR) upstream of the transcriptional start site (TSS) (Mavrich et al., 2008).

Nucleosomes have characteristic patterns along genes (see Fig. 1C-D): the best positioned nucleosome around the TSS is called the +1 nucleosome. Nucleosomes are evenly spaced downstream of the +1, but gradually decrease in the extent of positioning. Upstream of the +1 nucleosome at the promoter of genes, the DNA is depleted of nucleosomes and referred to as the nucleosome free region (NFR) (Mavrich et al., 2008; Shivaswamy et al., 2008).

Packaging of DNA into nucleosome imposes an obstacle for example for transcription factor binding or transcription, either by direct blocking of binding sites or the distortion of the bent DNA. ATP-dependent remodeler help to create a dynamic chromatin environment.

### 3.3 *Chromatin dynamics and reorganization*

Chromatin regulation comprises access to chromatin and the use of epigenetic marks to change the physical properties of the packed DNA and/or binding of non-histone proteins. This dynamic adaption is required during processes such as transcriptional activation or DNA repair.

Chromatin reorganization can be achieved by three major pathways: methylation of DNA, changes of the histones moieties by post-translational modifications or histone variant exchange, as well as alteration of the nucleosome architecture by ATP-dependent chromatin remodeler.

#### 3.3.1 DNA methylation

DNA is typically methylated at cytosines (m5C) in CpG islands by DNA methyltransferases (DNMTs) (Caiafa and Zampieri, 2005). Methylated DNA suppresses expression and leads to formation of compact and inactive heterochromatin. DNA methylation plays an important role in cell division and differentiation by altering the expression of genes (Bender et al., 1999). Some DNA methylation marks are inheritable and lead to genomic imprinting.

#### 3.3.2 Histone modifications

Post-translational modifications of histones can alter the biophysical properties of nucleosomes and thereby influence their interaction with DNA or binding partners. Mainly the long and flexible histone tails are dynamically modified for example by methylation, acetylation, ubiquitination, phosphorylation, SUMOylation and ADP-ribosylation. Chromatin modifiers or “writers” include lysine methyltransferases, histone acetyl transferases (HATs: e.g NuA4 and TIP60 acetylate H4 and H2A, H2A.Z, (Allard et al., 1999; Doyon et al., 2004), as well as ubiquitylases and kinases. After “writers” established a mark, “readers” bind to the respective modifications, whereas “erasers” are able to remove the modification. “Readers” contain specific domains that recognize for example acetylated lysines: *S.c.* Rsc4 (a subunit of RSC) interacts with H3K14ac thereby promoting expression (Kasten et al., 2004). “Erasers” such as Histone deacetylases (HDAC, e.g. NuRD) remove acetylation marks (Zhang et al., 1998).



Modifications of histone tails can act as epigenetic marks and thereby regulate for example transcription: H3K4 methylation is a mark for active chromatin (Rougeulle et al., 2003), whereas H3K9 methylation is linked to repression (Heard et al., 2001). Acetylated chromatin is usually found in transcriptionally active, more open euchromatin, while the more condensed, inactive heterochromatin lacks acetylation marks (Kurdistani and Grunstein, 2003).

Modification of histones is not limited to core histones, but can also affect histone variants: in response to DNA double-strand break, H2A.X is very rapidly phosphorylated at Ser139 ( $\gamma$ -H2A.X) by the ataxia telangiectasia mutated/ATM related (ATM/ATR) kinases in response to DNA damage (Rogakou et al., 1998).

Post-translation histone modifications have diverse functions in gene expression, repair of DNA damage and other DNA mediated processes such as mitosis.

### 3.3.3 ATP-dependent chromatin remodeler

ATP-dependent chromatin remodeler use the energy from ATP hydrolysis ( $\sim 7.3$  kcal/mole of free energy) to break contacts between histones and DNA in order to restructure nucleosomes thereby regulating the dynamic access to the packaged DNA. All remodeler share a conserved core ATPase, which belongs to the superfamily 2 (SF2) of DEAD/H-box helicases (Singleton et al., 2007). The bi-lobed Snf2 ATPase, consisting of two tandem RecA-like folds (DEXX and HELICc) uses ATP to directionally translocate along the minor groove of double stranded DNA (Singleton et al., 2007). In contrast to conventional helicases, remodeler ATPases do not have the “pin” motif (wedge domain) (Durr et al., 2005; Singleton et al., 2007), which is required for strand separation and therefore merely act as DNA translocases.

Chromatin remodeler are diverse in composition, structure and function. They catalyze various actions on their nucleosomal substrates, such as sliding (changing nucleosome position in *cis* or *trans*), eviction of octamers or dimers (removal of histones), exchange or incorporation of histone variants (changing the composition of nucleosomes) (see Fig. 2A). During sliding, the nucleosome is mobilized and the histone octamer is moved to a new position, thereby exposing originally occluded DNA. Most ISWI family remodeler can slide nucleosomeS to promote equally spaced nucleosomal arrays, whereas SWI/SNF remodeler randomize nucleosomes (Jaskelioff et al., 2000). Ejection can affect complete octamers leading to a removal of entire nucleosome thereby

exposing DNA. SWI/SNF family remodeler are able to evict nucleosomes, whereas ISWI family remodeler cannot perform this activity. Removal of histones can also involve only H2A/H2B dimers, leaving the central H3-H4 tetramer. Consequently, the DNA is exposed and the nucleosome is destabilized. Remodeler of the INO80 family are able to exchange H2A/H2B dimers with histone variants, such as H2A.Z (Htz1 in *S. c.*) (Mizuguchi et al., 2004; Papamichos-Chronakis et al., 2011).

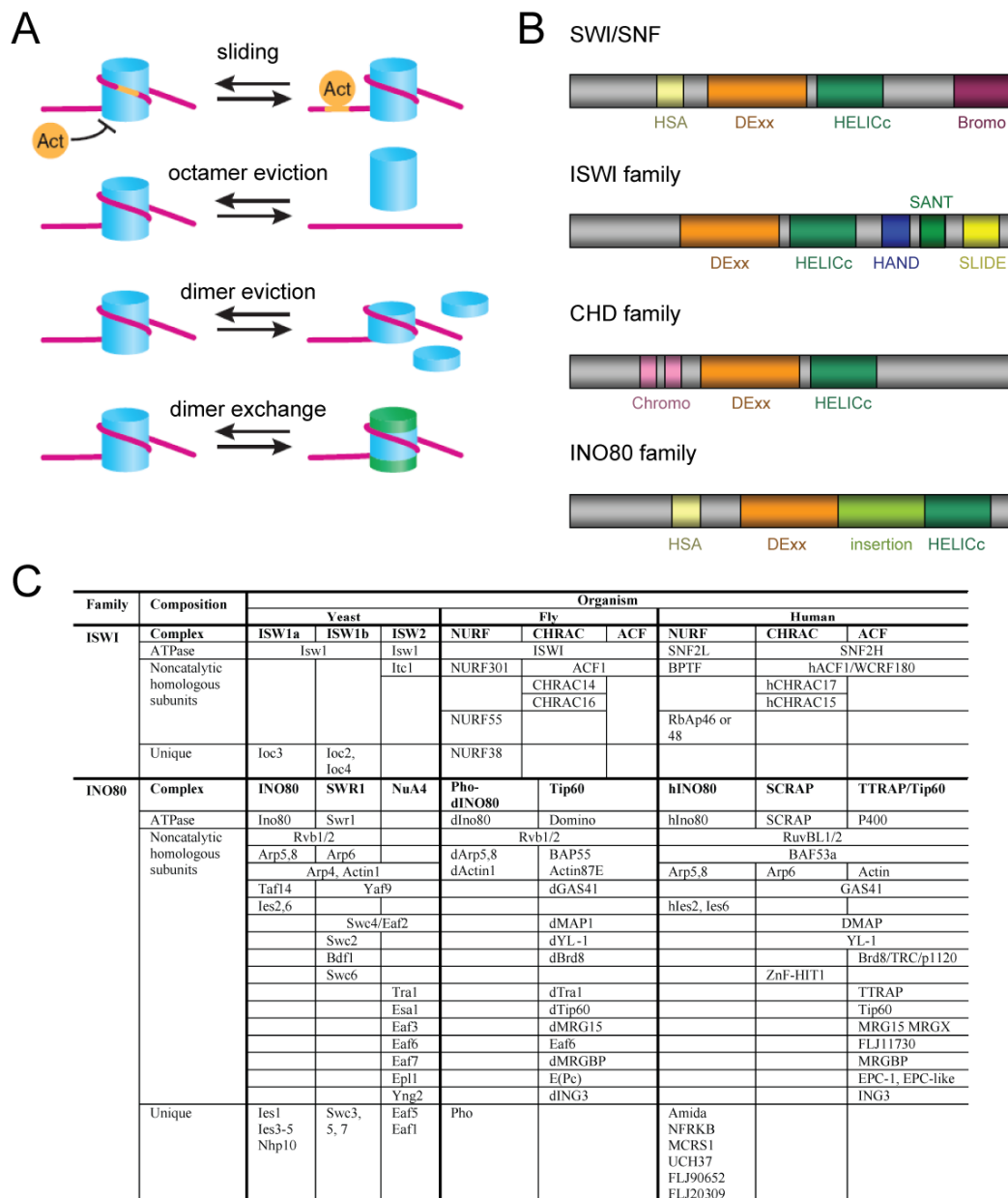


**Figure 2 Chromatin remodeler: their products, core ATPases and subunits in different species. A)** Nucleosome restructuring by chromatin remodeler includes nucleosome sliding, eviction of octamers or dimers and dimer exchange (adapted from (Cairns, 2007)); Act (orange) is an activator, which can interact with the DNA only after remodeling. Histone variants are depicted in green. **B)** The core ATPases of the

four major families of chromatin remodeler and their characteristic domains (adapted from (Clapier and Cairns, 2009)) C) ISWI and INO80 complexes and their accessory subunits in yeast, fly and human (adapted from (Clapier and Cairns, 2009) and (Bao and Shen, 2007)).

Conserved from yeast to human, the four major families of chromatin remodeler SWI/SNF, ISWI, Mi-2/CHD and INO80 family all contain a core SF2 ATPase subunit with unique accompanying domains, as well as optionally various additional accessory and regulatory subunits. While the central ATPase subunit facilitates DNA translocation, chromatin remodeling complexes of the different families have divergent remodeling activities. Most remodeler are functionally specialized and are usually not genetically redundant. The collection of chromatin remodeling complexes diverges in their enzymatic activity and reaction products, targeting, substrate preference and selection, mediated by their unique domains and additional subunits, which are for example responsible to bind certain posttranslational modifications.

### **3.3.3.1 SWI/SNF family of remodeler**

The multi-subunit, MDa large SWI/SNF (switching defective/sucrose non-fermenting) remodeling complexes was the first remodeler described in yeast (Cote et al., 1994). The ATPase of SWI/SNF family remodeler is characterized by the presence of an N-terminal HSA domain (helicase SANT domain), which recruits actin and actin related proteins, as well as C-terminal bromodomains, which are suggested to bind to acetylated lysines of histones (Mujtaba et al., 2007). Most eukaryotes contain two related SWI/SNF remodeler (Kasten et al., 2011): SWI/SNF and RSC (remodels the structure of chromatin) in yeast; BAP (Brahma associated protein) and PBAP (polybromo-associated BAP) in fly; BAF (Brg1 associated factors) and PBAF (polybromo-associated BAF) in humans. SWI/SNF remodeler have many activities in gene regulation, DNA repair, replication, proliferation, differentiation and tumor suppression; they can slide nucleosome and randomize nucleosomal arrays (Kasten et al., 2011). They are able to eject nucleosomes, but are not involved in chromatin assembly. Remodeling by RSC is enhanced by H4 acetylation (Kasten et al., 2004), whereas SWI/SNF lacks a regulation by the H4 tail or linker DNA.

### 3.3.3.2 ISWI family of remodeler

ISWI (imitation switch) remodeler are comparably small and contain only between 1-4 subunits (Yadon and Tsukiyama, 2011). Their ATPase subunit includes an N-terminal Snf2 motor and a tripartite C-terminal HAND, SANT, SLIDE (HSS) domain, which is a nucleosome recognition module (Grune et al., 2003) (see Fig. 3A-C). The *D.m.* HSS domain has an elongated dumbbell-like structure with the HAND-SANT domain connected to the SLIDE domain with a helical linker (Grune et al., 2003) (see Fig. 3B). The SANT domain (ySWI3, yADA2, hNCoR, hTFIIB) is structurally related to the c-Myb DNA-binding domain, however the ISWI SANT domain is negatively charged and thus probably involved in histone interaction, such as unmodified H4 tails (Grune et al., 2003). The juxtapositioned positively charged SLIDE domain (SANT-like ISWI) probably recognizes the linker DNA (Grune et al., 2003).

The ISWI ATPase can function on its own; however auxiliary additional subunits modulate the reaction with their specific domains: Acf1 (ATP-dependent chromatin assembly and remodeling factor) has a bromodomain and two PHD fingers (Eberharter et al., 2004). Acf1 in complex with ISWI changes the directionality of sliding and enhances the efficiency of regularly spaced chromatin (Eberharter et al., 2001; Fyodorov et al., 2004). The CHRAC (chromatin accessibility complex) complex contains the two histone fold proteins CHRAC14/16 in addition to ISWI and Acf1 (Corona et al., 2000; Hartlepp et al., 2005) to stabilize the interaction with the nucleosome, to enhance activity and to confer directionality.

Members of the ISWI containing chromatin remodeler slide nucleosomes (see Fig. 2B-C) in order to generate regularly spaced arrays. ISWI remodeler are able to translocate bidirectionally and processively along DNA thereby repositioning the nucleosome. Most remodeler of the ISWI family (ISWI, ACF and CHRAC) are involved in chromatin assembly and transcription repression by promoting the formation of regular nucleosomal arrays, for example during development (Stopka and Skoultchi, 2003). NURF (nucleosome remodeling factor) on the other hand promotes gene activation (Mizuguchi et al., 1997). ISWI family remodeler are also involved in replication initiation, timing and firing and replication of heterochromatin (Collins et al., 2002; Vincent et al., 2008). Recently, their involvement in DNA repair has been described (Erdel and Rippe, 2011; Smeenk and van Attikum, 2013).

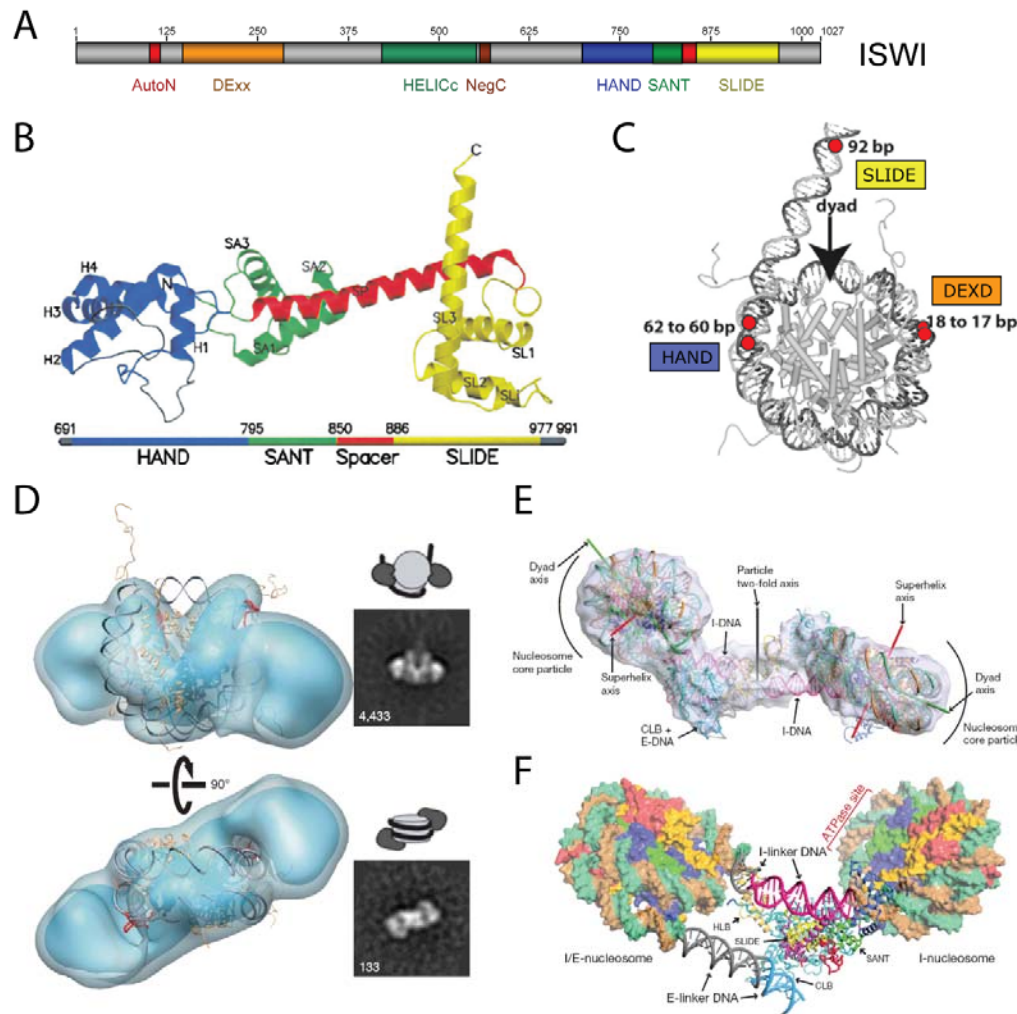


**Figure 3 ISWI family of chromatin remodeler.** **A)** Domain architecture of the core ATPase ISWI. ISWI has an N-terminal DEXD box ATPase domain, a HELIC domain, and a unique HAND, SANT, SLIDE motif at the C-terminus. **B)** Crystal structure of the *D.m.* HAND-SANT SLIDE (HSS domain) (Grune et al., 2003). **C)** Cross-linking studies revealed the interaction of the C-terminus with a mono-nucleosome (adapted from (Dang and Bartholomew, 2007)). **D)** Negative stain electron microscopy of the SNF2h-nucleosome complex in the presence of ADP·BeF<sub>x</sub> showed two SNF2h molecules interacting with one nucleosome (adapted from (Racki et al., 2009)). **E)** Cryo-EM structure of ISW1a(ΔATPase) interacting with two nucleosomes (Yamada et al., 2011). **F)** Model of ISW1a bridging two nucleosomes (Yamada et al., 2011).

ISWI remodeler are smaller than SWI/SNF or INO80 remodeler and make only limited contacts with the nucleosome and extranucleosomal DNA. However, they sense two functionally important stimuli: the histone tail of H4 and the linker DNA. The ISWI ATPase requires a basic patch (K<sub>16</sub>R<sub>17</sub>H<sub>18</sub>R<sub>19</sub>) on the N-terminal H4 tail for its remodeling activity (Clapier et al., 2001; Clapier et al., 2002; Ferreira et al., 2007), which is negatively regulated by H4K16 acetylation (Corona et al., 2002). It was speculated that the interaction with the basic H4 might be mediated via an acidic patch in the ISWI ATPase (Dang and Bartholomew, 2007). The ISWI ATPase binds at the SHL+2 position

(Dang and Bartholomew, 2007) (see Fig. 3C), where small distortions of the DNA can be accepted and which is adjacent to the SHL+1.5 location where the H4 tail protrudes. In addition to the H4 tail, ISWI also requires a certain length of linker DNA for full activity (Brehm et al., 2000). Thus, the interaction of the accessory domains with external DNA (Dang and Bartholomew, 2007) (see Fig. 3C) might be functionally important: the HAND domain cross-linked at the DNA entry/exit site, the SLIDE domain interacts with linker DNA.

Recently, Clapier and Cairns identified two new regulatory domains which negatively influence the ISWI activity (Clapier and Cairns, 2012): The AutoN and the NegC domain. The AutoN (N-terminal autoinhibitory region) negatively regulates ATP hydrolysis. The NegC domain is predicted to cross the two ATPase lobes which form the functional ATPase cleft. The NegC domain (equivalent to the C-terminal bridge in Chd1) couples ATP hydrolysis to productive DNA translocation. The AutoN contains a conserved basic patch that resembles the H4 basic patch. Both domains ensure that remodeling is only performed in presence of the correct nucleosomal features: Deletion of either AutoN or NegC domain enables sliding without the basic H4 tail or extranucleosomal DNA.

Another study demonstrated that the minimal conserved ATPase domain of ISWI (including the AutoN and NegC, but excluding the HSS domain) is able to bind and remodel nucleosome (Mueller-Planitz et al., 2013). Binding of DNA leads to a conformational change in the ATPase domain. Furthermore, the ATPase itself is not only involved in DNA binding, but also in H4 tail recognition. The HSS domain increases the affinity and specificity of the ATPase domain to the nucleosome.

Recently, it has been postulated that ISWI bind the nucleosomal substrate as a dimer and thereby enable bidirectional and processive translocation along nucleosomal DNA (Blosser et al., 2009; Racki et al., 2009). The human ISWI homolog SNF2h was visualized as a dimer on the nucleosome (Racki et al., 2009) (see Fig. 3D). The two ATPases face each other and take turns to engage either side of the nucleosome (discussed in more detail in section 3.4.2). Soon after, the Richmond lab applied a combination of crystallography and electron microscopy to analyze ISWI $\Delta$ ATPase and proposed that two nucleosomes can be bridged by one ISWI remodeler (Yamada et al., 2011) (see Fig. 3E). According to their model ISWI uses its own physical dimension to act as a protein ruler thereby determining the spacing of regular arrays (discussed in more detail in section 3.4.2).

Tracking the motion of DNA across the nucleosome using FRET analysis during ACF1 sliding reveal an initial step of 7 bp, followed by a stepsize of 3-4 bp (Blosser et al., 2009). The stepsize is preserved in several ISWI remodeler: *D.m.* ACF, *S.c.* ISW2, ISW1b (Deindl et al., 2013). The larger steps probably consist of 1 bp elementary steps (Deindl et al., 2013). The most intriguing finding of this study was that the translocation of DNA occurs first at the exit site of the nucleosome, where 7 bp of DNA are pushed out first, before the DNA is drawn into the nucleosome with 3 bp increments.

More detailed structural knowledge about the interaction of ISWI-containing remodeler including the ATPase and HSS domain as well as additional accessory subunits in complex with their natural nucleosomal substrate would be an essential starting point to improve the understanding of the mechanism of ATP-dependent chromatin remodeling.

### 3.3.3.3 CHD family remodeler

CHD (chromodomain, helicase, DNA binding) family remodeler are rather small and contain few subunits (Sims and Wade, 2011). The core ATPase subunit of CHD family remodeler is characterized by the presence of two tandem chromodomain at the N-terminus that bind methylated histones (Flanagan et al., 2005). Similar to ISWI remodeler, CHD remodeler require linker DNA for their activity (Bouazoune and Kingston, 2012). Most CHD remodeler are involved in sliding and ejection of nucleosome and thereby promote transcription. The NuRD/Mi-2 complex (nucleosome remodeling and deacetylase) however has repressive roles mediated by its deacetylation function (Denslow and Wade, 2007; Reynolds et al., 2012). Together with members of the ISWI family, CHD remodeler establish regular nucleosomal arrays with a defined linker length (Gkikopoulos et al., 2011; Pointner et al., 2012).

### 3.3.3.4 INO80 family remodeler

INO80 family remodeler are conserved MDa large, multi-subunit chromatin remodeler, which are defined by a split ATPase. The INO80 family includes INO80 (inositol requiring 80) and SWR1 (sick with Rat8). Higher order eukaryotes contain INO80, SCRAP (SNF2-related CREB-activator protein; a SWR1 homolog) and p400/TIP60 (TAT (transactivator of transcription) interactive protein 60 kDa) (see Fig. 2C and

Fig. 4)). Tip60 seems to be a fusion form of yeast SWR1 and yeast NuA4 (nucleosome acetyltransferase of H4) in higher eukaryotes and thus combines chromatin remodeling and histone variant exchange (mediated by the Snf2 ATPase p400) and histone acetyltransferase (HAT) activities (mediated by the HAT Tip60) within the same complex. Together INO80 and SWR1 regulate H2A.Z homeostasis by histone variant exchange: SWR1 exchanges H2A/H2B with the H2A.Z/H2B variant in a unidirectional and stepwise manner (Mizuguchi et al., 2004), whereas INO80 catalyzed the opposite reaction and removes H2A.Z/H2B dimers from nucleosomes (Papamichos-Chronakis et al., 2011). NuA4 acetylates histone H4 (Mitchell et al., 2008), but also the histone H2A and its variant H2A.Z/Htz1 (Babiarz et al., 2006; Keogh et al., 2006; Mizuguchi et al., 2004). INO80 is also able to slide nucleosomes, while SWR1 cannot (Nguyen et al., 2013).

INO80 family remodeler are extremely versatile and have very diverse functions in basically all DNA mediated processes, including replication, transcription, DNA repair and checkpoint pathways, but also telomere regulation, centromere stability, chromosome segregation and histone dimer exchange. The INO80 complex exhibits *in vitro* ATP-dependent 3'-5' DNA helicase activity (Shen et al., 2000), catalyzes nucleosome sliding (Shen et al., 2000), nucleosome spacing (Udugama et al., 2011), nucleosome eviction/displacement (Tsukuda et al., 2005) and H2A.Z-H2B dimer exchange with canonical H2A/H2B (Papamichos-Chronakis et al., 2011).

INO80 is involved in DNA replication and ensures proper chromosome segregation during regular cell division (Hur et al., 2010). INO80 associates with replication origins, is required for efficient progression of replication forks and reactivates stalled replisomes (Papamichos-Chronakis and Peterson, 2008; Shimada et al., 2008). INO80 participates in transcription via transcription factors (Cai et al., 2007), via the Rvb1/2 subunits (Jonsson et al., 2001) and regulation of H2A.Z eviction (Papamichos-Chronakis et al., 2011). INO80 is mainly found at the +1 nucleosome in promoters (Yen et al., 2012; Yen et al., 2013), where H2A.Z containing nucleosomes flank the nucleosome free region (Billon and Cote, 2012; Stargell and Gorovsky, 1994). H2A.Z nucleosomes are less stable and could thus facilitate promoter exposure thereby activating transcription. During DNA repair, INO80 is recruited to DNA double strand breaks (DSB) via direct binding to the DNA damage signal  $\gamma$ -H2A.X (van Attikum et al., 2004) mediated by the subunits Nhp10-Ies3 (Morrison et al., 2004), Arp4 (Downs et al., 2004) and Arp5 (Kitayama et al., 2009). INO80 also helps to expose DNA near the break to 5'-3' resection and evicts nucleosomes proximal to the break site (Tsukuda et al., 2005). In

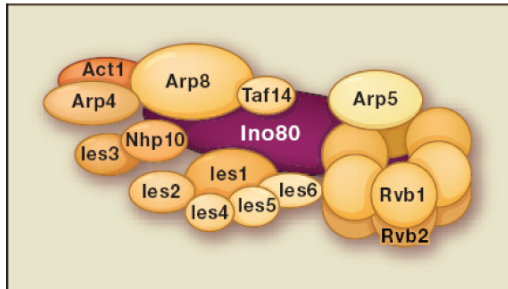


response to the DNA damage response pathway, INO80 itself is phosphorylated on its Ies4 subunit by Tel1/Mec1 kinases in yeast (ATM/ATR in mammals), which are required for DNA damage checkpoint (Morrison et al., 2007). Telomeres are regulated by the INO80 complex via its Ies3, Arp8 and Nhp10 subunits (Min et al., 2013; Yu et al., 2007). INO80 also participates in centromere stability (Chambers et al., 2012) and chromosome segregation (Measday et al., 2005). INO80 prevents polyploidy by ensuring appropriate chromosome segregation, probably by mediating proper H2A.Z localization as elevated H2A.Z levels lead to polyploidy (Chambers et al., 2012). Recently, it has been shown that the ATPase activity of INO80 is required for chromatin mobility, which is probably enhanced by nucleosome displacement (Neumann et al., 2012). INO80 can also function as a nucleosome spacing factor, which prefers longer linker length and moves nucleosomes from the end to the center (Udugama et al., 2011). INO80 has been described to reverse the incorporation of H2A.Z histone variant mediated by the SWR1 complex (Mizuguchi et al., 2004) by eviction of the unacetylated H2A.Z/H2B and exchange with the canonical H2A/H2B dimers in a unidirectional, stepwise manner (Papamichos-Chronakis et al., 2011). Incorporation of H2A.Z changes the biophysical properties of the nucleosome (Fan et al., 2002; Fan et al., 2004). The H2A.Z histone variant is enriched in actively transcribed chromatin at RNA polymerase II promoters at two specific nucleosomes one up- and downstream of the TSS (-1 and +1 nucleosome) (Billon and Cote, 2012; Stargell and Gorovsky, 1994), which is in agreement with enrichment of Ino80 and Arp5 enriched at these sites (Yen et al., 2012). H2A.Z incorporation into nucleosomes leads to subtle destabilization of the interphase between H2A.Z-H2B and (H3-H4)<sub>2</sub> tetramers (Suto et al., 2000). Regulation of H2A.Z distribution is important for genome integrity, dynamics (Papamichos-Chronakis et al., 2011; Wang et al., 2011), chromosome segregation (Krogan et al., 2004) and transcriptional control (Bargaje et al., 2012; Santisteban et al., 2011; Santisteban et al., 2000).

The catalytic subunit of the multi-subunit INO80 complex, the Ino80 ATPase contains a long insertion in the RecA2 fold, which is responsible for recruitment of the AAA+-ATPases Rvb1/Rvb2 and Arp5 (Jonsson et al., 2004). Furthermore, INO80 also contains a HSA domain, which comparable to the HSA domain of SWI/SNF remodeler recruits actin and Arps (actin related proteins): INO80 and SWR1 both contain actin and Arp4, INO80 specifically contains additionally Arp8 (Bao and Shen, 2007; Shen et al., 2000) (see Fig. 4). Rvb1/2, actin and the actin related proteins, Ies2 and Ies6 are conserved subunits in the INO80 complex from yeast to human. Ies1, Ies3-5, Taf14 and

Nhp10 are yeast specific subunits. In human INO80 assembles into three modules on the Ino80 scaffold: the N-terminus recruits metazoan specific subunits, which are dispensable for remodeling, the HSA domain interacts with Arp4, Arp8 and YY1, while the Snf2 ATPase assembles with the conserved Arp5, Ies2, Ies6 and Rvb1/2 (Chen et al., 2011).

A INO80 complex



B SWR1 complex

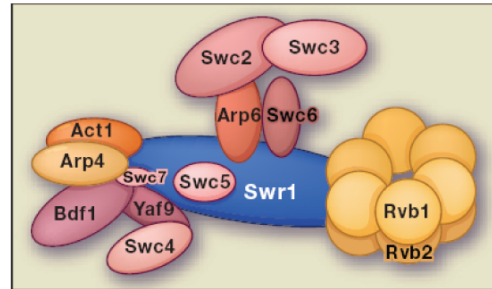


**Figure 4. Overview of subunit arrangement of INO80 chromatin remodeler INO80 and SWR1. A)** Subunits arrangement of INO80 based on the knowledge before this study. **B)** Subunit arrangement of SWR1. (Figure adapted from (Bao and Shen, 2007))

The AAA+-ATPases Rvb1 and Rvb2 are recruited to INO80 via the insertion in the Ino80 ATPase (Jonsson et al., 2004). Rvb1 and Rvb2 are homologs of the bacterial RuvB, which resolves Holliday junctions. Rvb1 and Rvb2 are involved in chromatin remodeling, snoRNA/RNP (Newman et al., 2000; Watkins et al., 2002; Watkins et al., 2004), c-myc (Wood et al., 2000) and  $\beta$ -catenin pathways (Bauer et al., 2000). Rvb1 and Rvb2 are essential (Jonsson et al., 2001) and have been implicated in cancer (Carlson et al., 2003) however their molecular function and contribution in the various associated complexes and pathways is not yet understood. Rvb1 and Rvb2 can assemble into homo-hexamers, hetero-hexamers and dodecamers (Jha and Dutta, 2009). Their oligomeric state and stacking arrangement, especially within complexes are still under debate. Rvb1 and Rvb2 consist of three domains: the ATPase core is build of domain I and III, interspaced by domain II. The crystal structure of the human RuvBL1 shows a hexameric arrangement (Matias et al., 2006). The crystal structure of Rvb2 is hexameric, however the domain II was missing in this structure (Petukhov et al., 2012). An atomic structure of Rvb1/2 with deletion of domain II revealed the adoption of two stacked hetero-hexamers with the remainder of the domain II facing towards each other (Gorynia et al., 2011). Several studies by electron microscopy revealed that Rvb1/2 can adopt hexameric and dodecameric arrangements with domain II or domain I/III facing each other: A negative stain EM structure of yeast Rvb1/2 revealed a hetero-hexameric assembly (Gribun et al., 2008). Analysis of yeast Rvb1/2 suggested alternative oligomeric states induced by His-

tags (Cheung et al., 2010). Cryo EM structures of human and yeast Rvb1/2 showed dodecameric arrangement with the interaction mediated by domain II (Lopez-Perrote et al., 2012; Torreira et al., 2008). In the cryo-EM analysis of the human Rvb1/2 it became evident that they coexist in two conformations, the transition from the compact and stretched form is driven by movements of the intrinsically flexible domain II (Lopez-Perrote et al., 2012; Petukhov et al., 2012). The negative stain structure of the human Rvb1/2 dodecamer is asymmetric with the bottom and top ring diverging (Puri et al., 2007; Torreira et al., 2008). The domain II with its OB-fold (oligonucleotide binding fold) shows similarities to the single strand binding protein RPA (replication protein A) and has been implicated in nucleic acid binding (Matias et al., 2006). Furthermore, the domain II might be involved in regulation of ATP hydrolysis by autoinhibition (Gorynia et al., 2011). The requirement of functional ATPase activity of Rvb1/2 seems to be context dependent; however Walker B mutants do not rescue the lethality of deletions mutants (Jonsson et al., 2001). For remodeling, the ATPase activity of Rvb1/2 is dispensable (Jonsson et al., 2004). Binding of Arp5 seems to be regulated by ATP, but the ATPase activity is not required for recruitment of the Arp5 subunit to the INO80 complex and (Jonsson et al., 2004).

Arp5 is one of three actin related proteins in INO80 and its presence is conserved through species. Arp5 is essential for INO80 activity (Shen et al., 2003). Arp5 is also able to fulfill role apart from the INO80 complex (Yen et al., 2012) and human Arp5 has been shown to shuttle between the cytoplasm and the nucleus (Kitayama et al., 2009).

Actin and the other actin-related proteins in INO80 Arp4 and Arp8 are recruited to the INO80 complex via the N-terminal HSA domain of the Ino80 subunits (Shen et al., 2003; Szerlong et al., 2008). The presence of polymerized actin in the nucleus is still under debate, however the presence of monomeric actin in chromatin remodeler has been proven (Kapoor et al., 2013). Arp4 and Arp8 have been crystallized and their deviating insertions explain why polymerization is prohibited (Fenn et al., 2011; Gerhold et al., 2012; Saravanan et al., 2012). Arp4 and Arp8 synergistically inhibit actin polymerization and sequester monomeric actin (Fenn et al., 2011). Arp4 and Arp8 can bind histones, Arp4 interacts with core histones (Harata et al., 1999); Arp8 binds preferentially H3 and H4 (Gerhold et al., 2012; Saravanan et al., 2012; Shen et al., 2003). Arp4 is also responsible for recruiting INO80 to DSB induced  $\gamma$ -H2A.X (Downs et al., 2004). The importance of Arp4 and Arp8 is emphasized by the fact that Arp4 is essential and Arp8 is required for proper INO80 activity (Shen et al., 2003).

Ies (INO80 subunit) subunits can be grouped into conserved and yeast specific: while Ies2 and Ies6 are also found in human INO80, Ies1 and Ies3-5 are yeast specific. Ies2 contains an uncharacterized PAPA-1 domain (PAP-1-associated protein-1 (Pim-1-associated protein-1), which has been implicated in protein-protein interaction (Kuroda et al., 2004)). The function of Ies2 remained elusive. Ies6 contains a conserved YL-1 domain and since its counterpart in SWR1, the YL-1 containing Swc2 subunit is responsible for H2A.Z binding (Wu et al., 2005), Ies6 might fulfill a similar role in INO80. Furthermore, Ies6 is required to prevent polyploidy formation by aberrant chromosome segregation (Chambers et al., 2012).

Ies3 interacts with Nhp10 (Shen et al., 2003) and is implicated in binding to telomeres (Yu et al., 2007). Ies4 gets phosphorylated in response to DSB by Mec1/Tel kinases and insures proper S phase checkpoint activation (Morrison et al., 2007).

Nhp10 (non-histone protein 10) is a yeast specific INO80 subunit. Nhp10 belongs to the high mobility group proteins (HMG), which have a highly conserved DNA binding domain (Ray and Grove, 2009, 2012). Nhp10 binds preferentially distorted, bent DNA (Ray and Grove, 2012) and is not required for chromatin remodeling (Shen et al., 2003), but responsible for proper replication (Vincent et al., 2008) and DSB repair (Morrison et al., 2004). A sequence specific motif for Nhp10 has been suggested (Badis et al., 2008), but could not be confirmed in a high resolution ChIP-exo study of INO80 (Yen et al., 2013).

Taf14 (TATA binding protein-Associated Factor) contains a YEATS domain (Yaf9-ENL-AF9-Taf14-Sas5). The YEATS domain of Yaf9 (Yeast homolog of the human leukemogenic protein AF9), a SWR1 subunit has structural similarities to Asf1, a histone chaperone for H3 and H4 (Wang et al., 2009). The Taf14 YEATS domain adopts similar folds compared to the YEAST domain of Yaf9 (Zhang et al., 2011).

The multi-subunit INO80 complex has divergent functions in DNA associated processes. Its overall structure and a complete subunit topology however were not known.

### **3.3.3.5 Models for chromatin remodeling mechanism**

The exact mechanism of nucleosome sliding is still enigmatic; however two major models are discussed: the twist diffusion and the loop propagation model (Bowman, 2010; Saha et al., 2006). In both cases, three strong regions of histone–DNA contacts have to be overcome during sliding: a strong central contact around the dyad and two energetically

weaker contacts at SHL+2.5 and SHL-2.5 (Hall et al., 2009). Interestingly, the latter contacts are in close proximity to the SHL2 region that has been shown to allow bulging of the DNA (Luger et al., 1997; Ong et al., 2007; Richmond and Davey, 2003; Suto et al., 2003) and is concomitantly the site where chromatin remodeler bind the nucleosomal DNA (Dang and Bartholomew, 2007).

One idea to achieve nucleosome remodeling is that the DNA is shifted around the histone octamer by twist diffusion ((Bowman, 2010), see Fig. 5A). According to this model, single base pairs are twisted during contact of the chromatin remodeler to the minor groove. This twist can be transferred gradually from the linker DNA over the nucleosomal DNA resulting in a shift of the DNA relative to the histone octamer by the size of the distortion. A drawback of the twist diffusion model is that ATP-dependent remodeler are not inhibited by physical barriers that would prevent DNA rotation such as DNA hairpins or nicks (Saha et al., 2006; Schwanbeck et al., 2004; Zofall et al., 2006). Therefore, this model might apply to thermal motion of nucleosomes, but is probably not the mechanism for sliding by ATP-dependent chromatin remodeler.

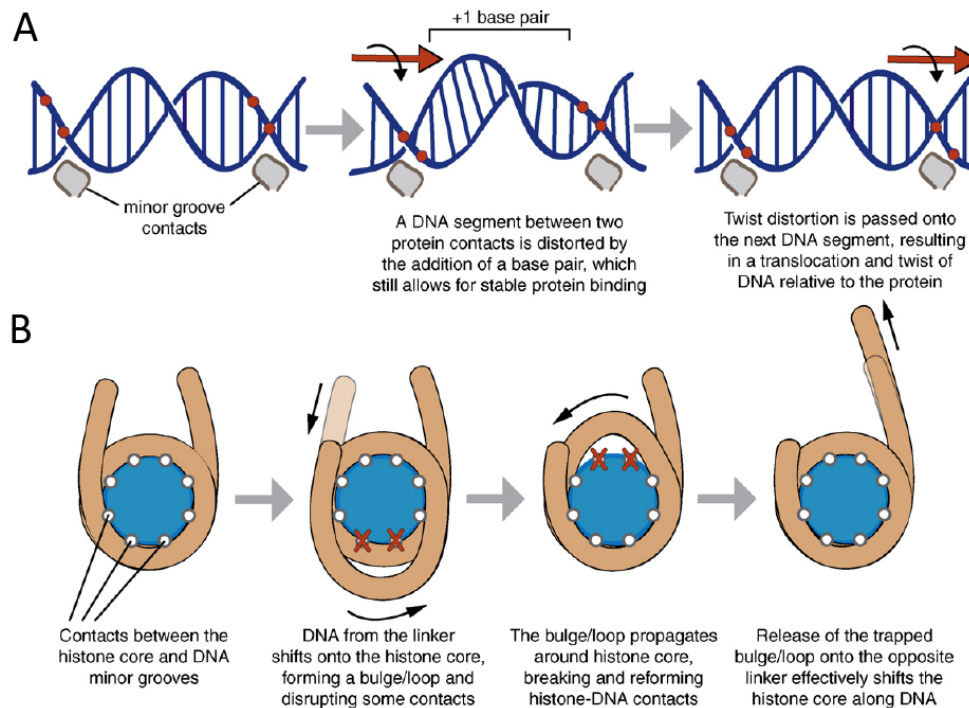


**Figure 5 The two major models for chromatin remodeling** (adapted from (Bowman, 2010)). **A)** According to the twist-diffusion model, a 1bp twist of DNA is propagated around the nucleosome. **B)** The looping model suggests that a loop of DNA is passed over the nucleosome leading to a relocation of the DNA in respect to the histone octamer.

The currently most favored model is the so called DNA loop propagation model ((Bowman, 2010), Fig. 5B). According to this model, the DNA is peeled off the nucleosome surface, catalyzed by the action ATP dependent chromatin remodeling complexes. The emerging transient DNA bulge or loop is propagated over the nucleosome surface in a one-dimensional diffusion. DNA histone contacts are disturbed at the leading edge of the loop. Finally, the loop propagation leads to a relocation of the DNA relative to the intact histone octamer.

However, in order to analyze, how remodeling is conducted from a mechanistic point of view, further and deeper structural knowledge about chromatin remodeler is required.

### **3.3.4 Other influences on chromatin structure**

Despite the influences on chromatin dynamics so far, many more factors contribute to the structure and rearrangements of chromatin. The role of long non coding RNA in chromatin is just emerging (Goto and Nakayama, 2012; Volpe and Martienssen, 2011). But also processes and their involved machineries, such as transcription influence nucleosomes (Hughes et al., 2012). Furthermore, histone chaperones, which typically shield histone-DNA contacts, play important roles for example in transcription (Gadad et al., 2009).

## **3.4 Structural information about chromatin remodeler**

### **3.4.1 SWI/SNF family remodeler**

Most electron microscopy (EM) structures of chromatin remodeler that have been solved to date are members of the SWI/SNF family: two SWI/SNF remodeler and five RSC remodeler (Leschziner, 2011) (see Fig. 6). All those reconstructions are low-resolution EM and do not exceed 20Å resolution. EM reconstructions of the SWI/SNF family share common features: they are rather globular, C-shaped with a central cavity or depression that could accommodate a nucleosome.

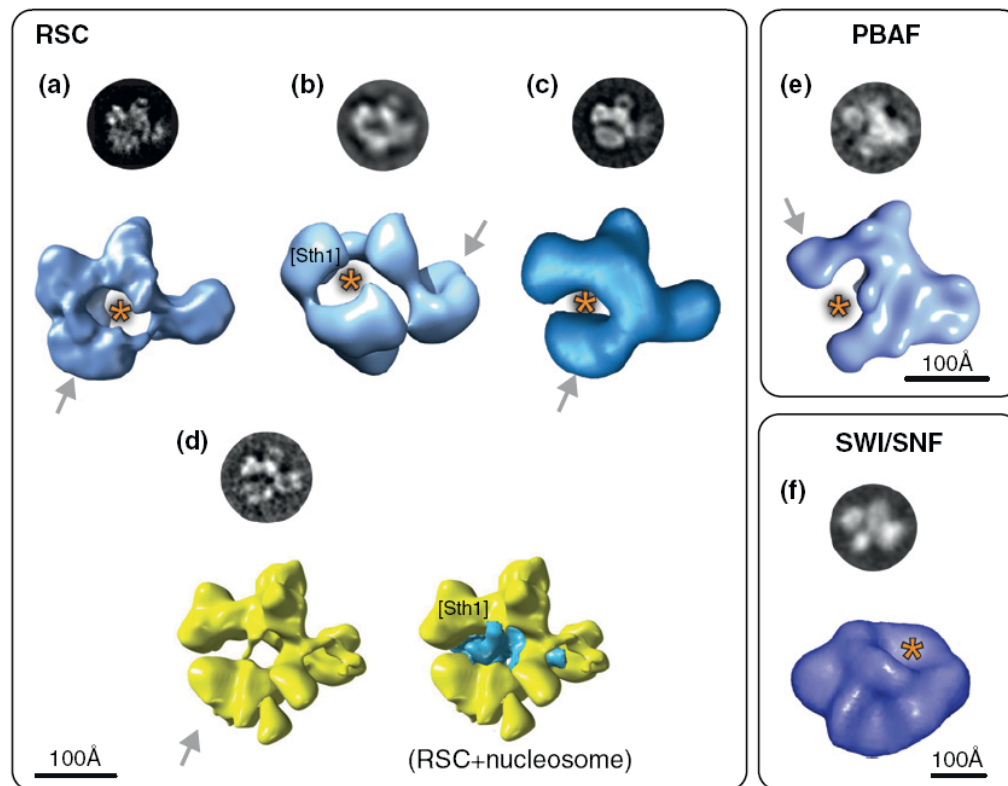


**Figure 6 Electron microscopy reconstructions of members from the SWI/SNF family (adapted from (Leschziner, 2011)):** Two-dimensional class average and the respective 3D reconstruction. Yeast RSC remodeler (a) (Asturias et al., 2002), (b) (Leschziner et al., 2007), (c) (Skiniotis et al., 2007), (d) (Chaban et al., 2008), e) the human RSC ortholog PBAF (Leschziner et al., 2005) and f) yeast SWI/SNF (Smith et al., 2003). 3D reconstructions from negative stain EM are depicted in blue, the cryo-EM map in yellow. Grey arrows indicate location of observed flexibility. 2D class averages from experimental data correspond to the respective 2D reconstructions. Orange asterisks mark the proposed binding site for the nucleosome. Sth1 marks the proposed location of the core ATPase of RSC.

Both structures of yeast SWI/SNF, first with negative stain EM (Smith et al., 2003), later with cryo-EM (Dechassa et al., 2008) are very similar. SWI/SNF is globular and contains a shallow depression that has the dimension to accommodate a nucleosome. According to the size of the depression, the nucleosome however cannot be engulfed completely by SWI/SNF. This conclusion could be confirmed using DNA footprinting and photoreactive site-specific cross-linking: only one side of the nucleosomal DNA is in contact with the SWI/SNF remodeler (Dechassa et al., 2008).

All four yeast RSC remodeler and the human RSC ortholog PBAF are very similar to each other. Similar to the SWI/SNF remodeler they are also rather globular and have a C-shaped arrangement of four globular domains with a deep cavity that could dimensionally and sterically accommodate a nucleosome (Asturias et al., 2002; Chaban et al., 2008; Leschziner et al., 2005; Leschziner et al., 2007; Skiniotis et al., 2007). Unlike



SWI/SNF they could engulf the nucleosome almost completely (Smith et al., 2003). Direct evidence for nucleosome binding in the observed cavity came from 2D image analysis of PBAF (Leschziner et al., 2005) and the first cryo-EM reconstruction of a RSC-nucleosome complex (Chaban et al., 2008). Furthermore, conformational flexibility was observed in RSC and PBAF reconstructions: in RSC one lobe showed open and closed conformations (Leschziner et al., 2007; Skinotis et al., 2007). RSC preferentially adopted the “closed” conformation in presence of a peptide mimicking acetylated histone H3 (Skinotis et al., 2007), which is known to activate RSC remodeling.

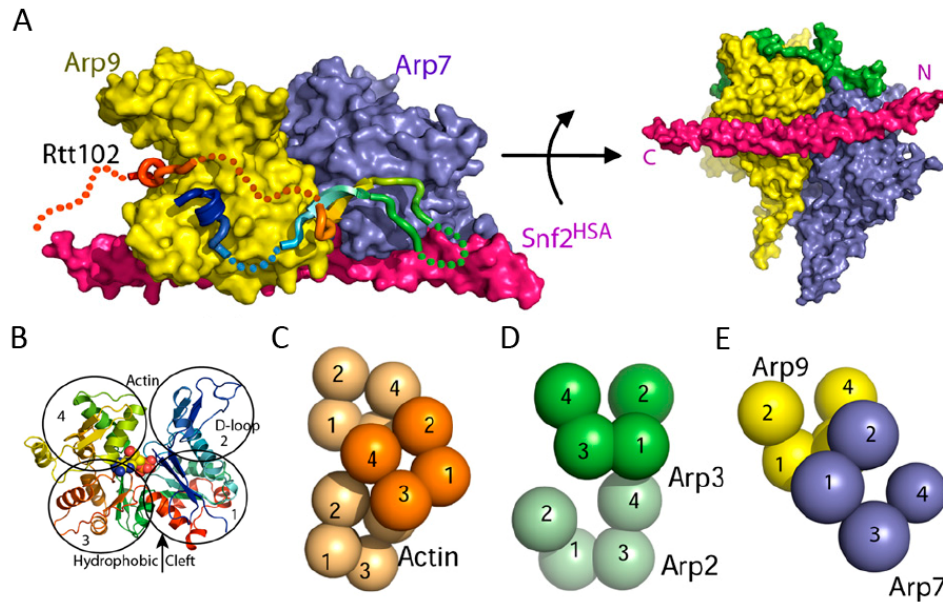


**Figure 7. Structure of the Snf2<sup>HSA</sup>-Arp7-Arp7-Rtt102 module of the SWI/SNF complex** (adapted from (Schubert et al., 2013)). **A)** Surface representation of the structure with the elongated SNF2<sup>HSA</sup> alpha helix in purple, Arp7 in blue, Arp9 in yellow and Rtt102 in rainbow colors. **B)** Definition of the domain organization in actin. **C-D)** Schematic representation of actin-actin interactions with domain organization: **B)** ARP and actin interactions, **C)** Arp2, Arp3 interactions, **D)** Arp9, Arp7 interactions.

To date, only few subunits of the SWI/SNF remodeler have been crystallized: The high resolution X-ray structure of Arp7, Arp9, Rtt102 assembled on the SWI/SNF HSA domain offered unique insights into the assembly of actin related proteins (Schubert et al., 2013) (see Fig. 7), which are also found in other chromatin remodeler, such as INO80. The structure shows that the SWI/SNF<sup>HSA</sup> domain spans the Arp7-Arp9-(Rtt102) interface as an extended  $\alpha$ -helix. In contrast to conventional actin-polymerization in actin fibers, Arp7 and Arp9 are rotated/shifted and the respective interfaces are distinct from actin polymers.



### 3.4.2 ISWI family remodeler

ISWI family chromatin remodeler are smaller and contain far less subunits as SWI/SNF or INO80 and are thus expected to contact the nucleosome to a lesser extent. Before EM was performed, the first indirect structural study of an ISWI-nucleosome complex was done using photoreactive cross-linking and footprinting (Dang and Bartholomew, 2007). This revealed that the HSS domain of ISWI is contacting the linker DNA, whereas the ATPase motor is bound approximately two turns of DNA away from the dyad axis at the SHL+2 position (Dang and Bartholomew, 2007), a critical point in the nucleosomal DNA and the site of DNA translocation (Saha et al., 2006; Zofall et al., 2006).

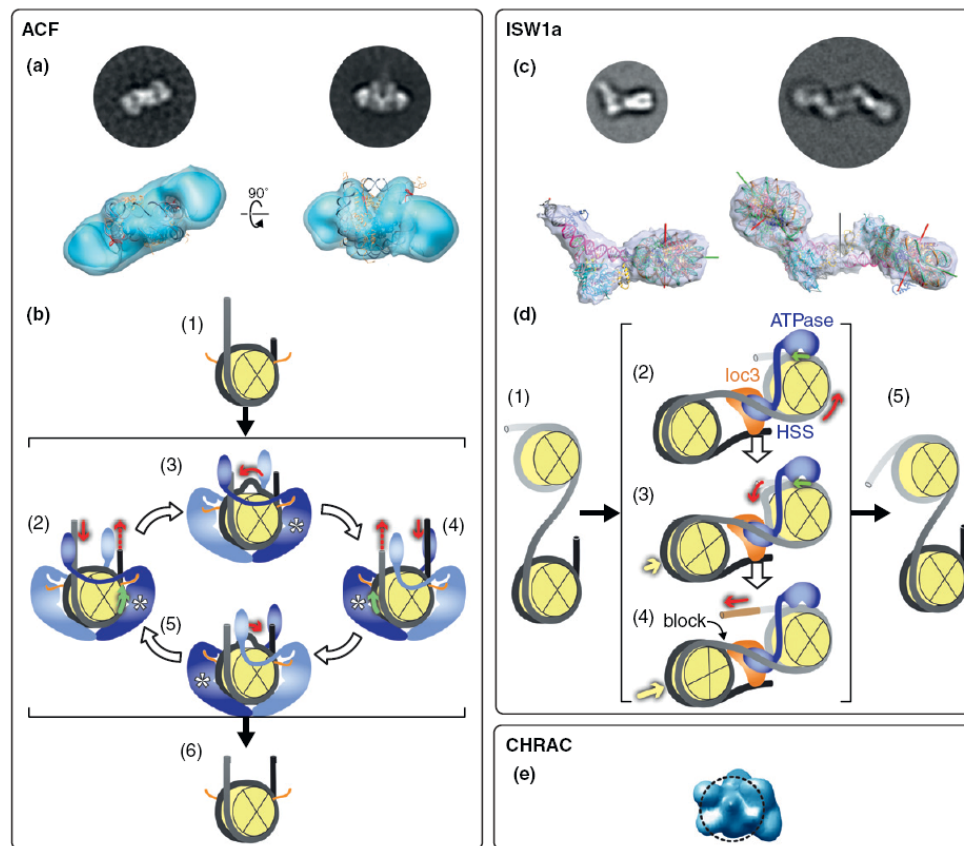


**Figure 8 Three-dimensional EM reconstructions of ISWI remodeler and respective models for remodeling** (adapted from (Leschziner et al., 2007)). **A and C)** Two-dimensional class-averages and the respective three-dimensional EM reconstructions. **B and D)** Suggested mechanisms for remodeling: the remodeler is marked in blue, the nucleosome in yellow. **A)** The negative stain EM structure of ISWI, the core ATPase of the ACF complex shows that human ISWI interacts with the nucleosome as a dimer (Racki et al., 2009). **B)** Model of ISWI-ATPases at the nucleosome taking turns in active translocation (asterisk marks the active monomer, engaged H4 histone tail in orange). The HSS domain helps by interacting with the linker DNA. **C)** The Cryo-EM structure of ISW1a( $\Delta$ ATPase) reveals that the complex can interact with mononucleosomes or space two mononucleosomes (Yamada et al., 2011) **D)** A model for ISW1a explains how the protein dimensions are used as a ruler to measure the distance between two nucleosomes. **E)** Negative stain structure of human CHRAC complex reveals a multi-lobed structure (Hu et al., 2008).

Recently three EM studies about ISWI containing remodeler were published (see Fig. 8). The first EM structure analyzed the entire human CHRAC complex (chromatin accessibility complex: hSNF2H, hACF1, hCHRAC15, hCHRAC17, (Hu et al., 2008)), which revealed a multi-lobed structure with no apparent nucleosome binding site.

The Narlikar lab analyzed the human ISWI homolog SNF2H using negative stain EM (Racki et al., 2009). They found two SNF2H bound to one nucleosome on opposite sites. The authors could detect the ATPase domain of SNF2H, which has been shown to bind at SLH +2 (Dang and Bartholomew, 2007), however they were not able to visualize the linker DNA and the HSS domain, which is primarily involved in linker DNA binding (Dang and Bartholomew, 2007; Grune et al., 2003). The authors proposed a model for ISWI in establishing evenly spaced arrays: a cooperative, dimeric motor of ISWI performs an “alternating action” instead of a “tug of war”. Taking turns, only one ATPase is active at a time, preferably translocating towards the longer linker DNA until the DNA is equalized on each side of the nucleosome.

Two years later, the lab of Richmond combined x-ray crystallography and EM to study yeast ISW1a, a complex of the ATPase subunit Isw1a and its accessory subunit Ioc3 (Yamada et al., 2011). In the crystal structure of Isw1a( $\Delta$ ATPase)-Ioc3 ( $\equiv$ Isw1a<sup>HSS</sup>, Ioc3) in complex with DNA it became obvious that ISW1a( $\Delta$ ATPase) is able to bind two strands of DNA simultaneously. The HSS domain contacts the DNA in the minor groove sequence independently. Using cryo-EM, the authors demonstrated that one ISW1a( $\Delta$ ATPase) can bridge two nucleosomes by binding to the two linker DNA strands. Based on their findings, an alternative model for ISW1a’s ability to evenly space nucleosomes was proposed: ISW1a functions as a sterical ruler by taken its own dimension to physically “measure” the distance between two adjacent nucleosomes. However, interactions between ISW1a( $\Delta$ ATPase) and the nucleosome is restricted to linker DNA and DNA directly next to the DNA entry site and no interaction of the remodeler and the histones could be observed. Furthermore, the nucleosome constructs yielding the di-nucleosomal structure contained linker DNA only on one side, and it might thus be possible that the authors artificially connected two nucleosomes via their two sole linker DNAs. Another surprise is the different orientation that ISW1a( $\Delta$ ATPase) adopts in the monomeric form compared to the dimeric nucleosome complex.

The two EM studies on ISWI remodeler come to opposing conclusions: Racki et al. detected two ISWI ATPases on one nucleosome (the HSS domain and the linker not being visible), whereas Yamada et al. detected one ISW1a( $\Delta$ ATPase) bound to two

nucleosomes (in this case only the HSS domain of ISWI and Ioc3 are visible). It remains to be seen, which model is correct and further structural analysis is required. Additionally, a structure of ISWI in complex with the nucleosome showing both the ATPase as well as the HSS domain is still missing.

### 3.4.3 CHD family remodeler

To date members of the CHD family of remodeler have been structurally analyzed by crystallography, but EM studies are not yet available.

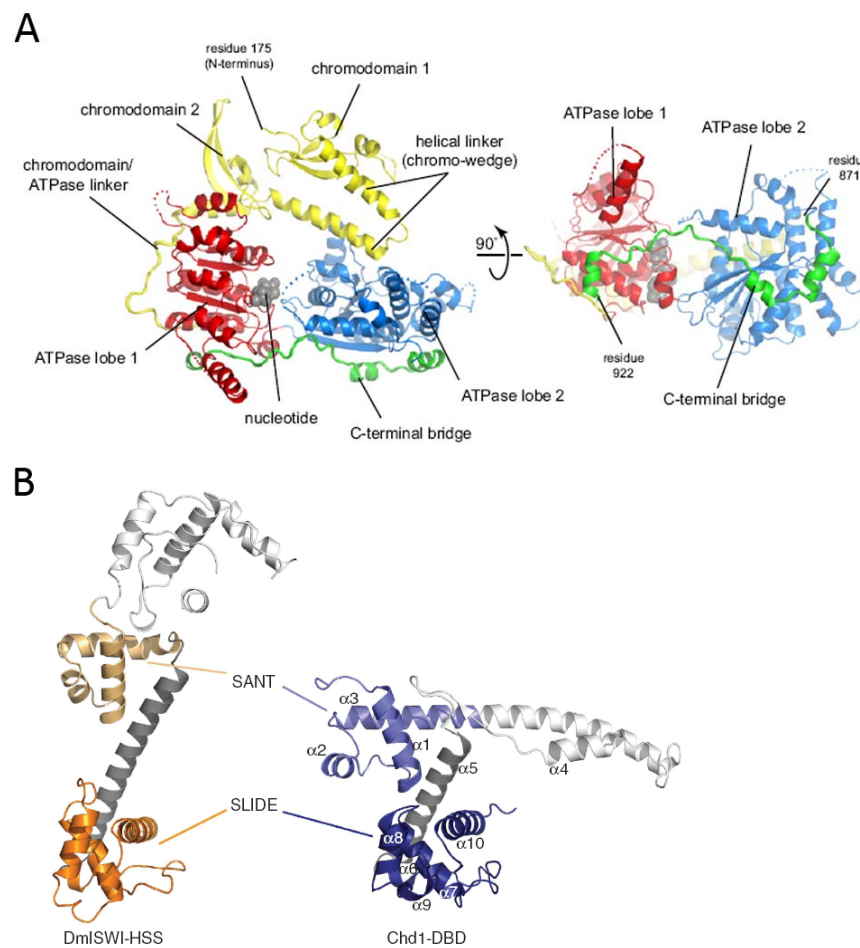


**Figure 9. Crystal structures of Chd1.** **A)** The structure of the Chromo- and ATPase domain of Chd1 explain how the chromodomains block the DNA binding site build by the two ATPase lobes (Hauk et al., 2010). **B)** Comparison between the *D.m.* ISWI HSS domain and the Chd1 DNA-binding domain, which is structurally homologous to the SANT-SLIDE domain of ISWI (Ryan et al., 2011).

The structure of the yeast Chd1 revealed that the N-terminal chromodomains block the DNA binding surface and prevent a proper closure of the RecA-like lobes

(Hauk et al., 2010) (see Fig. 9A). The chromodomains prevent activation of the ATPase by naked DNA. The autoinhibition is mediated by an acidic helix that contacts both lobes of the ATPase fold thereby occluding the central cleft.

X-ray crystallography of the C-terminal DNA binding domain of Chd1 revealed previously unrecognized structural homology with ISWI remodeler (Ryan et al., 2011) (see Fig. 9B): the DNA binding motif resembles the SANT-SLIDE domain of ISWI (Grune et al., 2003). The homology was not expected given the low sequence conservation, but mutations in the DNA-binding surface of the Chd1 SANT-SLIDE domain negatively influence its activity (Ryan et al., 2011).

For deeper structural understanding, we must await structure of the entire Chd1 remodeler in complex with the nucleosomal substrate.

#### **3.4.4 INO80 family remodeler**

There was no overall 3D structural information about the complete INO80 complex or SWR1, another member of the same family. However, few studies analyzed subunits of the INO80 complex. Crystal structures of the homologous Snf2 ATPase Rad54 (Durr et al., 2005; Thoma et al., 2005) revealed the arrangement of the two ATPase lobes, their interaction with DNA and how the ATPase might be active. For the insertion domain of the split Ino80 ATPase no structural information is available, as there is none for the N-terminus of Ino80. The HSA domain may adopt an elongated  $\alpha$ -helical fold as described for the HSA domain of SWI/SNF complex (Schubert et al., 2013). The structures of the Rvb1/2 complexes from x-ray crystallography and EM showed the AAA<sup>+</sup>-ATPases only in their isolated forms, where they can adopt homo- and hetero-hexamers as well as dodecameric arrangements ((Gorynia et al., 2011; Lopez-Perrote et al., 2012; Matias et al., 2006; Puri et al., 2007; Torreira et al., 2008). Information about the assembly and orientation of Rvb1/2 within complexes was not described so far. Actin, Arp4 and Arp8 have been crystallized (Fenn et al., 2011; Gerhold et al., 2012; Saravanan et al., 2012; Vorobiev et al., 2003). Both Arp4 and Arp8 exhibit the conserved actin fold and additional insertions, which explain their inability to polymerize as actin. In an EM study, Arp8 was found to dimerize via the N-terminus and interact with the nucleosome in a dimeric form (Saravanan et al., 2012), however the stoichiometry of Arp8 in the INO80 complex has not been analyzed so far. Arp5 has not been crystallized. There is also not structural information available about Ies1-6. The YEATS domain of Taf14 has been

solved by NMR (Zhang et al., 2011) and crystallography (Simpson 2012): The YEATS domain fold is similar to the YEATS domain of Yaf9 (Wang et al., 2009). Nhp10 contains two HMG-boxes (HMO2, HMG-B), of which homologous domain have been structurally analyzed: the NMR structure of the related *S.c.* Nhp6 HMGB-box in complex with DNA revealed a non-sequence specific interaction (Masse et al., 2002).

In summary, information about the 3D structure of INO80 and members of the INO80 family was missing. For a pseudo-atomic interpretation, several crystal structures of subunits would also be a prerequisite.

### ***3.5 Hybrid methods in structural biology***

In order to gain structural information about multi-subunit complexes, integrated structural methods are applied for a complete or detailed description, when one single technique is not sufficient. Hybrid methods combine several structural approaches to understand the three-dimensional function and organization of large and/or dynamic complexes.

Commonly high resolution information from X-ray crystallography and nuclear magnetic resonance (NMR) is combined with low resolution data gained from techniques such as small angle x-ray scattering (SAXS), electron microscopy or chemical cross-linking and mass-spectrometry (XL-MS), but also biochemical information from interaction studies can be applied integrated (reviewed in (Lander et al., 2012)).

X-ray crystallography allows the interpretation at an atomic resolution; however the ability to crystallize is a clear bottle neck. Furthermore, large amount of highly concentrated protein is required. NMR also offers high resolution structural information, however the size of the analyzed protein or protein complex is limited to approximately 30-70 kDa. X-ray crystallography and NMR often allow us to study only one or few subunits or domains of larger assemblies.

Electron microscopy and single particle analysis on the other hand is not limited by size, the bigger the complex the better it is suited for EM. Additionally, smaller quantities and less concentrated protein samples are required. In cryo-EM, the protein complexes are visualized in an aqueous, quasi native buffer environment, which resembles close to physiological conditions circumventing the possible drawbacks of crystal lattice formation in crystallography. EM is able to dissect different dynamic or transient states of macromolecular assemblies, which are not amenable to other structural

methods. EM is an ideal structural method to study large and dynamic assemblies. The resolution of EM structures varies from nano meter range to almost atomic resolution for symmetric assemblies. Negative staining enhances the signal-to-noise ratio, but preservation artifacts such as flattening, low pH of the heavy metal stain and drying the sample hamper the resolution. Under cryo conditions, the signal-to-noise ratio is lower, but the specimen can be observed in a closer to native, hydrated state, structural data is not limited to the surface and the resolution is better.

Electron density maps can be interpreted at pseudo-atomic resolution by fitting high resolution crystal structures as applied recently on the ATP synthase (Lau and Rubinstein, 2012). However, this depends on the availability of those structures and sometimes requires further knowledge about the subunit topology or location. In EM, subunits of complexes can be located by analysis of deletion mutants, antibody staining or tagging of subunits

Chemical cross-linking and mass spectrometry is ideally suited to complement structural analysis, such as EM. Chemical cross-linking and mass spectrometry is a novel technique that offers an unbiased approach to study the interaction surfaces in proteins or protein complexes (Herzog et al., 2012; Leitner et al., 2012; Walzthoeni et al., 2012). Commonly a bifunctional cross-linker covalently connects to lysine residues, which are in close proximity and thereby suggest interaction between the two cross-linked proteins. XL-MS offers a domain resolution of the protein-protein interaction network. The information gained from XL-MS has been used on several complexes to complement EM data, for example fitting of crystal structures into an EM density of whole polycomb repression complex PRC2 was supported by XL-MS (Ciferri et al., 2012).

The application of integrative approaches on important and challenging complexes maximizes the precision, completeness and efficiency of structural characterization of the individual methods. Therefore, we used a combination of EM and XL-MS to tackle the large chromatin remodeler, INO80.

## 4 Aims of the Projects

### 4.1 ISWI remodeler complexes

The first presented research project aims at determining the structure of the *Drosophila melanogaster* (*D.m.*) ISWI-containing chromatin remodeling complexes using electron microscopy, followed by single particle analysis and three dimensional reconstructions at the highest possible resolution. A main focus is the common catalytic core subunit, the ATPase ISWI (Imitation Switch). The mechanism of chromatin remodeling will be elucidated by observing the chromatin remodeler ISWI, the heterodimeric complex ACF (ATP-utilizing chromatin assembly and remodeling factor), as well as the CHRAC complex with two additional histone fold proteins (CHRAC14, CHRAC16) (see Fig. 2C) on their substrate, the nucleosome. If a structure of a remodeler in complex with a nucleosome can be solved, we are planning to extend the mono-nucleosomal substrate to a more physiological context of poly-nucleosomal arrays.

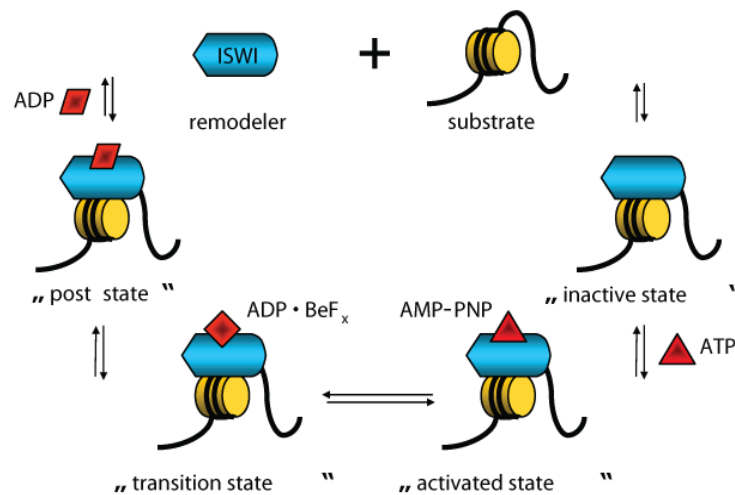


**Figure 10** The presumed cycle of chromatin remodeling could be trapped at different states using adequate ATP analogs.

To learn more about the cycle of chromatin remodeling, the remodeler-nucleosome complexes will be trapped in different nucleotide states using ATP analogs (see Fig. 10). Three-dimensional structures of the consecutive steps would help to understand the structural basis of the remodeling reaction.

## 4.2 INO80 remodeling complex

The second presented research project aimed at solving the structure and topology of the multi-subunit 1.3 MDa of the chromatin remodeler INO80 from *Saccharomyces cerevisiae*. Structural knowledge about the INO80 complex was scarce, the topology was largely unknown and information about the overall structure or interaction with the nucleosomal substrate was missing.

Thus, our goal was to obtain three-dimensional information about the INO80 complex using electron microscopy (EM). This would enable a comparison with other large chromatin remodeler from the SWI/SNF family, but also to speculate about nucleosome interaction. We aimed at the highest possible resolution for an INO80 structure, preferably under cryo-conditions to be able to gain as much information as possible about the overall shape and the presence and interaction of subunits. The structure could then be further interpreted by localization of subunits by analysis of deletion mutants, antibody staining or subunit tagging.

Furthermore, we planned to clarify the subunit topology of the INO80 complex by chemical cross-linking and mass spectrometry (XL-MS). This hybrid approach would allow us to at least partially interpret the EM density, but also to design new constructs for other structural methods such as crystallography.

It was also unclear, how INO80 would bind to the nucleosome. For that reason we planned to analyze the interaction of INO80 with the nucleosome with an integrated approach of biochemical binding studies of deletion mutants, complemented with structural methods from XL-MS and EM.

Ultimately, we would like to build a pseudo-atomic model of the entire INO80 complex by docking of available high-resolution crystal structures into the EM density of INO80 supported by XL-MS and molecular dynamics.

A three-dimensional structure of the INO80 in combination with the knowledge about the complete subunit topology in combination with data about the interaction with the nucleosome would allow us to speculate about the mechanism of nucleosome sliding and histone variant exchange. Additionally, this thorough structural analysis with hybrid methods would set the basis for designing further experiment to understand the mechano-structural mechanism of the INO80 complex.



## 5 Results

### 5.1 Reconstitution of nucleosomes

All four *D.m.* core histones were expressed recombinantly in *E. coli* (see Fig. 11A, C) and subsequently purified according to a modified protocol (see Fig. 11B). The most time consuming step, the inclusion bodies purification was substituted by direct use of the whole cell extract in a denaturing environment containing 8 M urea (in collaboration with the Becker group).

The purification of histone H4 is shown exemplarily for all four histones. The cells were lysed with a buffer containing 8 M urea to dissolve the histones from the inclusion bodies (see Fig. 11D). The lysate was sonicated to trim the DNA and subsequently pelleted to remove cell debris and aggregated proteins. About 50% of histone H4 was indeed soluble in the urea buffer (see Fig. 11D). H4 was not lost during filtering of the lysate with miracloth and a syringe filter (see Fig. 11D). About 90% of H4 bound to the SP Sepharose chromatography column (see Fig. 11D-E). The washing steps with increasing salt concentrations were effective in removing high molecular weight contaminations (see Fig. 11D-E). H4 eluted from the SP Sepharose material at ~500 mM NaCl (see Fig. 11E). Subsequently, anion exchange chromatography removed most of the DNA contamination, and H4 was detected in the flow through (see Fig. 11F). For all histones about 2-5 mg per L cell culture could be purified (see Fig. 11C).

Purified, lyophilized histones were mixed under unfolding conditions in equimolar amounts with 120% H2A-H2B excess and refolded to reconstitute octamers. Canonical octamers were separated from H2A-H2B dimers by size exclusion chromatography (see Fig. 11G-H).

The DNA used for mono-nucleosomes was based on the 601 positioning sequence from Widom, which was optimized for nucleosome positioning by SELEX (Lowary and Widom, 1998). The DNA fragments were either cut out from plasmids or amplified by PCR. In case of Cy3-labelled DNA for MicroScale Thermophoresis, the label was introduced into the DNA by using 5' Cy3 labeled primers in the PCR reaction.

Mononucleosomes were reconstituted using the salt gradient dialysis method. In order to determine the optimal ratio between DNA and octamers, the amount of octamers was titrated to a constant amount of purified DNA (see Fig. 11I).

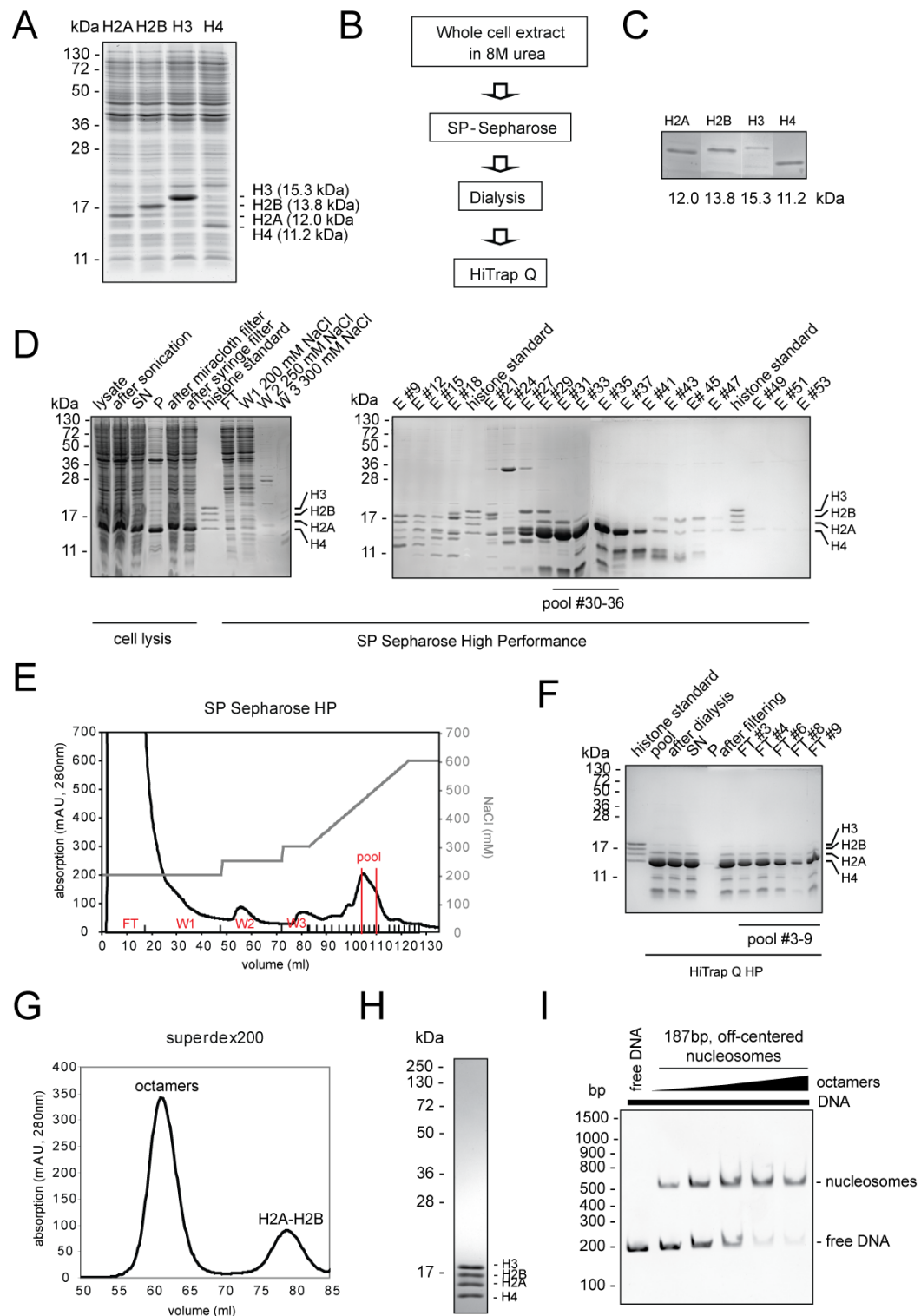


**Figure 11. Reconstitution of nucleosomes.** **A)** Expression of all four *D.m.* histones was monitored by 18% SDS PAGE and Coomassie staining. **B)** Schematic representation of *D.m.* core histone purification with 8 M urea. **C)** All four core histones were purified and analyzed by 18% SDS PAGE and Coomassie staining. **D)** Exemplary purification of H4 using a cation exchange chromatography, analyzed by 18% SDS PAGE, stained with Coomassie. SN = supernatant, P = pellet, FT = flow through, W = wash, E = elution. **E)** Elution profile for H4 on a SP Sepharose. **F)** The FT of a HiTrap Q contained DNA free H4. **G)** Size exclusion elution profile of octamers and H2A-H2B dimers. **H)** Purified octamers after gel filtration. **I)**

Example for a reconstitution of 187 bp long, off-centered nucleosomes by titrating increasing amounts of octamers to a constant amount of 187 bp long DNA.

Using this method, mono-nucleosomes with various length of linker DNA were reconstituted, namely core nucleosome with no linker DNA (147 bp), off-centered nucleosomes with 20 bp linker DNA (167 bp), off-centered nucleosomes with 40 bp linker DNA (187 bp), as well as centered nucleosomes with 20 bp linker DNA on each side (187 bp). Additionally, for remodeling assays by INO80 nucleosomes were assembled on 359 bp of the INO1 gene without the 601 positioning sequence.

## **5.2 *ISWI* chromatin remodeler**

### **5.2.1 Purification of *D.m.* ISWI-containing chromatin remodeler**

From fly ISWI remodeler family, I purified the core ATPase ISWI expressed in *E. coli*; the *D.m.* ACF complex, consisting of ISWI and Acf1 expressed in insect cell culture and the small histone fold like proteins *D.m.* CHRAC14 and CHRAC16 expressed in *E. coli* (domains and proteins length are depicted in Fig. 12).

The *D.m.* ISWI WT and Walker mutants were expressed recombinantly in *E. coli* and purified to near homogeneity following the purification protocol that is schematically represented (see Fig. 13). ISWI was purified with an N-terminal His<sub>6</sub>-tag, which can be cleaved off using TEV protease. In a first affinity purification step with Ni-NTA agarose, His<sub>6</sub>-ISWI was enriched and most bacterial contaminations were removed. After TEV protease cleavage, the uncleaved His<sub>6</sub>-ISWI was separated from cleaved ISWI using a second Ni-NTA step. In order to get rid of contaminating DNA, an anion exchange (MonoS) was performed. Finally, homogeneity was achieved by size exclusion chromatography in which ISWI elutes as a single peak with no or only minor aggregation. In addition to the WT, Walker A (K159R) and Walker B mutants (D256A, E257A) were purified. The yield of purified *D.m.* ISWI was ~ 3 mg per L cell culture. An ATPase assay (Henrike Klinker, Becker group, data not shown) proved that the protein was active.

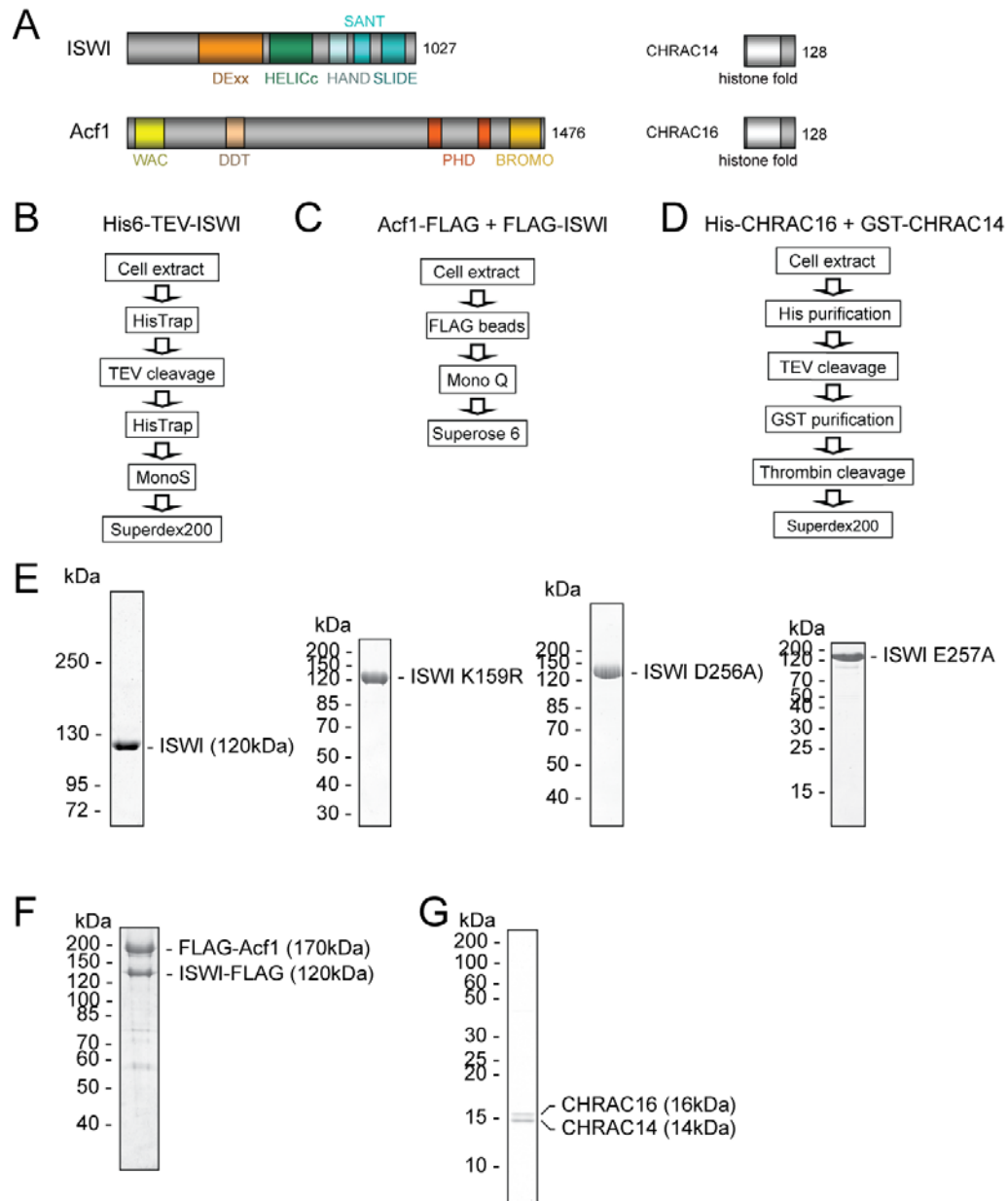


**Figure 12. Purification of *D.m.* ISWI-containing chromatin remodeler.** (A) Domain motifs in ISWI remodeler: ISWI contains an ATPase domain (orange DEXx box and green HELICc), a HAND domain (light blue), a SANT domain (turquoise) and a SLIDE domain (blue). Acf1 contains a WAC domain (WSTF/Acf1/cbp146, yellow), a DDT domain (DNA-binding homeobox-containing proteins in different transcription and chromatin remodeling factor, orange), two PHD domains (red) and a C-terminal bromodomain (orange). The two CHRAC proteins possess a histone-fold motif (Hartlepp et al., 2005). (B) The procedure for purification of His<sub>6</sub>-TEV-ISWI from *E. coli*. (C) Purification procedure for a FLAG-tagged ACF complex expressed in insect cells. (D) Purification procedure for the two CHRAC subunits GST-thrombin-CHRAC14 and His<sub>8</sub>-TEV-CHRAC16. (E-G). All components could be purified to near homogeneity. The final samples were analyzed by 15% SDS PAGE and Coomassie staining. (F) Purified WT and mutant ISWI (K159R, D256A, E257A). (F) The dimeric ACF complex composed of Acf1 and ISWI. (G) The two CHRAC proteins CHRAC14 and CHRAC16.

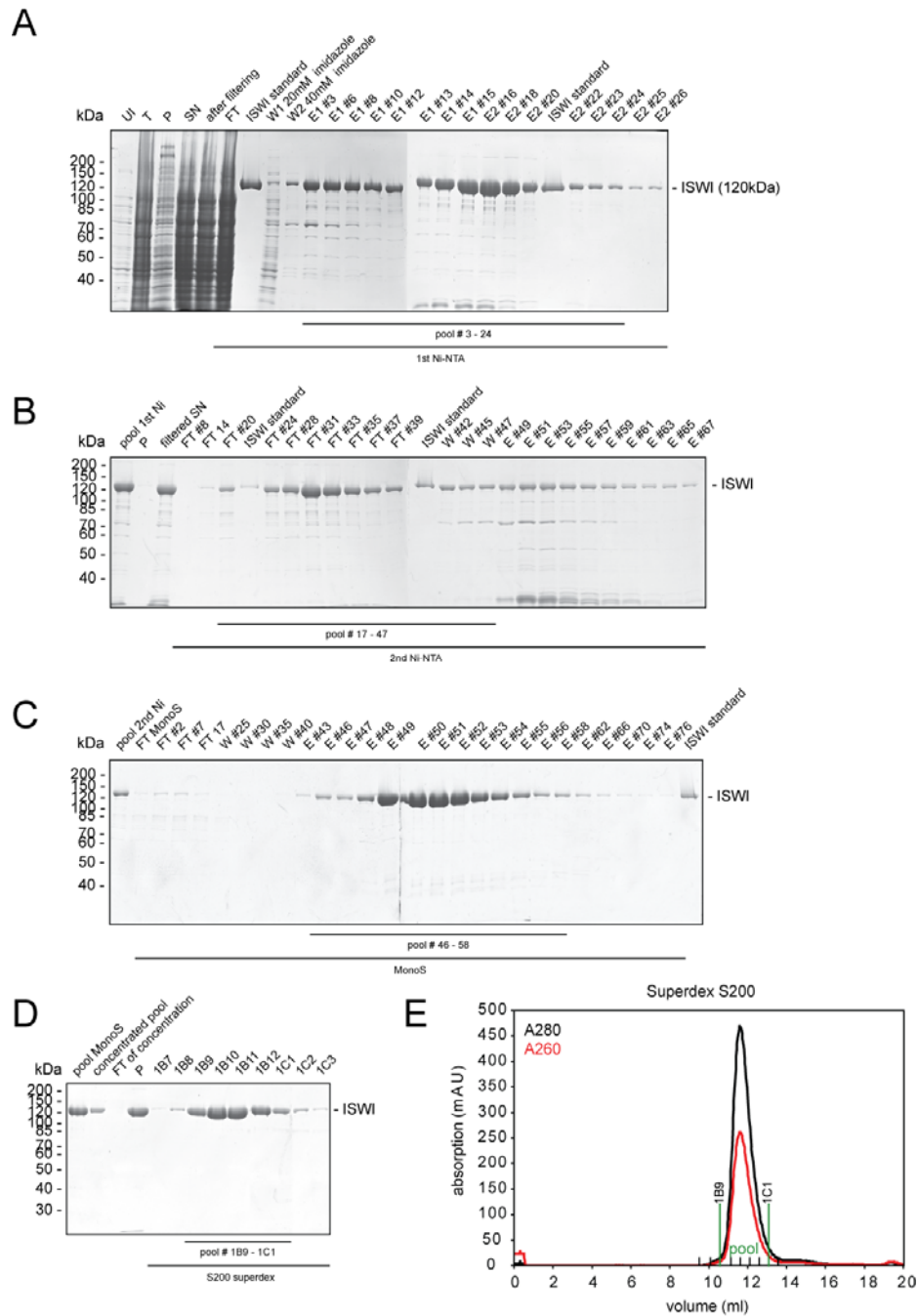


**Figure 13. Purification of *D.m.* ISWI from *E. coli*.** (A) - (D) The purification was monitored by 15% SDS PAGE stained with Coomassie. (A) Ni-affinity purification removed most bacterial contaminations. (B) A second Ni-affinity purification after TEV protease cleavage was used to remove uncleaved His<sub>6</sub>-ISWI. (C) The ion exchange using a MonoS mainly removed contaminating DNA. (D) A final size exclusion chromatography ensured homogeneity of the complex. (E) The chromatographic profile of the gel filtration shows that ISWI was homogenous.

The *D.m.* ACF complex - FLAG-ISWI and Acf1-FLAG - complex was expressed in Sf21 insect cells using the baculovirus system and purified using the mentioned purification procedure (see Fig. 14). After affinity purification via the FLAG tag on ISWI

and Acf1, the DNA was removed by anion exchange chromatography (MonoQ). Gel filtration was required to separate monodisperse ACF from higher oligomers. The yield of pure ACF was ~30 µg per L cell culture. The purified amount was enough for initial experiments; however aggregation problems limited the yield and the quality of the preparation. An ATPase assay (Henrike Klinker, Becker group, data not shown) proved that the protein complex was enzymatically active.

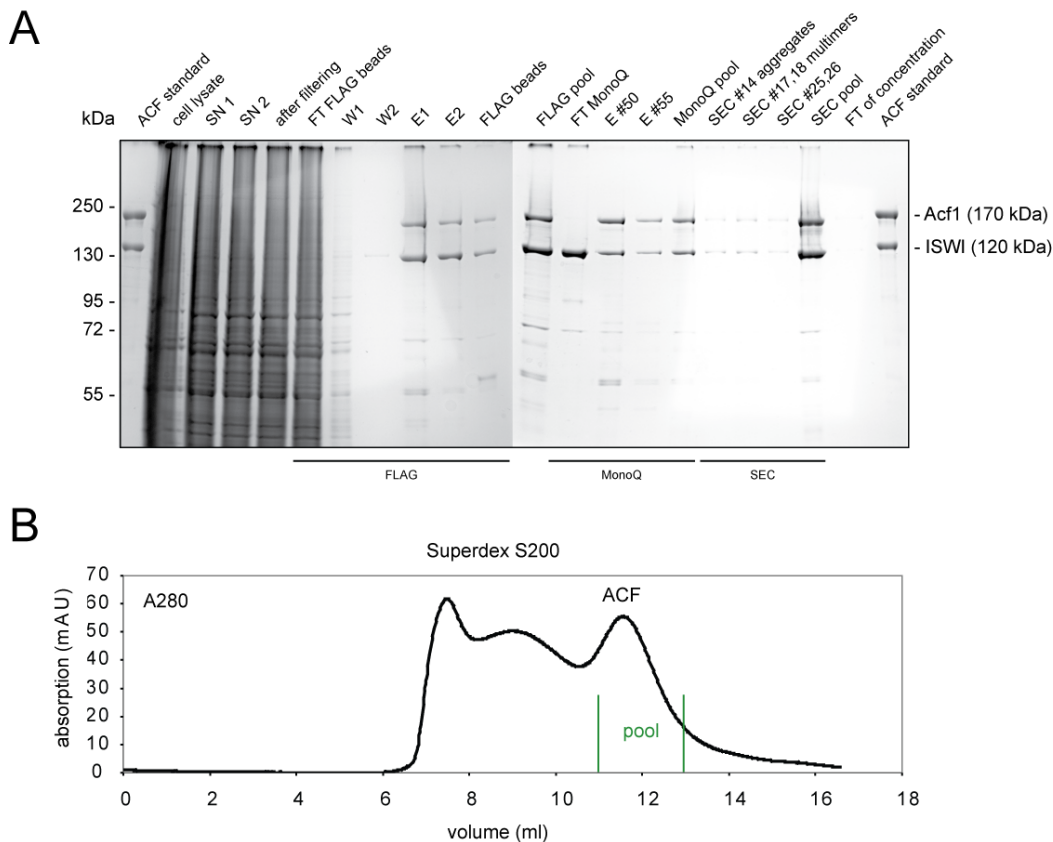


**Figure 14. Purification of *D.m.* dimeric ACF complex from insect cells. (A)** The process of purification was monitored with 8% SDS PAGE stained with Coomassie. **(B)** SEC profile from ACF purification.

CHRAC14 and CHRAC16, two histone fold subunits belonging to the *D.m.* CHRAC complex (ISWI, Acf1, CHRAC14, CHRAC16, see Fig. 15) were expressed recombinantly in *E. coli* as GST-Thrombin-CHRAC14 and His<sub>8</sub>-TEV-CHRAC16. The purification was performed with a tandem affinity purification procedure according to Hartlepp et al., 2005 with minor modifications (see methods section 7.2.4.3, Fig. 12D). Ni-NTA affinity purification was used to enrich the two CHRAC proteins. The His-tag from CHRAC16 was removed by TEV cleavage. For the second affinity purification step, the GST-tag of CHRAC14 was bound to GST sepharose and the complex was eluted by thrombin cleavage.

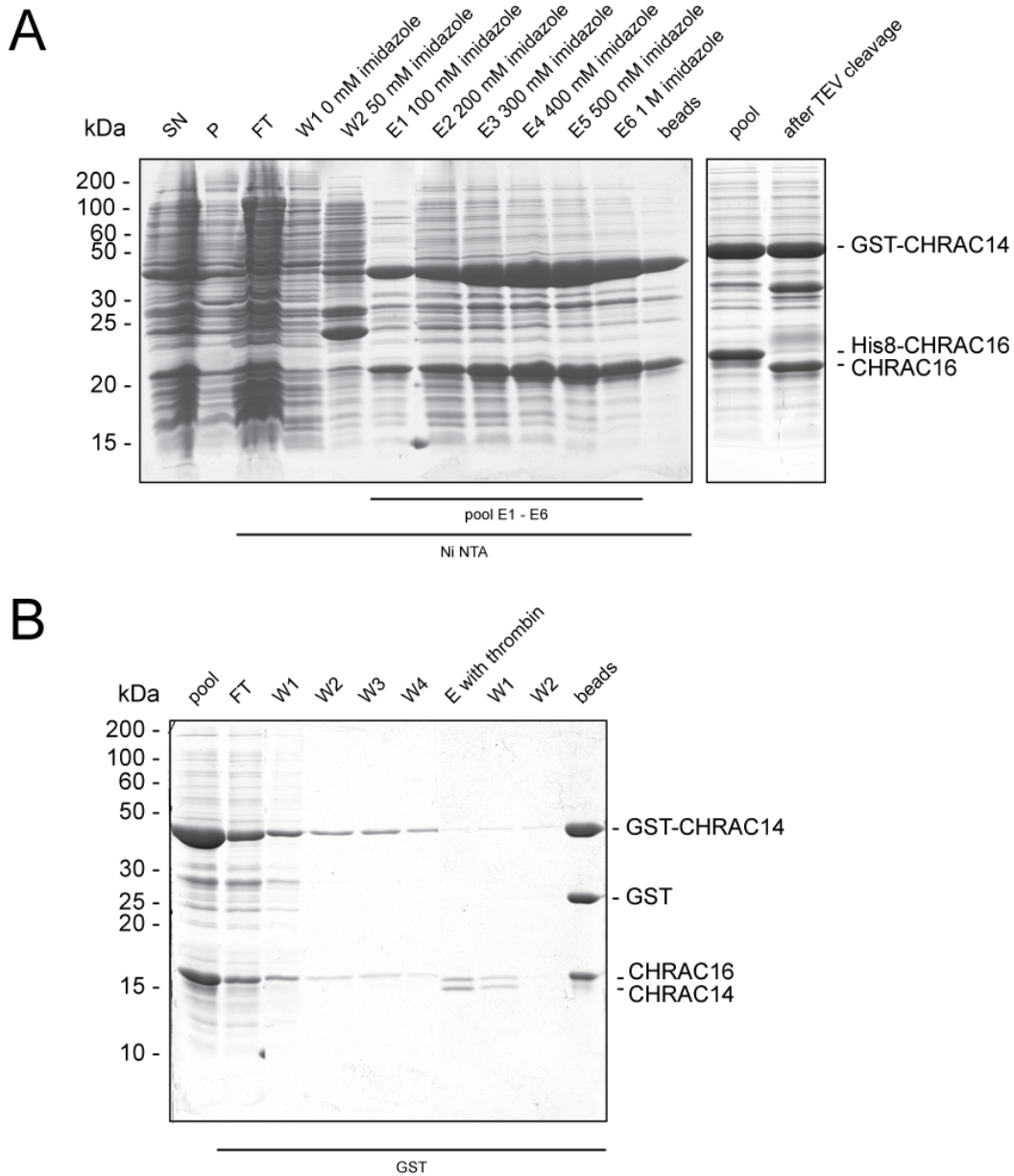


**Figure 15. Purification of *D.m.* CHRAC14/16 from *E. coli* by tandem affinity purification.** (A) Ni-NTA affinity purification followed by TEV cleavage resulted in purified GST-CHRAC16 and CHRAC14. The progress was monitored by 15% SDS PAGE stained with Coomassie. (B) After the second affinity purification with GST, the complex was cleaved off by thrombin and resulted in pure CHRAC14/16 complex. The purification was again monitored by 15% SDS PAGE and Coomassie staining.

## **5.2.2 Reconstitution of ISWI nucleosome- complexes**

### **5.2.2.1 Following complex formation using electrophoretic mobility shift assay**

Complex formation between ISWI family chromatin remodeler and their substrate were monitored using electrophoretic mobility shift assays (EMSA). After incubating the chromatin remodeler of the ISWI family with DNA or nucleosomes on ice or at room temperature, the sample was separated on a 4-5% native PAGE. Nucleosome-bound complexes migrated slower in the gel, while aggregates remained in the pockets.

Both ISWI and the ACF complex bound DNA, although with a weaker affinity compared to mono-nucleosomes (see Fig. 16). ISWI requires a certain length of linker DNA in order to bind to mono-nucleosomes (Brehm et al., 2000). Accordingly, 147 bp long core nucleosome as well as off-centered nucleosomes with 20 bp linker (167 bp) were bound with very low affinity by ISWI, while 187 bp long nucleosomes were bound by one or two ISWI molecules (see Fig. 16C). ISWI moves centered nucleosome to the end (Eberharter et al., 2001). Hence centered 187 bp long nucleosomes were preferred over 187 bp long off-centered nucleosomes. Thus, these 187 bp long centered mono-nucleosome with a 20 bp linker on both sides were used for subsequent experiments.

In the case of the ACF complex (ISWI, Acf1) the linker length was less critical: 147 bp long core nucleosomes were not shifted, but 20 bp linker were already sufficient for complex formation, although the 187 bp long nucleosomes seemed to be the preferred substrate (see Fig. 16D). 187 bp long, centered nucleosomes were bound by one or two ACF molecules, whilst the off-centered version apparently accommodated just one ACF molecule.

Upon titration of the remodeler, it became apparent that ISWI and ACF did not only form a stoichiometrical 1:1 complex with a nucleosome. The shifts indicated that one nucleosome was bound by one or up to three ISWI molecules (see Fig. 16E). In the case of ACF, one nucleosome was bound by one or two ACF molecules (see Fig. 16F). Aggregation was a joint aspect, which in the case of ISWI prevented a quantitative shift into distinct complexes.

The two histone fold subunits CHRAC14/16 seemed to enhanced binding of two remodeler to one nucleosome (see Fig. 16G).



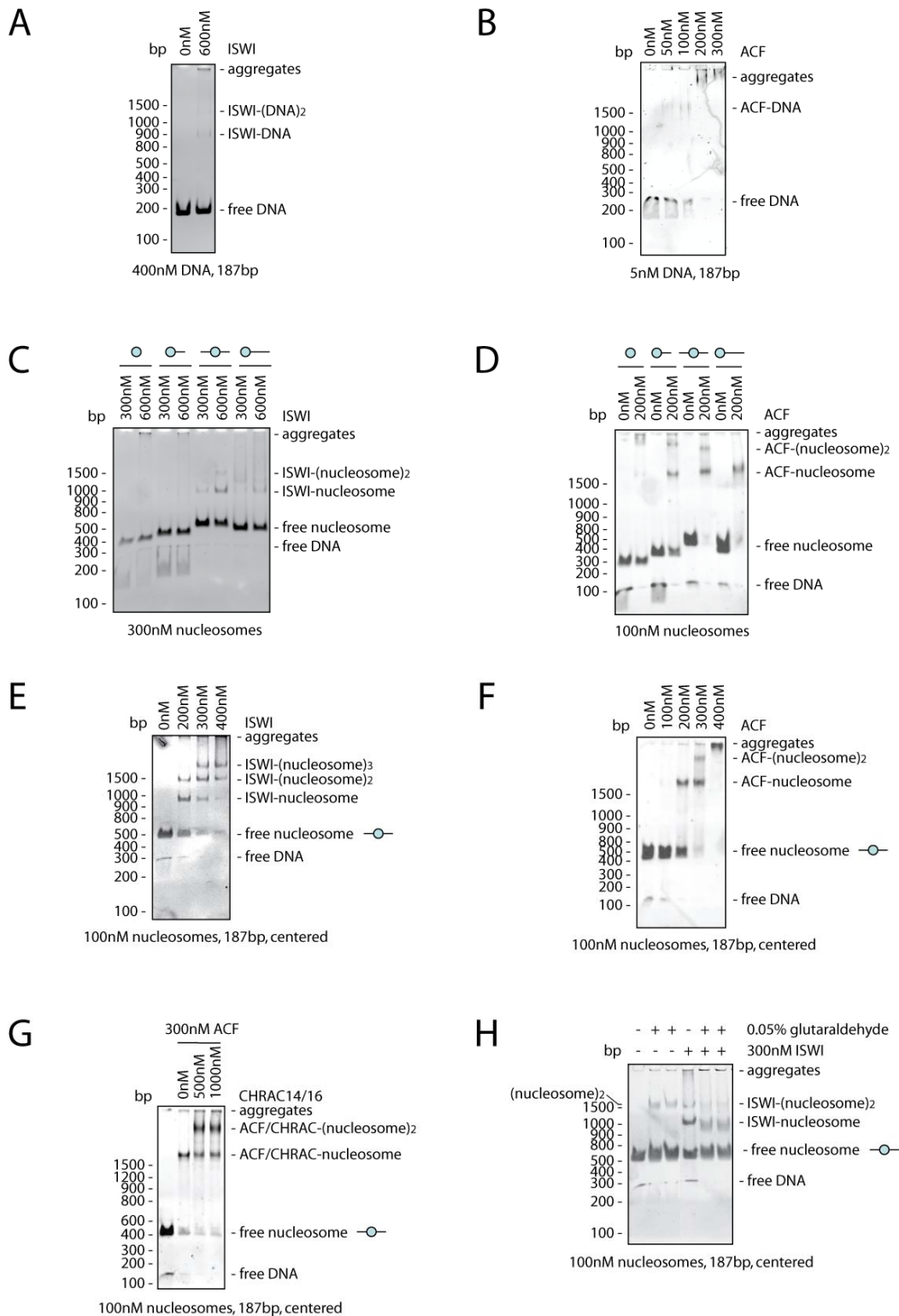


**Figure 16. Assessment of the affinity of ISWI-remodeler to the nucleosome by EMSA.** Increasing amounts of complexes were incubated with nucleosomes, separated by 5% native PAGE and stained with SybrGreenI. **(A)** ISWI and **(B)** ACF complex bound DNA. **(C)** ISWI interacted preferentially with 187 bp long, centered nucleosomes. **(D)** ACF complex bound 187 bp long nucleosomes with the highest affinities. **(E)** Titration of ISWI to 187 bp long, centered nucleosomes revealed the formation of dimeric and trimeric complexes. **(F)** Titration of ACF to 187 bp long, centered nucleosomes showed that ACF could interact

with nucleosomes as a monomer or dimer, but eventually started to aggregate with the substrate. **(G)** CHRAC14/16 increased formation of a dimeric complex. **(H)** Cross-linking with glutaraldehyde stabilized the complexes.

In order to stabilize the complexes of ISWI with the nucleosome, they were fixed using the cross-linker glutaraldehyde. The control reaction without ISWI however showed that nucleosomes cross-linked to themselves under those conditions (see Fig. 16H).

ISWI and ACF bound preferentially nucleosome with longer linker DNA and were able to multimerize as monomers and dimers, but also showed a high tendency to aggregate together with their substrates.

### 5.2.2.2 Measuring binding affinities in solution using MicroScale Thermophoresis

Unfortunately staining of nucleosomes with SybrGreenI proved to be non-linear (data not shown), thereby complicating the quantification of the shifts to calculate the half maximal effective concentration ( $EC_{50}$ ). For this reason, binding affinities were measured in solution under close to native conditions using the novel and powerful MicroScale Thermophoresis (MST, NanoTemper technology, (Dühr and Braun, 2006), see Fig. 17).

The NanoTemper Technology is based on Thermophoresis, an effect that leads to a diffusion of a molecule along a temperature gradient. This thermophoretic motion depends on the hydration shell of a molecule that changes upon binding of for example a ligand (see Fig. 17A). Through measuring the changes in thermophoresis by monitoring the fluorescence of a labeled binding partner with a Monolith NanoTemper, binding affinities could be determined.

For MST measurements, the DNA component was fluorescently labeled with Cy3. The concentration of the DNA or nucleosome was constant and increasing amounts of the remodeler were titrated to yield binding curves.

A Cy3 labeled 187 bp long double-stranded DNA was used to measure the binding affinity of ISWI to DNA. The half maximal effective concentration ( $EC_{50}$ ) of ISWI to DNA was 1101  $\pm$  124 nM (see Fig. 18A). MST confirmed the conclusion from the band shift assay: one molecule of DNA could accommodate two ISWI molecules (Hill-coefficient 2.08  $\pm$  0.42).

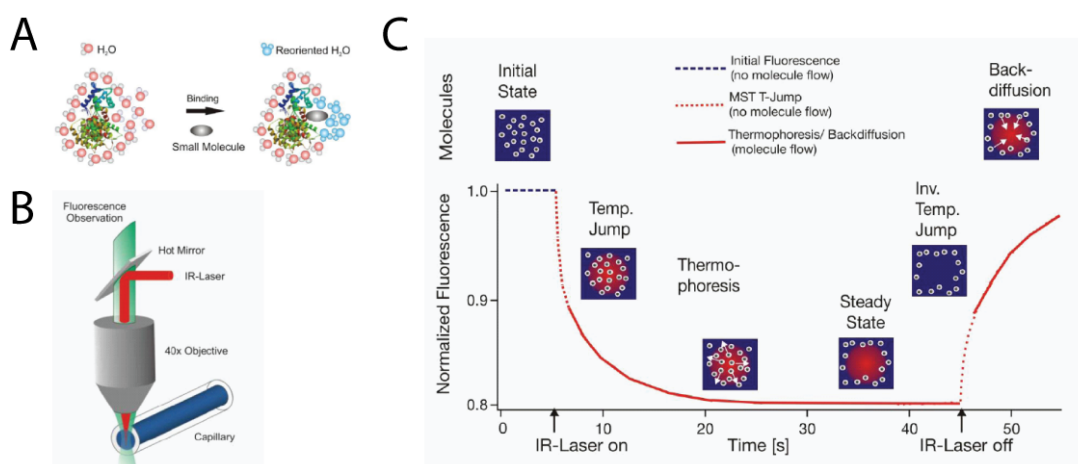


**Figure 17. MicroScale Thermophoresis (MST) measurement using the Monolith NanoTemper.** (A) The hydration shell of a molecule changes upon binding of a small molecule and thereby influences the thermophoretic behavior of the particle. (B) The setup of the NanoTemper includes an IR laser for local heating of the sample in the capillary. Simultaneously, the fluorescently labeled sample is observed and changes in the intensity due to the movement of the molecules are recorded. (C) Switching the IR laser leads to a diffusion of the molecules along the established temperature gradient until a steady state level is reached. After turning the laser off an inverse fast temperature jump can be observed and the molecules diffuse back.

Furthermore, ISWI WT had a higher affinity towards centered mono-nucleosomes (187 bp = 20N20) compared to naked DNA (see Fig 18A):  $EC_{50}$  (ISWI WT, DNA) = 1101  $\pm$  124 nM compared to  $EC_{50}$  (ISWI WT, nucleosome) = 598  $\pm$  29 nM, verifying the results from EMSA.

#### 5.2.2.2.1 A pre-transition state analog increased the affinity of ISWI to nucleosomes

The next step was to analyze the effect of ATP and ADP on the affinity of ISWI towards the nucleosomal substrate. The addition of ATP should trigger ATP hydrolysis and thus lead to remodeling of the centered nucleosome resulting in an off-centered nucleosome. During the course of remodeling, ISWI remodeler are expected to engage the nucleosome and dissociate again after remodeling. Indeed, the affinity of ISWI wild type towards a centered mono-nucleosome drastically decreases in the presence of ATP: from an  $EC_{50}$ (ISWI WT, no nucleotide, nucleosome) = 598  $\pm$  29nM to  $EC_{50}$ (ISWI WT, ATP, nucleosome) = 5249  $\pm$  2161nM (see Fig. 18B). The addition of ADP leads to a slight drop in affinity from  $EC_{50}$ (ISWI WT, no nucleotide, nucleosome) = 598  $\pm$  29 nM to  $EC_{50}$ (ISWI WT, ADP, nucleosome) = 953  $\pm$  8 nM (see Fig 18B). This was anticipated,

as ADP mimics the “post-state” were the affinity of ISWI to the nucleosome has to be reduced in order to dissociate from the remodeled substrate.

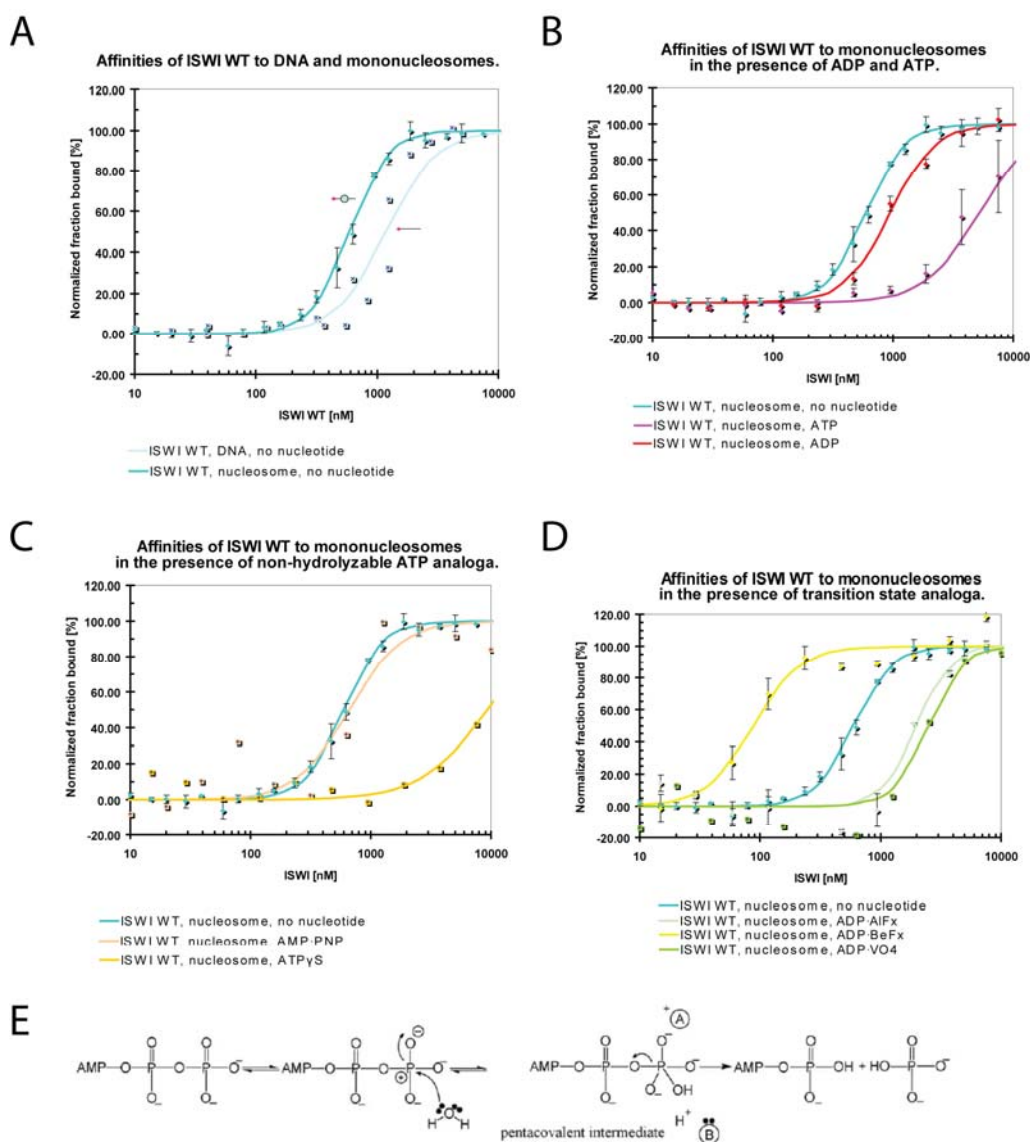


**Figure 18. Binding affinities of ISWI to mono-nucleosomes were measured by MST in the presence of various ATP analogs. (A)** ISWI WT had a higher affinity to mono-nucleosomes compared to naked DNA. **(B)** The addition of ADP or ATP reduced the affinity of ISWI towards a nucleosome. **(C)** AMP-PNP had similar affinity as the apo state and was probably not hydrolyzed. In the presence of ATP $\gamma$ -S, the affinity dropped drastically to level of ATP and could thus probably be hydrolyzed. **(D)** The pre-transition state analog (ADP·BeF<sub>x</sub>) led to a higher affinity compared to post-transition state analog (ADP·AlF<sub>x</sub>, ADP·VO<sub>4</sub>). **(E)** During ATP hydrolysis, a pentacovalent intermediate is formed, which can be mimicked by the pre- and post-transition state analogs. See also Table 1.

Non-hydrolyzable ATP analogs were also tested (see Fig. 18C). The addition of ATP $\gamma$ -S reduced the affinity of ISWI to a mono-nucleosome to  $EC_{50}$ (ISWI WT, ATP $\gamma$ -S, nucleosome) = 9323 nM, which was in the range of the affinity in the presence of ATP. Thus it could be concluded that ATP $\gamma$ -S was hydrolyzed by ISWI and not suitable to

mimic an ATP bound state. The addition AMP·PNP on the other hand did not change the binding affinity of ISWI to the nucleosome ( $EC_{50}(\text{ISWI WT, AMP·PNP, nucleosome}) = 661 \text{ nM}$ ). This phenomenon can be explained by two possibilities: AMP·PNP was bound and contrary to ATP $\gamma$ -S could be hydrolyzed and thus mimics a true ATP bound, activated state. Another explanation could be that ATP $\gamma$ -S was not binding to ISWI.

During ATP hydrolysis, the ATP is attacked by a water molecule and a penta-covalent intermediate is formed (see Fig. 18E). ADP·BeF<sub>x</sub> (most likely ADP·BeF<sub>3</sub>) mimics the pre-transition state with the water molecule ready to attack the  $\gamma$ -phosphate. ADP·AlF<sub>x</sub> (most likely ADP·AlF<sub>4</sub>) and ADP·VO<sub>4</sub> on the other hand are post-transition state analogs, mimicking the state during hydrolysis, where the ATP has already been hydrolyzed, but the inorganic phosphate is not yet released from the active center. Compared to the apo state, the addition of the pre-transition state analog ADP·BeF<sub>x</sub> led to an increase in the affinity ( $EC_{50}(\text{ISWI WT, ADP·BeF}_x, \text{nucleosome}) = 88 \pm 12 \text{ nM}$ , see Fig. 18D). This seems reasonable, given that the pre-transition state has to have the highest affinity in order not to “loose” the substrate during the course of remodeling. ISWI in presence of the two post-state analogs, ADP·AlF<sub>x</sub> and ADP·VO<sub>4</sub> (see Fig. 18D) on the other hand showed a decreased affinity towards a nucleosome compared to the apo state. This can be reasoned with the fact, that after ATP hydrolysis, the duty of remodeling by the enzyme has been fulfilled and the substrate is ready to be released again. Compared to the affinity in the presence of ATP, the addition of post-transition state analogs led to a decrease in affinity, which could be due to the fact, that the inorganic phosphate mimetics could be released.

**Table 1. MST binding affinities of ISWI WT with DNA or mono-nucleosomes, in presence or absence of ATP or ATP analogs.**

remodeler	substrate	nucleotide	EC50 [nM]	Hill coefficient [n]
ISWI WT	DNA	no nucleotide	1191 ± 124	2.08 ± 0.42
ISWI WT	nucleosome	no nucleotide	598 ± 29	2.71 ± 0.19
ISWI WT	nucleosome	ATP	5249 ± 2181	1.91 ± 0.67
ISWI WT	nucleosome	ADP	953 ± 8	2.35 ± 0.10
ISWI WT	nucleosome	AMP·PNP	661.00	2.00
ISWI WT	nucleosome	ATP $\gamma$ S	9323.00	1.57
ISWI WT	nucleosome	ADP·BeF <sub>x</sub>	88 ± 12	2.21 ± 0.14
ISWI WT	nucleosome	ADP·AlF <sub>x</sub>	1981 ± 127	3.12 ± 0.11
ISWI WT	nucleosome	ADP·VO <sub>4</sub>	2501.00	3.00

In summary, ISWI had a higher affinity towards its nucleosomal substrate in presence of the pre-transition state analog ADP·BeF<sub>x</sub>.

#### **5.2.2.2.2 Influence of Walker mutants on the binding affinity to nucleosomes**

ISWI belongs to the DEXX box subgroup of the Snf2 ATPases family of helicases. The conserved Walker A motif (also called P or phosphate loop) bind to the  $\alpha$ - and  $\beta$ -phosphates and is therefore responsible for ATP coordination (see Fig. 18E). The Walker B motif or DEAH box coordinates the magnesium ion, which activates the attacking water molecule by polarization and thereby accounts for ATP hydrolysis.

In order to analyze the binding behavior not only in the presence of ATP analogs, I also introduced mutations in the Walker motif, in order to abolish ATP binding or ATP hydrolysis.

To eliminate ATP binding, the lysine (K) in the Walker A motif (GKT/S) was mutated to alanine (ISWI K159R) (see Fig. 19A). The binding affinity of ISWI K159R ( $EC_{50}$ (ISWI K159R, no nucleotide, nucleosome) = 1003  $\pm$  173 nM) to a mono-nucleosome was reduced compared to the wild type ISWI ( $EC_{50}$ (ISWI WT, no nucleotide, nucleosome) = 598  $\pm$  29 nM). This shift was in the same range as the addition of ADP ( $EC_{50}$ (ISWI WT, ADP, nucleosome) = 953  $\pm$  8 nM). While the binding affinity of ISWI WT drastically dropped in the presence of ATP ( $EC_{50}$ (ISWI WT, ATP, nucleosome) = 5249  $\pm$  2161 nM), the ATP binding deficient mutant ISWI K159R did not respond significantly to the addition of ATP as expected ( $EC_{50}$ (ISWI K159R, ATP, nucleosome) = 1250  $\pm$  119 nM). The catalytically inactive K159R mutation, a dominant negative null mutant *in vivo* (Corona et al., 1999; Deuring et al., 2000), has lost its ability to bind ATP.

Mutations in the Walker B motif do not abolish ATP binding, but prohibit ATP hydrolysis. Two different mutations were analyzed: the aspartic acid (D) or the glutamic acid (E) in the DEAH box of the Walker B motif was mutated to alanine (ISWI D256A, ISWI E257A).

The affinity of ISWI D256A ( $EC_{50}$ (ISWI D256A, no nucleotide, nucleosome) = 660 nM) to a nucleosome was similar to the wild type ISWI ( $EC_{50}$ (ISWI WT, no nucleotide, nucleosome) = 598  $\pm$  29 nM) (see Fig 19C). Upon the addition of ATP, the ISWI D256A ( $EC_{50}$ (ISWI D256A, ATP, nucleosome) = 1520 nM) showed a reduced affinity towards a nucleosome compared to the NTP free state. This effect, however was not as drastic as it was observed for the wild type ISWI ( $EC_{50}$ (ISWI WT, ATP,

nucleosome) = 5249 +/- 2161 nM). ISWI D256A was therefore probably still capable to partially hydrolyze ATP.

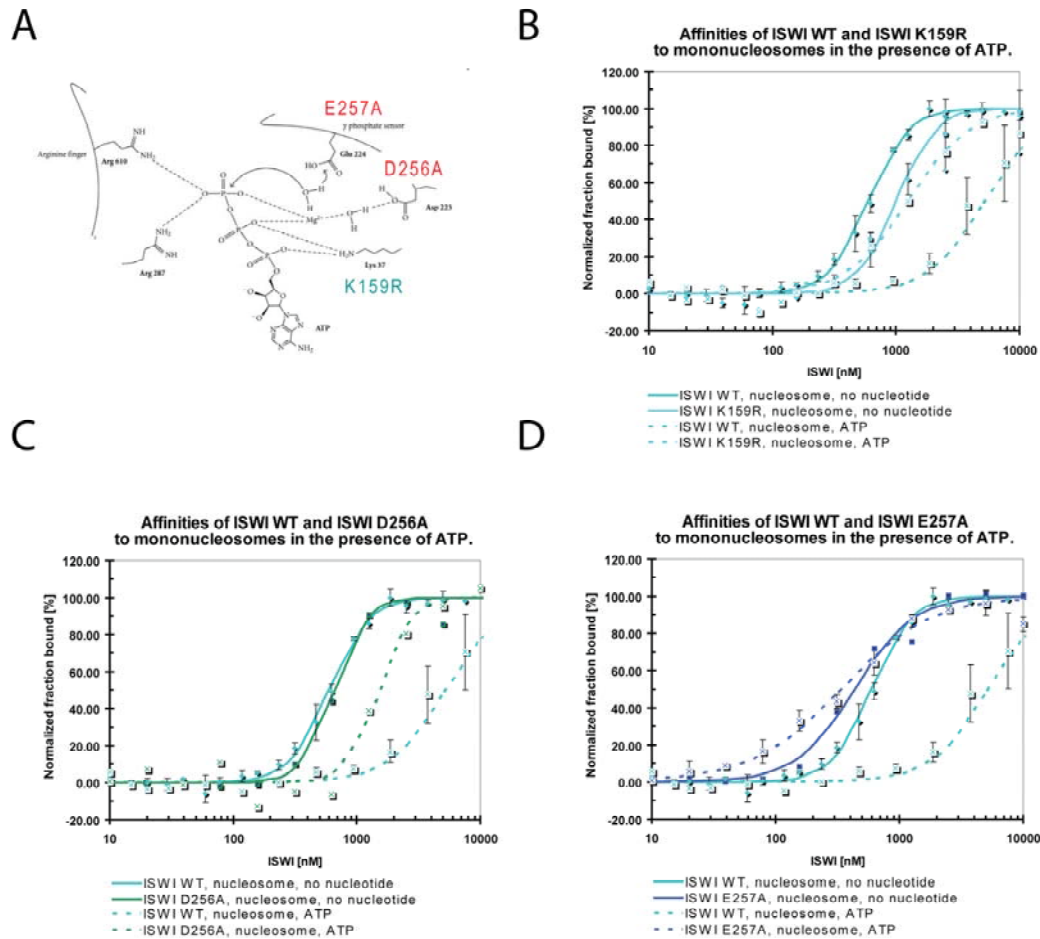


**Figure 19. Binding affinities of ISWI and Walker A and Walker B mutants to mono-nucleosomes were measured by MST without NTP or in the presence of ATP. (A)** Walker A and Walker B mutants and their role in ATP hydrolysis. **(B)** The Walker A mutant ISWI K159R cannot bind ATP and thus affinities did not change upon addition of ATP. **(C)** The Walker B mutant ISWI D256A apparently partially hydrolyzed ATP, since the affinity decreased in response to ATP, but to a lesser extent compared to ISWI WT in presence of ATP. **(D)** The ISWI Walker B mutant E257A was unable to hydrolyze ATP and showed slightly increased affinities compared to ISWI WT. See also Table 2.

The second Walker B mutant ISWI E257A ( $EC_{50}$ (ISWI E257A, no nucleotide, nucleosome) = 433 nM) had a marginally higher affinity towards the mono-nucleosome compared to wild type ISWI ( $EC_{50}$ (ISWI WT, no nucleotide, nucleosome) = 598 +/- 29 nM) (see Fig. 19D). In this case, the presence of ATP had no significant effect on the binding behavior of ISWI E257A. This indicated, that ISWI E257A ( $EC_{50}$ (ISWI E257A, ATP, nucleosome) = 340 +/- 66 nM) is truly impaired in ATP hydrolysis.



**Table 2. Monolith NanoTemper binding affinities.**

remodeler	substrate	nucleotide	EC50 [nM]	Hill coefficient [n]
ISWI WT	DNA	no nucleotide	1191 ± 124	2.08 ± 0.42
ISWI WT	nucleosome	no nucleotide	598 ± 29	2.71 ± 0.19
ISWI WT	nucleosome	ATP	5249 ± 2181	1.91 ± 0.67
ISWI WT	nucleosome	ADP	953 ± 8	2.35 ± 0.10
ISWI WT	nucleosome	AMP·PNP	661.00	2.00
ISWI WT	nucleosome	ATP <sub>γ</sub> S	9323.00	1.57
ISWI WT	nucleosome	ADP·BeF <sub>x</sub>	88 ± 12	2.21 ± 0.14
ISWI WT	nucleosome	ADP·AlF <sub>x</sub>	1981 ± 127	3.12 ± 0.11
ISWI WT	nucleosome	ADP·VO <sub>4</sub>	2501.00	3.00
ISWI K159R	nucleosome	no nucleotide	1003 ± 173	2.80 ± 0.15
ISWI K159R	nucleosome	ATP	1250 ± 119	1.78 ± 0.14
ISWI D256A	nucleosome	no nucleotide	660.00	3.28
ISWI D256A	nucleosome	ATP	1520.00	3.35
ISWI E257A	nucleosome	no nucleotide	433.00	1.84
ISWI E257A	nucleosome	ATP	340 ± 66	1.20 ± 0.11

In summary, the Walker A mutation in ISWI led to a decreased affinity to nucleosomes, and could not bind ATP. Walker B mutant D256A bound nucleosomes equally effective as the WT, however ATP was still partially hydrolyzed. The Walker B mutant E257A showed a slight increase in affinity to nucleosomes, and was not capable of ATP hydrolysis.

### ***5.2.2.2.3 Indication for cooperate binding of an ISWI dimer to the nucleosome***

The affinity of ISWI WT to the nucleosome showed a Hill coefficient above 1 (2.71 ± 0.19), indicating a positive cooperativity of probably two ISWI molecules that bind to the nucleosome. This is in agreement with a recent study from the Narlikar lab (Racki et al., 2009). According to this study, the human homolog of ISWI, SNF2h acts as a dimeric motor on the nucleosome. The authors present a low resolution negative stain structure, which shows two SNF2h molecules binding on opposing sites on a mono-nucleosome in an activated ATP state with ADP·BeF<sub>x</sub> (see Fig. 18D).

The method for the determination of binding affinities by MicroScale Thermophoresis is a powerful novel technique. The obtained results are consistent with the data obtain from the human homolog SNF2h (Racki et al., 2009). According to a fluorescence binding assay in this study SNF2h had a K<sub>1/2</sub> of 633 ± 48 nM and a Hill coefficient of 1.8 ± 0.12 (Racki et al., 2009), compared to ISWI EC<sub>50</sub>= 598 ± 29 nM



and a Hill coefficient =  $2.71 \pm 0.19$  (this study). In the presence of ADP the  $K_{1/2}$  drops to  $971 \pm 90$  nM in the case of SNF2h (Racki et al., 2009), compared to the  $EC_{50} = 953 \pm 8$  nM of ISWI (this study). The pre-transition state analog  $ADP \cdot BeF_x$ , which was also used for determining the structure, resulted in a  $K_{1/2}$  of SNF2h of  $262 \pm 14$  nM. The effect I observed for ISWI was even more drastic, the  $EC_{50}$  went down to  $88 \pm 12$  nM in the presence of  $ADP \cdot BeF_x$ .

#### ***5.2.2.2.4 Low in solution affinities prevent EM analysis***

The binding affinity of ISWI WT to a nucleosome ( $EC_{50}$ (ISWI, no nucleotide, nucleosome =  $598 \pm 29$  nM) was significantly lower than the results obtained from gel shift experiments indicate (see Fig. 16, 18). According to the EMSA results, about 50% of the nucleosomes were already shifted at an ISWI concentration of  $\sim 200$  nM. On the other hand the in solution thermophoretic experiment indicated that 50% of the nucleosomes should be shifted at a significantly higher concentration of 600 nM. Furthermore, samples that according to the EMSA result should contain approximately 50% ISWI-nucleosome complexes hardly showed any complex formation when analyzed via negative staining (see Fig. 20A-B).

Therefore, approximate  $EC_{50}$  values estimated from EMSA were compared with results from MST (see Fig. 20C). This experiment illustrated, that in the EMSA complex formation and aggregation started at lower concentrations compared to the thermophoretic in solution measurements (red crosses). The “caging effect” of the dense polyacrylamide gel matrix can stabilize complexes, but also the low ionic strength of the running buffer or the increase in local concentration, when the gel is started could account for this effect. Thus the affinities were overestimated in gel by EMSA compared to in solution measurements by MST, which gave a more native like picture.

Unfortunately, the affinity of ISWI towards a mono-nucleosome is too low to directly analyze the complexes using electron microscopy. At a concentration of  $\sim 600$  nM ISWI, only 50% of the nucleosomes would be shifted. The grid on the other hand was already overcrowded at concentrations  $> 200$  nM ISWI, making it impossible to distinguish single particles. At 200 nM ISWI, however hardly any ISWI –nucleosome complexes should be formed (see Fig. 20C), which was indeed confirmed by negative stained images (see Fig. 20B).

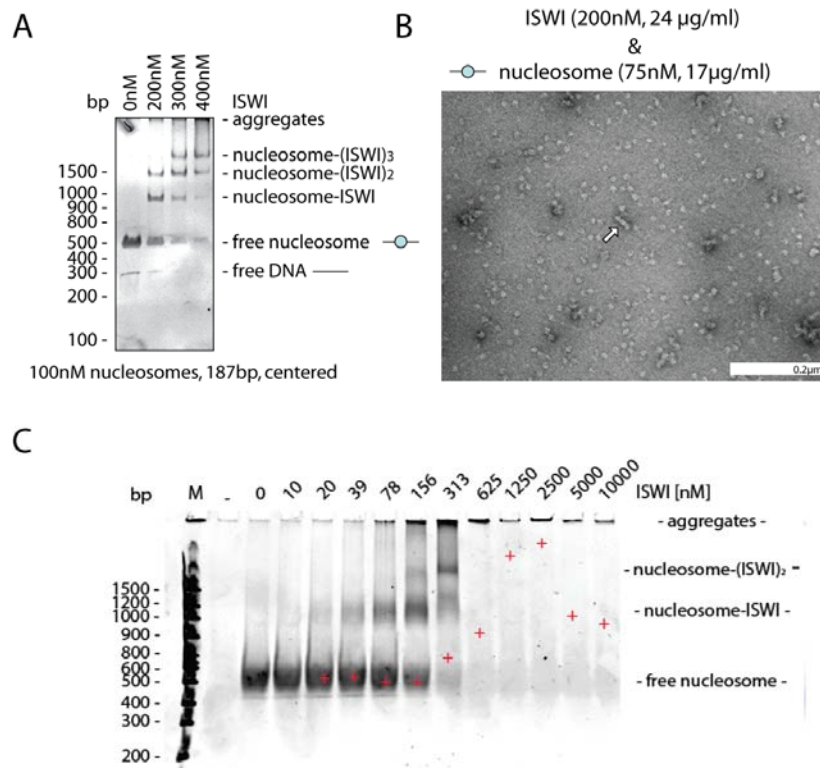


**Figure 20. Gel shift assays led to an overestimation of complex formation compared to in solution measurements.** (A) According to the EMSA results ~50% of the nucleosomes were shifted at approximately 200 nM ISWI. (B) Micrographs of negatively stained “ISWI-nucleosome complexes” did not contain 50% complexes as indicated by the EMSA results. (C) The comparison of EMSA and MST results (red crosses) showed that in solution complex were formed at significantly higher concentrations of ISWI as indicated by the gel shift experiment.

To overcome the problem of overcrowding and the concomitant underrepresentation of complexes due to the low binding affinity ( $EC_{50}(\text{ISWI WT, no nucleotide, nucleosome}) = 598 \pm 29 \text{ nM}$ ), I tested, whether the presence of nucleotide and ATP analogs improved the affinity of ISWI towards mono-nucleosome. Most of the tested nucleotides, such as ATP, ADP, non-hydrolyzable ATP analogs (AMP·PNP, ADP· $\gamma$ S), as well as the post-transition state analogs (ADP·AlF<sub>x</sub>, ADP·VO<sub>4</sub>) had either no effect on the affinity or a negative impact. The pre-transition state analog ADP·BeF<sub>x</sub> was the only one which showed a decreased half maximal effective concentration of  $88 \pm 12 \text{ nM}$ . This would be suitable for further analysis via electron microscopy. Another promising candidate is the Walker B mutant ISWI E257A in the presence of ATP with an  $EC_{50}$  of  $340 \pm 66 \text{ nM}$ . This mutant is able to bind ATP, however hydrolysis is impaired. The ISWI E257A mutant thus mimics an activated ATP bound state, similar to the state

induced by the pre-transition state analog ADP·BeF<sub>x</sub>. This analog was used for structure determination of the human ISWI homolog SNF2H (Racki et al., 2009).

### 5.2.2.3 Negative staining of ISWI-nucleosome complexes

For electron microscopy, the samples are deposited onto a glow-discharged carbon-coated copper grid and stained with 2% uranyl acetate (UA) (see Fig. 21A). To improve the data quality, different types of heavy metal with various pH values have been tested, as well as a method that inverts the charge of the grid. For both remodeler and nucleosomes, conventional glow-discharging (negative air plasma) and the use of 2% uranyl acetate proved to be most suitable. While ISWI can be stained efficiently, ACF tended to aggregate on the grid (see Fig. 21A). Free nucleosomes had a preferred orientation on the grid that impedes a proper three-dimensional reconstruction.

Three software packages EMAN2, Sparx and IMAGIC (Frank et al., 1996; Tang et al., 2007; van Heel et al., 1996) were used to process nucleosomes (see Fig. 21B-C). They all use the common line algorithm to calculate initial models. However, the workflow for all three packages was ceased after alignment given the preferred orientation of the nucleosomes on the grid. Alignment results revealed huge differences in the software in handling the round nucleosomes (see Fig. 21C). EMAN2 reference-free class averages show nearly no details, whereas K-means class averages of Sparx tempted into speculating about DNA turns. IMAGIC applies multi-statistical analysis (MSA) with Eigen Images and multi-reference alignment (MRA), thereby allowing a more detailed analysis of the class averages and their quality.

Given that the binding affinity of ISWI towards the nucleosome was too low for direct analysis on the grid, I studied ISWI-nucleosome complexes with increased half maximal effective concentrations. In the presence of ADP·BeF<sub>x</sub> the affinity was high enough for direct observation of complexes on the grid. However, the distribution and staining of the particles was dreadful (data not shown), and the data could not be processed further. Similarly, the use of ISWI E257A mutant with the addition of ATP increases the affinity; however the particles on the grid are not suitable for single particle analysis.

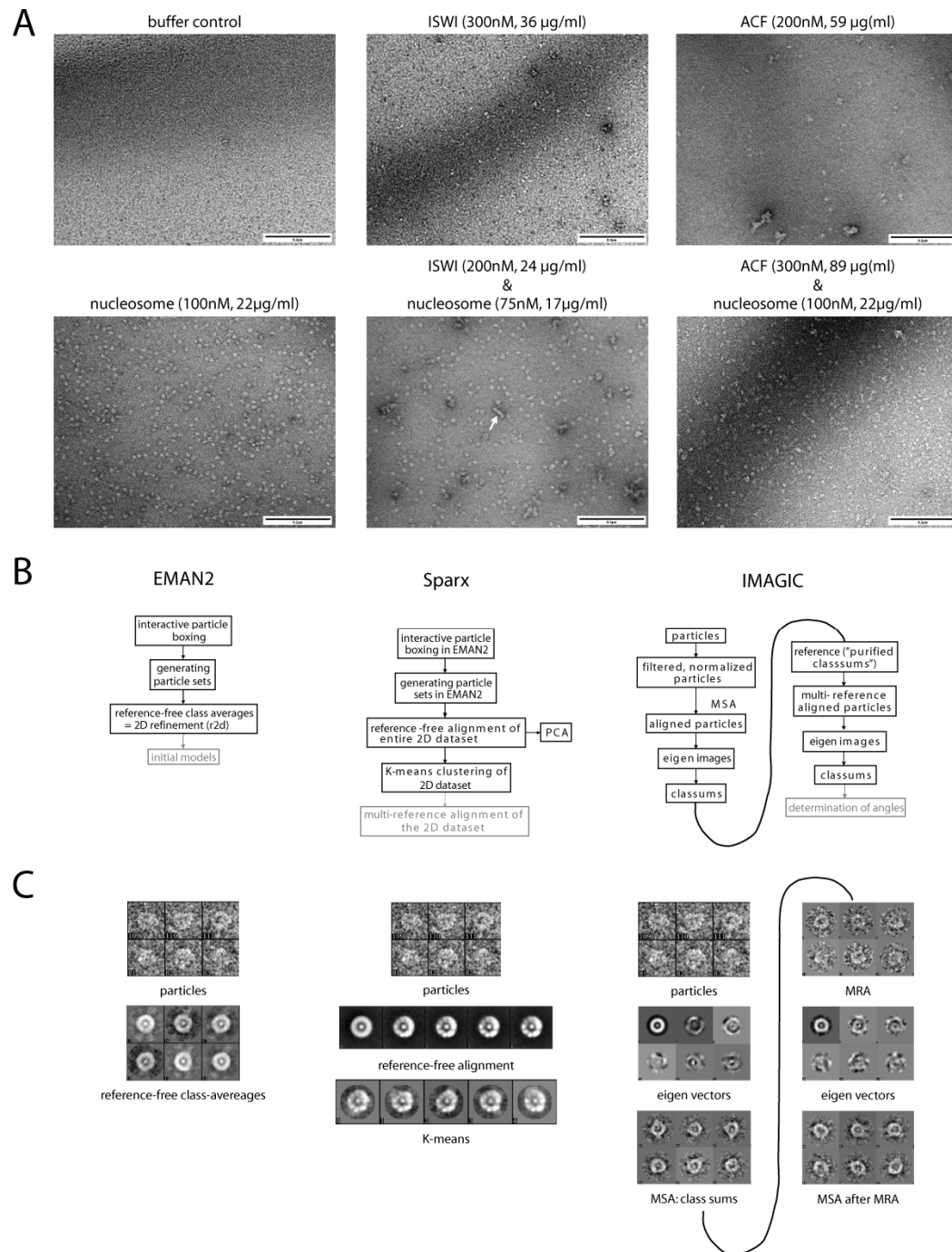


**Figure 21. Electron microscopy of ISWI remodeler and nucleosomes. (A)** Negative stain images with 2% UA at 110 kx magnification (scale bar 0.2µm). **(B)** Work flow of processing packages EMAN2, Sparx and IMAGIC **(C)** Images of pre-processing of mono-nucleosomes revealed a preference for top views.

Recently, a negative stain structure of the human ISWI homolog SNF2h was published (Racki et al., 2009). The resolution of this structure, which shows two SNF2h molecules binding to one nucleosome in an activated ATP state ( $\text{ADP} \cdot \text{BeF}_x$ ), is limited and thus the authors could not deduce any mechanistic detail of the structural basis of

chromatin remodeling. In order to improve not only the binding affinity, but to also improve the data quality, the ISWI-nucleosome complexes have to be purified further in order to get rid of aggregation contamination and to separate ISWI-nucleosome from ISWI<sub>2</sub>-nucleosome complexes. Reduction of the heterogeneity of the sample would result in an increased resolution and thus enable the visualization of the interaction in greater detail.

## 5.2.3 Purification of the nucleosome-ISWI complex

### 5.2.3.1 GraFix

One of the major problems was the heterogeneity of the sample preparation. A homogenous sample may help to increase the resolution of the EM reconstruction publishes on ISWI so far (Racki et al., 2009). The ISWI-nucleosome sample contained free nucleosomes, several remodeler-nucleosome complexes as well as free remodeler and aggregates. The data quality of the ISWI-nucleosome complexes was not therefore suitable for further analysis by electron microscopy and single particle analysis.

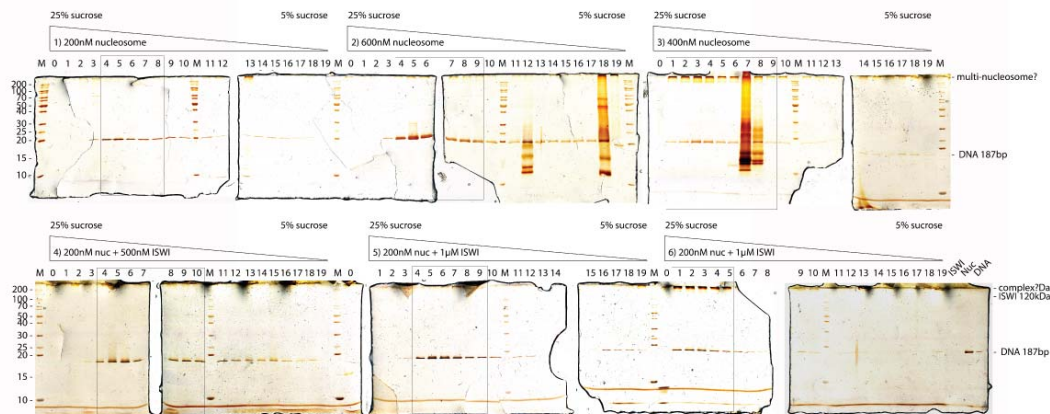


**Figure 22. Separation of nucleosomes, nucleosome-ISWI complexes with GraFix revealed aggregation problem.** Nucleosomes alone were run in sucrose gradients without glutaraldehyde. Cross-linking with glutaraldehyde however induced aggregation. Adding increasing amounts of ISWI induced aggregation, which was further enhanced upon cross-linking.

Simple cross-linking was no option given the unspecific cross-linking between two nucleosomes (see Fig. 22). One alternative could be GraFix (Gradient and fixation) (Kastner et al., 2008). According to this method, the sample is centrifuged through a sucrose or glycerol gradient with increasing concentration of a cross-linker. Simultaneous

cross-linking and centrifugation prevents non-specific cross-links as well as the formation of aggregates. Furthermore, GraFix has been shown to improve the quality of samples.

Unfortunately, upon adding glutaraldehyde to a sucrose gradient led to aggregation of ISWI-nucleosome complexes (see Fig. 22). GraFix was therefore not suitable to separate the various complex species from each other.

### 5.2.3.2 Size exclusion chromatography

Another method to increase homogeneity is size exclusion chromatography. ISWI and nucleosomes can be separated by size exclusion chromatography (see Fig. 23A).

Mixing of ISWI and nucleosome led to aggregation (see Fig. 23B), and only free excess ISWI eluted from the column and was detected in a silver-stained SDS PAGE. Different buffer conditions, the addition of ATP or the use of Walker mutants did not change this behavior. The complex between remodeler and nucleosome was not stable enough for gel filtration and was thus not applicable for further purification.

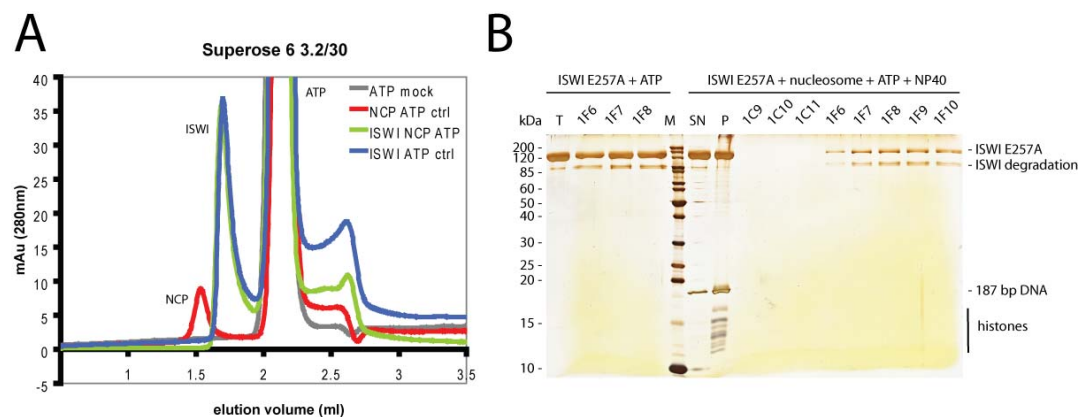


**Figure 23. Size exclusion chromatography of ISWI –nucleosome complexes.** **A)** ISWI (blue) and nucleosomes (red) eluted at different volumes of a Superose 6 3.2/30 column. **B)** Silver-stained 15% SDS PAGE of samples after the gel filtration revealed that ISWI remodeler and the substrate aggregated (pellet P), and only ISWI can be detected after gel filtration on a silver stained SDS-PAGE.

As the affinity of ISWI to nucleosomes was not high enough for EM purposes and the complex could not be purified further, the project was ended at this stage. ADP·BeF<sub>x</sub> improved complex formation at concentrations that can be used for EM, however a structure of the human ISWI homolog was published applying these conditions (Racki et al., 2009).



### 5.3 INO80 chromatin remodeler

#### 5.3.1 Structural analysis of the INO80 complex by electron microscopy

The 1.3 MDa INO80 was endogenously purified to near homogeneity from *S. cerevisiae* with a FLAG-tag (see Fig. 24A-B; for details see (Tosi et al., 2013)). To verify the activity of the purified complex, we performed an ATP dependent remodeling and ATPase assays (described in more detail in section 5.3.7).

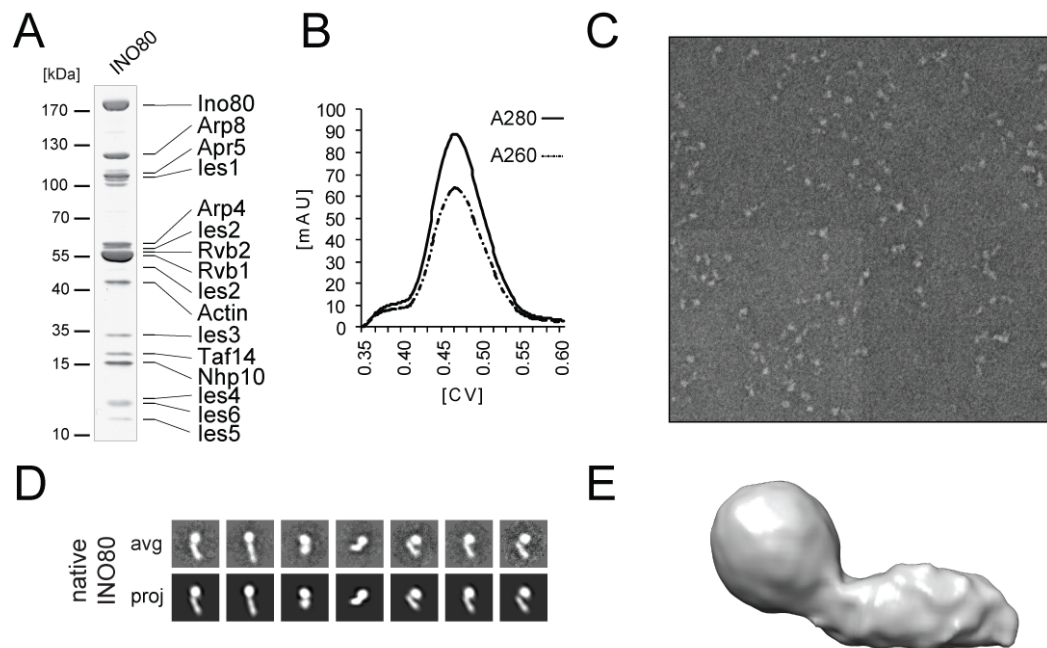


**Figure 24. Native INO80 complex.** **A)** Coomassie-stained SDS-PAGE of endogenously purified INO80 from *S. cerevisiae*. **B)** INO80 eluted from gel filtration with a homogenous peak. **C)** Micrograph of negatively stained, native INO80 showed elongated particles with a globular domain. **D)** Comparison of class averages with corresponding projections of native INO80 (EMAN2). **E)** Initial model of native INO80 calculated with EMAN2. (Figures adapted from (Tosi et al., 2013)).

In order to determine a 3D structure, freshly purified INO80 was subjected to negative stain EM. Analysis of stained micrographs revealed an elongated shape of the INO80 complex: INO80 has a globular domain connected to an elongated rod, resembling a “falling star” or embryo (see Fig. 24C-E). However, it became obvious that a fraction of INO80 particles was dissociated into the globular domain and the elongated rod (see Fig. C and Fig. 25), leading to a very heterogeneous dataset. The disintegration of INO80 was enhanced upon freezing of INO80 (see Fig. 25). Using the common line methods, initial models were calculated from intact INO80 particles and subjected to refinement with EMAN2 (see Fig. 23E). The projections of the structure were in good agreement

with the class averages (see Fig. 24D). The resolution of the structure was limited to  $\sim 50$  Å at a Fourier Shell Correlation (FSC) of 0.5. The resolution was probably limited by the instability and heterogeneity of the sample.

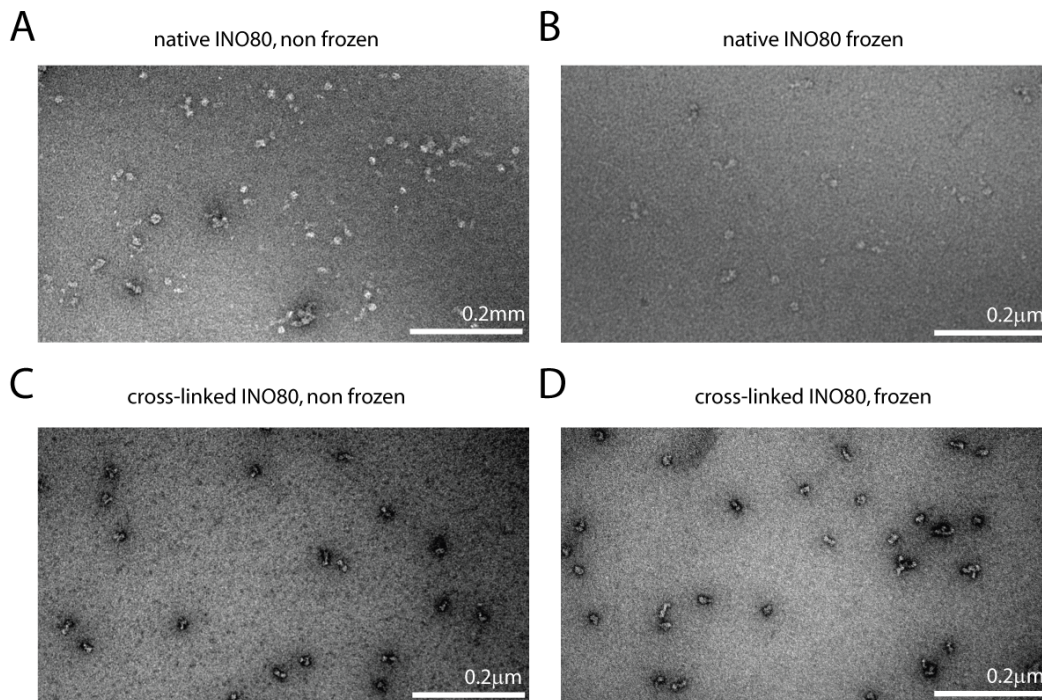


**Figure 25. The effect of freezing on the integrity of INO80.** Micrographs show negatively stained INO80 particles. **A)** Native non-frozen INO80 showed both intact and broken particles. **B)** Native INO80 mainly was split into head and cone after freezing in liquid nitrogen. **C)** INO80, stabilized by cross-linking showed intact elongated particles. **D)** Cross-linked INO80 stayed intact also after freezing.

In order to stabilize INO80, we mildly cross-linked fresh INO80 preparations with glutaraldehyde, ensuring that no aggregations were induced. Cross-linked INO80 still eluted as a homogenous peak at gel filtration and showed no aggregation in negative staining (see Fig. 25).

Particles from negatively stained micrographs were selected manually. Reference-free class averages were calculated from mildly fixed INO80 with EMAN2 (Tang et al., 2007) and ISAC (iterative and stable alignment and clustering) (Yang et al., 2012). Stabilization of INO80 preserved the overall shape of INO80, but considerably enhanced the quality of the particles (see Fig. 25 and 26B). Initial models were calculated from both 2D classification techniques using common lines reconstruction in EMAN2 and resulted in very similar initial models. Furthermore, the initial models from native and fixed specimen were comparable. The initial 3D structure of stabilized INO80 was first refined with EMAN2 and subsequently subjected to iterative projection matching and refinement



with Spider (Frank et al., 1996) to a resolution of  $\sim 22$  Å (at FSC = 0.5) (see Fig. 26C and E). The correctness of the initial models was confirmed by using geometrical object such as an ellipsoid or a cylinder, which refined to similar structures (see Fig. 26D).

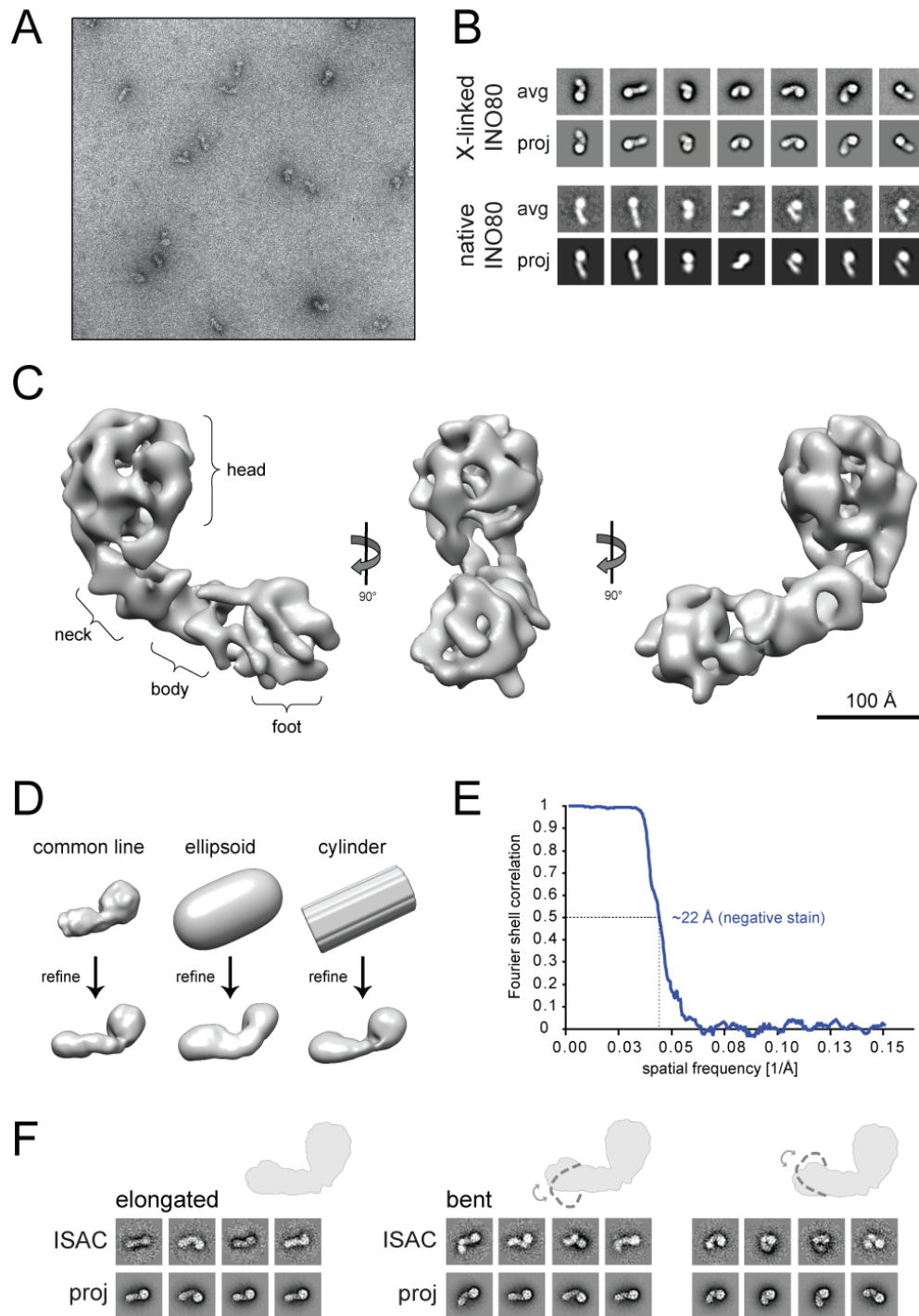


**Figure 26. Electron microscopy analysis of stabilized INO80.** **A)** Micrograph of negatively stained mildly fixed INO80. **B)** Comparison between fixed and native class averages and their corresponding projections by EMAN2. **C)** 3D reconstruction of fixed INO80 showed an elongated embryo-like shape with a globular head, a neck and a body and foot domain. **D)** Geometrical objects, such as ellipsoid or cylinder

refined to similar structures as the common line model. **E)** According to the Fourier shell correlation (FSC) at 0.5, the resolution of the negative stain structure is  $\sim 22$  Å. **F)** Reference-free class averages from ISAC (Yang et al., 2012) were correlated to projections of the elongated INO80. In the bent classes, the foot was bent inside or outside and the ISAC classes did not correlate to projections of the refined model. (Figure adapted from (Tosi et al., 2013)).

The majority of class averages from negatively stained INO80 was in good agreement with the final 3D EM structure, however a subset of classes from reference free alignment by ISAC could not be assigned to projections of the final elongated EM reconstruction and showed bent conformations (see Fig. 26F). This indicated a conformational flexibility of INO80 in the distal foot region, leading to open and closed states of the remodeler. The flexibility in the foot region probably also prohibited higher resolution.

In order to avoid staining artifacts we subjected freshly purified and stabilized INO80 to cryo electron microscopy (cryo-EM) (see Fig. 27). The negative stain structure was filtered at 35 Å and used as a reference for iterative projection matching and alignment by Spider. After sorting out bent conformations, the final resolution was determined at 17.5 Å at FSC = 0.5 (see Fig. 27C). The flexibility in the foot region of the negative stain structure was confirmed under cryo conditions as the local resolution in the foot of INO80 was inferior compared to the remaining head and body (see Fig. 27D).

The final 3D structures of fixed INO80 from negative staining and cryo-EM revealed an asymmetric, elongated embryo-like shape with distinct structural modules (see Fig. 26C and 27A): a globular head is connected via a neck region to a rod-like body-foot. The overall dimensions of the structure are  $\sim 310$  Å x 210 Å x 160 Å. The globular head accounts for approximately half of the volume of INO80 and has a diameter of  $\sim 120$  Å. The head is positioned laterally on one side of the conical neck-body-foot structure, creating a sharp kink in INO80 with a prominent groove.

The elongated structure of INO80 is surprisingly different from EM structures of other large remodeler, such as RSC and SWI/SNF remodeler (reviewed in (Leschziner, 2011)). Remodeler of the SWI/SNF family are rather globular and contain a central cleft, which has been shown to accommodate the nucleosome (Chaban et al., 2008). The EM structure of INO80 contains no such cavity, which suggests that INO80 has a different mechanism of binding to the nucleosome. The discovered flexibility of the foot region suggests that the INO80 can undergo considerable conformational changes that could be involved in nucleosome interaction or remodeling.

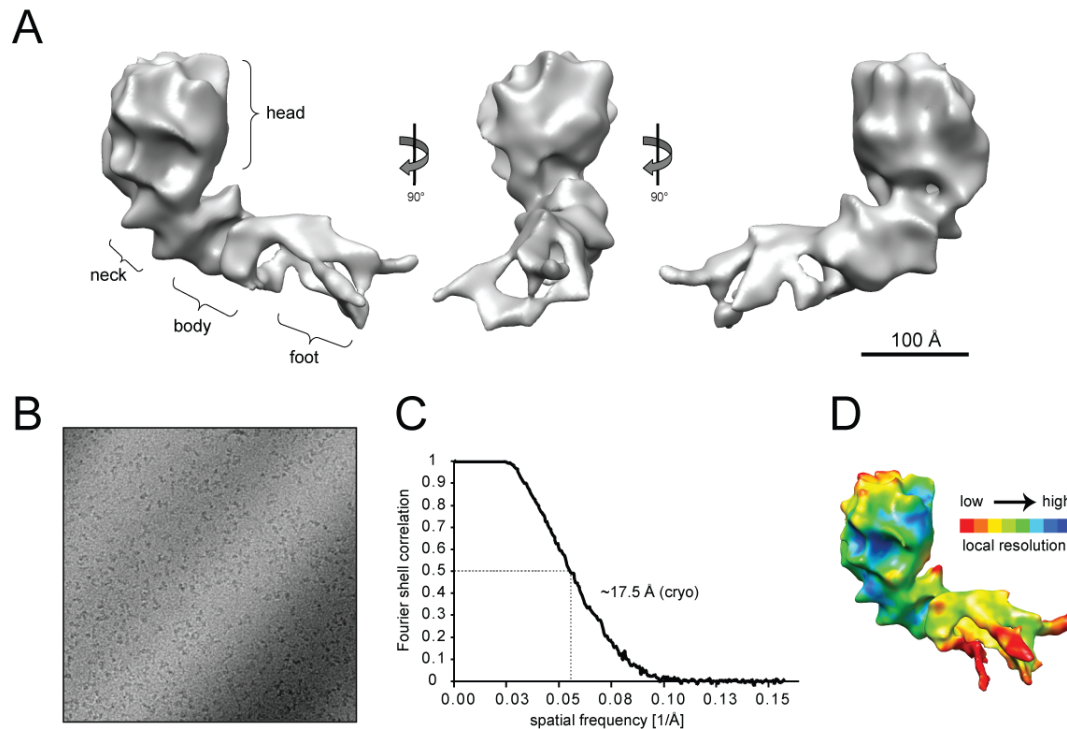


**Figure 27. Cryo electron microscopy.** **A)** 3D reconstruction from cryo-EM showed a very similar structure as negative stain EM with a globular head connected to the body-foot cone via a neck domain. **B)** Micrograph of cryo-EM of fixed INO80 recorded on a Tecnai Spirit (FEI). **C)** The resolution of the cryo-EM structure was 17.5 Å according to the FSC at 0.5. **D)** The local resolution of the cryo structure revealed that the flexible foot was least resolved. (Figure adapted from (Tosi et al., 2013)).

In summary, our analysis established an overall 3D structure of the 1.3 MDa INO80 remodeling complex revealing a distinct elongated, modular shape, which probably undergoes large-scale conformational changes.

### 5.3.2 A Rvb1/2 dodecamer is located in the head of the INO80 complex

The globular head is an ideal candidate to harbor the AAA<sup>+</sup>-ATPases Rvb1/2 given its volume and shape. Indeed a model of the yeast dodecameric Rvb1/2 (for details see (Tosi et al., 2013)) fit the dimensions of the head module (see Fig. 28A).

We calculated rotational cross-correlation in the isolated head volume and found six maxima spaced by ~60° in the negative stain and cryo structures (see Fig. 28C and F). The six-fold symmetry axis is oriented approximately parallel to the body-foot cone of INO80. Detection of the six-fold symmetry confirms the location of the Rvb1/2 complex in the head of INO80 and validates the quality of the INO80 structure (see Fig. 28B and E). Additionally, the symmetry axis enables us to position the AAA<sup>+</sup> folds of Rvb1/2.

One immediate result from positioning the Rvb1/2 AAA<sup>+</sup>-ATPases into the head, was that the volume (~600 kDa) and the roundish shape of the head are compatible with a Rvb1/2 dodecamer, but not with a hexameric Rvb1/2 complex. A model of Rvb1/2 dodecamer composed of two stacked hexamers derived from crystal structures of the human orthologs (Gorynia et al., 2011; Matias et al., 2006) could be fit into the head module of the INO80 structure (see Fig. 28A).

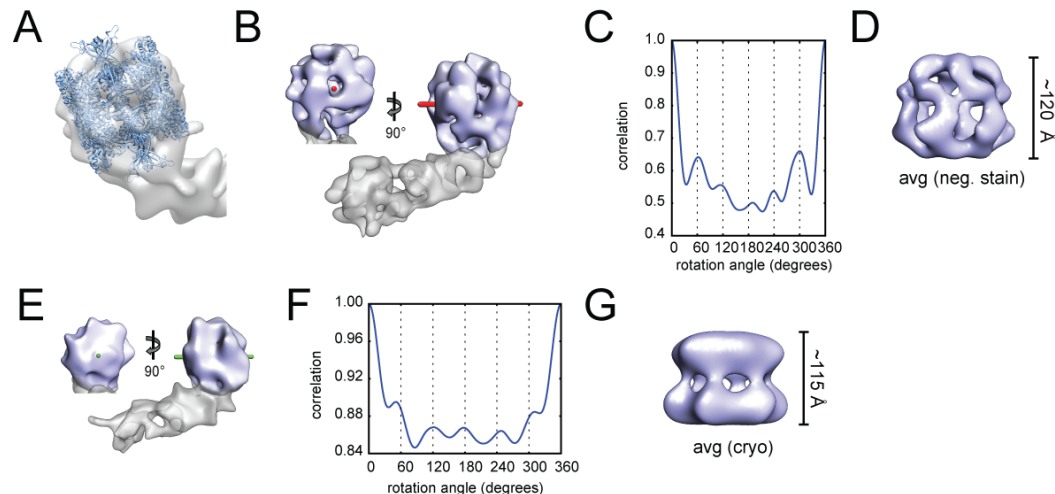


**Figure 28. AAA<sup>+</sup>-ATPase Rvb1/2 in the head of INO80.** **A)** Two hexamers of the human Rvb1 could be accommodated in the head of INO80. **B)** The symmetry axis in the head (red) of the negative stain structure of INO80 is approximately parallel to the body-tail cone. **C)** The cross-correlation between the two isolated head volumes of the negative stain structure revealed a six-fold symmetry with six maxima spaced by ~60°. **D)** The Rvb1/2 head of the negative stain structure averaged with applied six-fold symmetry. **E)** The symmetry axis in the head (green) of the cryo stain structure of INO80 is in the same location as the axis in the negative stain structure. **F)** Cross-correlation between two isolated head volumes of the cryo-structure also showed a six-fold symmetry with six maxima spaced by ~60°. **G)** Averaged head module of the cryo-EM structure with applied six-fold symmetry. (Figure adapted from (Tosi et al., 2013)).

Application of the six-fold symmetry yields averaged head modules (see Fig. 28 D and G), which were in good agreement with EM structures of isolated Rvb1/2 complexes, however the Rvb1/2 stacks were more compact in INO80 compared to any isolated structures (Lopez-Perrote et al., 2012). Recently, it has been demonstrated that isolated Rvb1/2 complexes can adopt different conformations (Lopez-Perrote et al., 2012) and AAA<sup>+</sup>-ATPases can undergo substantial conformational rearrangements during their ATP hydrolysis dependent cycle. One possibility might be that the Rvb1/2 dodecamer are stabilized in one particularly compact conformation in the INO80 environment.

The peripheral head module of INO80 harbors the AAA<sup>+</sup>-ATPases Rvb1/2 as a dodecameric.

### 5.3.3 Mapping of subunit interactions XL-MS

To interpret the 3D EM structure, we needed information about the subunit topology of the multi-subunit containing INO80 complex. We applied an approach using chemical cross-linking followed by mass spectrometry (Herzog et al., 2012) to determine a complete subunit interaction map with domain resolution (Tosi et al., 2013).

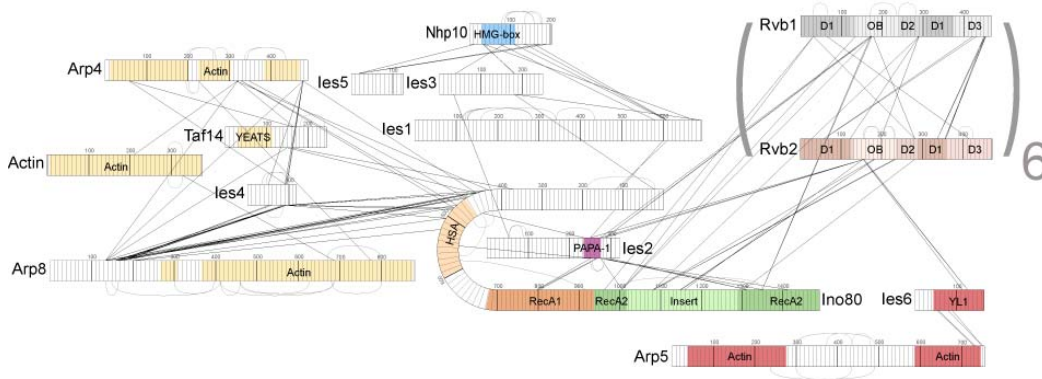


**Figure 29. Cross-linking network of INO80 subunits.** Inter-links between different subunits (black lines) and intra-cross-links within one subunit with a minimal distance of 30 amino acids between the cross-link sites (grey lines) are depicted. Ino80 (HSA in dark yellow, RecA1 in orange, RecA2 in green, insertion domain in light green) provides a scaffold for sub-complexes: Act1, Arp4, Arp8, Ies4 and Taf14 (yellow) at the HSA domain of Ino80; Nhp10 (blue), Ies1, Ies3, Ies5 at the N-terminus of Ino80; Rvb1 (grey) and Rvb2 (coppery), Arp5 and Ies6 (red) at the C-terminus of Ino80; Ies2 (purple) has a special structural role. (Figure adapted from (Tosi et al., 2013)).

In four experiments, we identified 212 unique intra-links (cross-links within the same polypeptide) and 116 inter-links (cross-links between two polypeptides), respectively (see Fig. 29). We validated our approach by confirming that intra-links on available crystal structures or homology models fulfilled the distance restraint of  $\leq 30$  Å (Herzog 2012) (see (Tosi et al., 2013)).

INO80 subunits clustered into four modules on the Ino80-Ies2 scaffold (see Fig. 29; for a detailed description see (Tosi et al., 2013)): the non-conserved Nhp10 module comprised Nhp10, Ies1, Ies3, Ies5 and the N-terminus of Ino80; the conserved Arp8-module is composed of Act1, Arp4, Arp8, Ies4, Taf14 and the HSA domain of Ino80; the Rvb1/2 module at the RecA2 domain and the insertion of Ino80; and the Arp5 module with Arp5 and Ies6 close to the Rvb1/2 module. These data is in agreement with previously published biochemical analysis on the modular organization of INO80 (Chen et al., 2011; Jonsson et al., 2004; Szerlong et al., 2008), but further extends it.

The defined structural modules were confirmed by purification of sub-complexes and verified *in vivo* by analysis of subunit composition of INO80 complexes from  $\Delta arp5$ ,  $\Delta arp8$  or  $\Delta nhp10$  strains (see (Tosi et al., 2013)).



Our complete interaction topology of all INO80 subunits is compatible with, but also greatly extends previously published results on the modular architecture of INO80 and adds information about domain and motif resolution of the interactions.

### 5.3.4 The Rvb1/2 dodecamer

Taking into account the information from XL-MS, we can further interpret the Rvb1/2 dodecamer in the head of the INO80 structure. Rvb1/2 monomers contain three domains (Matias et al., 2006). Domain 1 and 3 form the AAA+ATPase core, connected by domain 2 with its oligonucleotide binding (OB)-folds. Analysis was performed on a molecular model of yeast dodecameric Rvb1/2 (for details see (Tosi et al., 2013)).

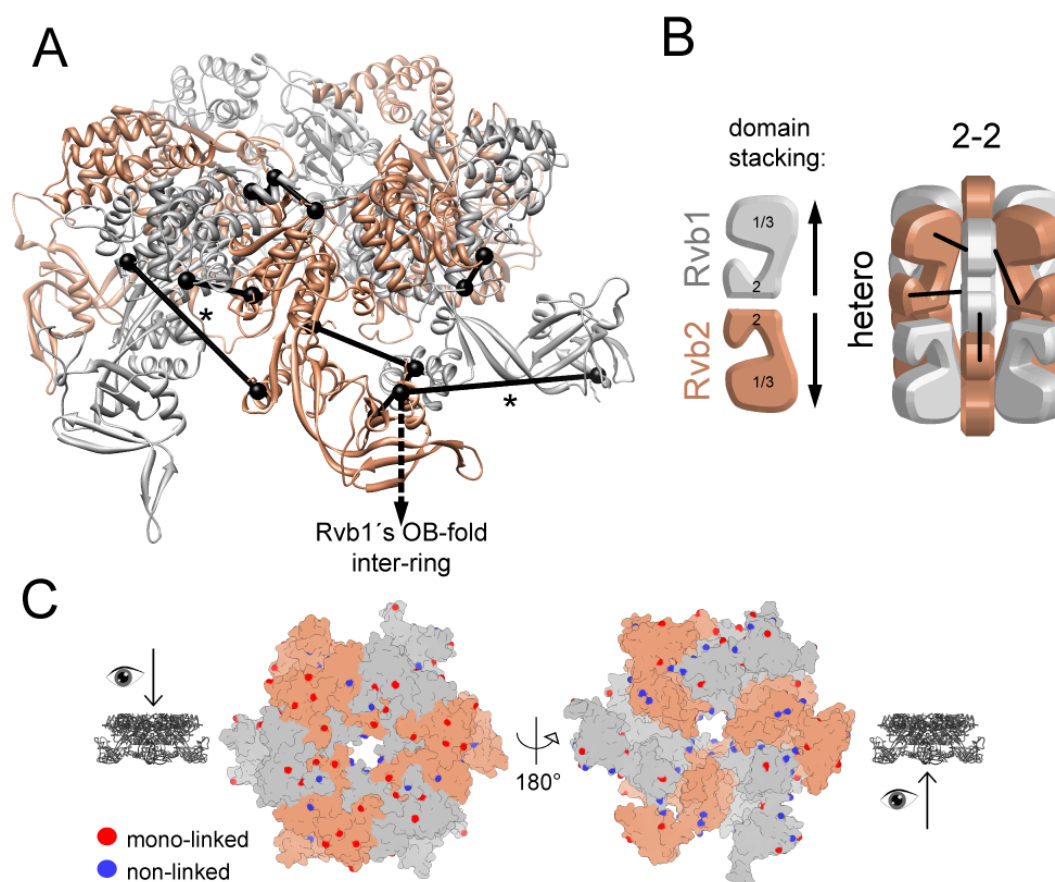


**Figure 30. Arrangement and stacking of the AAA<sup>+</sup>-ATPases Rvb1 and Rvb2 dodecamer.** **A)** Cross-links between the ATPase domain 1/3 and domain 2 of Rvb1 (grey) and Rvb2 (coppery) restrained the topology to a hetero-hexameric arrangement. The asterisks mark cross-links in flexible regions. **B)** Of all possible stacking arrangements of the Rvb1/2 rings, only hetero-hexamers with a domain 2-2 stacking fulfilled the cross-links (black). **C)** Mono-linked lysines (red) on the convex side of the hetero-hexameric Rvb1/2 rings indicated solvent exposure. Non-linked lysines (blue) were mainly found on the concave side of the Rvb1/2 hexamer. This implied that the two stacked rings interact via their domain 2 at the concave side. (Figure adapted from (Tosi et al., 2013)).

Among all possible different stacking arrangements of homo- and hetero-hexamers, the cross-link restraints were only fulfilled within two stacked hetero-hexamers (see Fig. 30A-B; see (Tosi et al., 2013) for details). Stacking of the two rings was determined by analyzing mono-links (lysine, modified only by lysine, but not cross-linked): ~80% of lysines on the convex side of the Rvb1/2 hetero-hexamer, but only on ~10% of lysines on the concave side were mono-linked, suggesting that the convex surface is solvent exposed in the dodecamer, while the concave surface is more protected (see Fig. 30C; see (Tosi et al., 2013) for details).

The dodecamer of Rvb1/2 in INO80 is composed of two hetero-hexameric Rvb1/2 rings, which stack via their OB-folds in domain 2. Taking the six-fold symmetry axis into account, the OB-folds of the Rvb1/2 in the equatorial plane face the neck of INO80.

### 5.3.5 The Snf2 domain

Numerous cross-links between the Rvb1/2 head and the ATPase domain of Ino80 indicated that the Snf2 fold is located in close proximity to the Rvb1/2 head in the neck region of the INO80 structure (Tosi et al., 2013). The neck harbors a bi-lobed density patch that resembles the characteristic Snf2 fold (see Fig. 31) (Durr et al., 2005; Thoma et al., 2005).

Indeed the *Danio rerio* (*Dro*) Rad54 Snf2 domain (crystal structure: (Thoma et al., 2005)), a homolog of the Ino80 Snf2 domain fit well into the density at the neck with a cross-correlation coefficient of 0.87 (see Fig. 31). The docking orientation of the Snf2 domain was further restrained by the inter-links of Rvb1/2 clustered in the RecA2 lobe of the Snf2 domain. The cross-links were in agreement with this position and the additional density could harbor the 30 kDa insertion domain in the Ino80 Snf2 fold. Ies2 cross-linked on top of the Ino80 Snf2 ATPase and to the OB-folds of Rvb1/2 suggesting a position of the PAPA-1 containing Ies2 on top of the neck domain, “sealing” the Ino80 ATPase.

The groove between the head and the neck domain could potentially accommodate nucleosomal DNA bound to the Snf2 domain of Ino80 in the neck. Furthermore, the DNA binding OB-folds of Rvb1/2 are in close proximity and could stabilize the interaction with the DNA. It is also tempting to speculate about a coordinated binding of DNA by the Snf2 ATPase domain and the OB-folds of Rvb1/2.

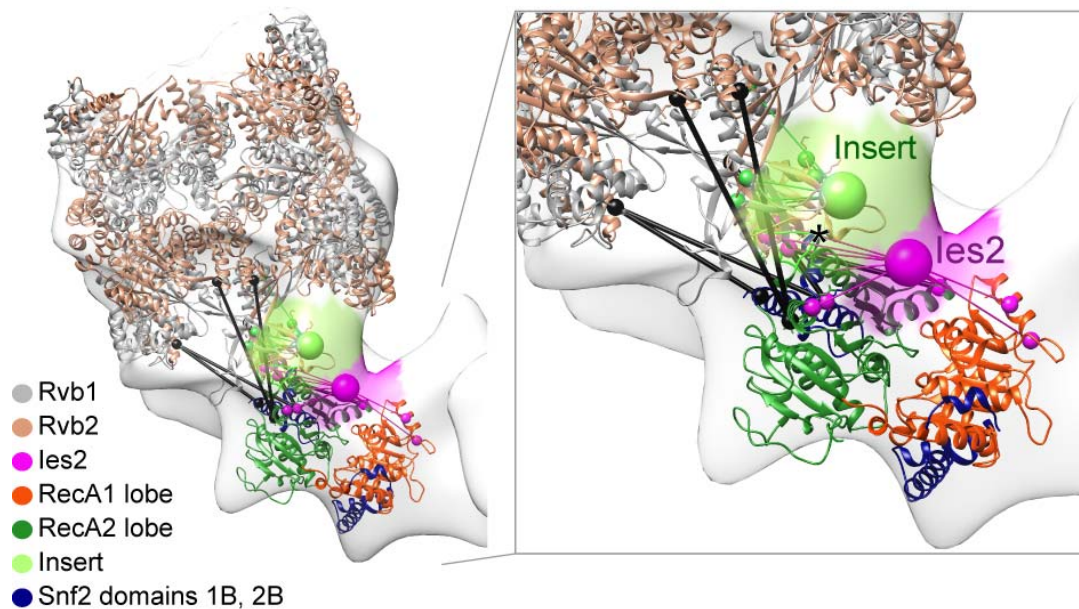


**Figure 31. Snf2 ATPase of INO80.** *Dro* Rad54 (Thoma et al., 2005) was used as a model for the homologous Snf2 ATPase domain of Ino80 and was docked into the neck region of the electron density (grey) and oriented by the cross-links to Rvb1/2 (black). Small spheres represent lysines of RecA1, RecA2 of Ino80 and OB-folds of Rvb1/2 that cross-linked to Ies2 (pink) or the insertion of Ino80 (light green). Ies2 was localized on top of the Snf2 fold (pink ball). The asterisk marks remaining density which could account for the insertion domain of Ino80. (Figure adapted from (Tosi et al., 2013)).

Our hybrid approach enabled us to position the Snf2 domain in the neck of the INO80 structure, in close proximity to the Rvb1/2 head module.

### 5.3.6 Localization of Nhp10-, Arp8- and Arp5- modules

The Rvb1/2 dodecamer is located in the head, the Snf2 Ino80 ATPase in the neck region. In order to localize the remaining modules of INO80 in the 3D structure, we performed DID-labeling (Flemming et al., 2010) of individual subunits. GST-FLAG-DID2 and His<sub>6</sub>-Dyn2 were purified via affinity chromatography with GST or Ni<sup>2+</sup>-NTA agarose, respectively and by subsequent size exclusion chromatography (see Fig. 32). INO80 subunits were C-terminally tagged with DID1 in a  $\Delta dyn2$  background. After affinity purification of INO80, the DID-tag was assembled by addition of DID2 and Dyn2 and enriched by a second affinity purification via the GST-tag of DID2. Further purification of the INO80 complex was performed equivalent to the WT via ion exchange and gel filtration.



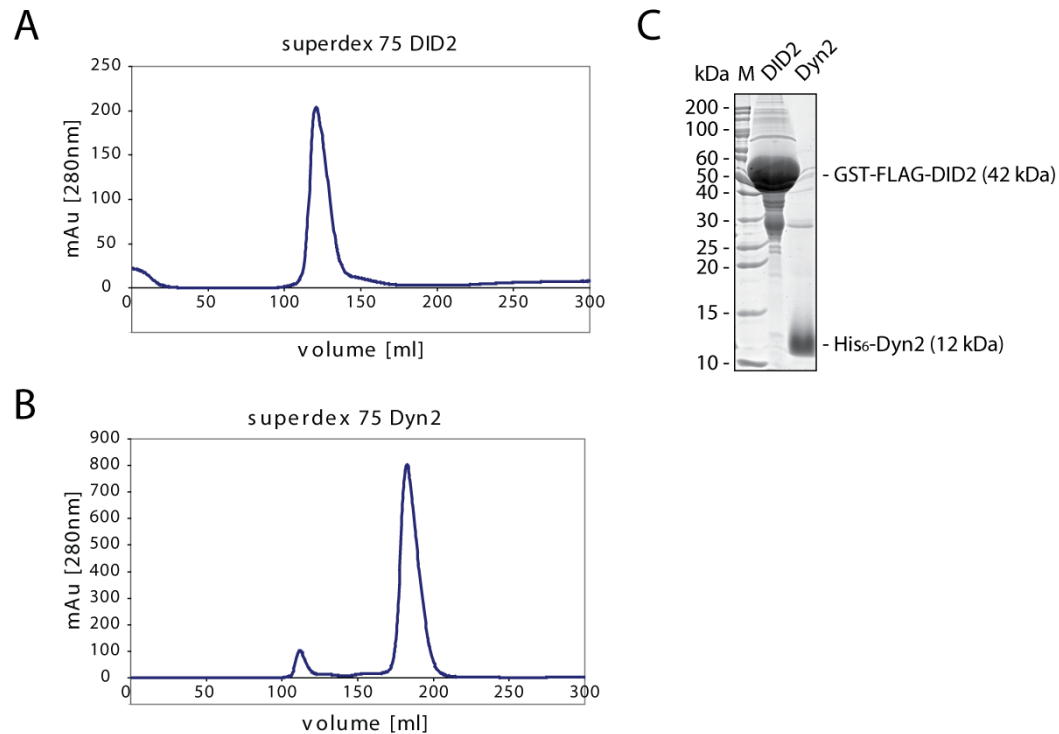


**Figure 32. Purification of GST-FLAG-DID2 and His6-Dyn2 via affinity purification and gel filtration.** A) Size exclusion profile of DID2. B) Size exclusion profile of Dyn2. C) Coomassie stained 15% SDS-PAGE of DID2 and Dyn2 after size exclusion chromatography.

Arp4 was DID-tagged as a representative of the Arp8-module (Ino80<sup>HSA</sup>, Act1, Arp4, Arp8, Ies4, Taf14). In single particles from negatively stained INO80 the DID-tag of Arp4 was protruding from the foot of INO80 (see Fig. 33A). The peripheral location of the module is in agreement with a lack of cross-links from the Arp8-module to other modules of the INO80 complex.

The Nhp10-module (Ino80<sup>N-term</sup>, Nhp10, Ies1, Ies3, Ies5) was localized by direct DID-tagging of Nhp10. Visualization of INO80 particles showed the DID-tag being located at the body of INO80 (see Fig. 33A). This rather central location of the yeast specific Nhp10-module is confirmed by the detection of cross-links between Ies3 and Ies2 (see Fig. 33A).

The Arp5 module (Arp5, Ies6) was indirectly localized by DID-tagging of its interacting subunit Ies6. The DID-tag on Ies6 was at the neck of the INO80 particles. This location of the Arp5-module was proposed already by cross-links of Ies6 to Rvb2, which is found in the head module. Furthermore, the EM structure harbors unaccounted density in the neck region behind the Snf2 fold, which resembles the dimensions of an actin fold (see Fig. 33B, (Tosi et al., 2013)).

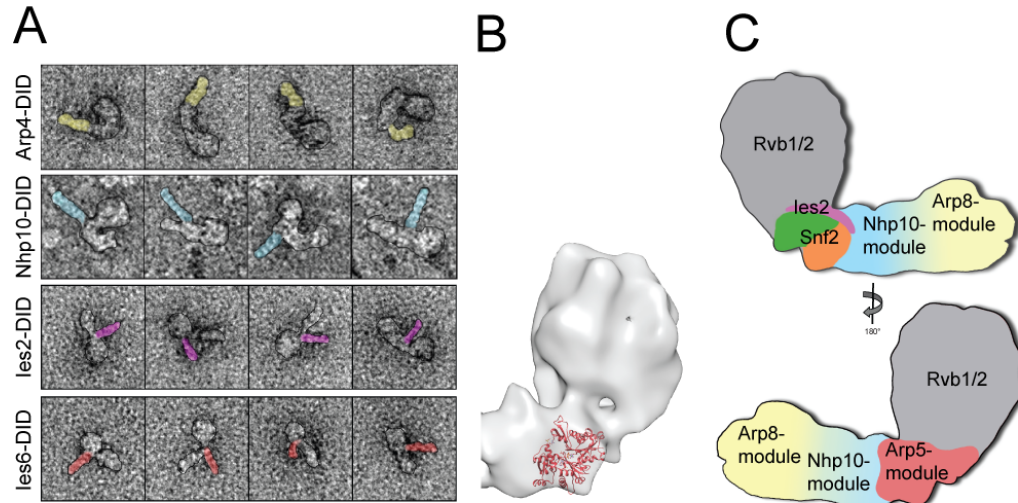


**Figure 33. DID-labeling for subunit localization.** **A)** Negative staining of single particles revealed the position of Arp4 (yellow) at the foot, Nhp10 (blue) at the body, Ies2 (pink) and Ies6 (red) at the neck. **B)** Unaccounted density at the back of the ATPase could account for Arp5 (actin fold depicted in red). **C)** Rvb1/2 (grey) is located in the head, Snf2 (RecA1 in orange, RecA2 in green) in the neck topped by Ies2 (pink) and backed by Arp5 (red). The Nhp10 module (blue) is situated in the body and the Arp8 module (yellow) in the foot. (Figure adapted from (Tosi et al., 2013)).

To confirm the proposed localization of Ies2, we analyzed INO80 particles with DID-labeled Ies2 and detected the DID-tag also close to the neck of the INO80 structure (see Fig. 33A). This result fits nicely with our inferred localization from XL-MS and EM analysis, which anticipated that Ies2 is sitting on top of the Snf2 fold in the neck region (see Fig. 33C).

In summary, combining data from EM, XL-MS and DID-labeling we propose the following INO80 module topology: the head contains the Rvb1/2 dodecamer, the neck harbors the Snf2 Ino80 ATPase fold, Ies2 and the Arp5-module, the Nhp10-module is situated in the body and the Arp8-module is located in the distal foot region of INO80.

### 5.3.7 Functional analysis of INO80 modules

In order to dissect the role of the INO80-modules, we analyzed their contribution in substrate binding by EMSA, stimulation of ATPase activity and the remodeling reaction.

INO80 bound to its nucleosomal substrate in EMSA. INO80 was able to shift core nucleosomes without the presence of extra-nucleosomal DNA, however a longer linker DNA enhanced the affinity of INO80 to nucleosomes, as observed before (see Fig. 34A) (Udugama et al., 2011). Centered and off-centered nucleosomes with equal total DNA length were bound with similar affinities (see Fig. 34A)

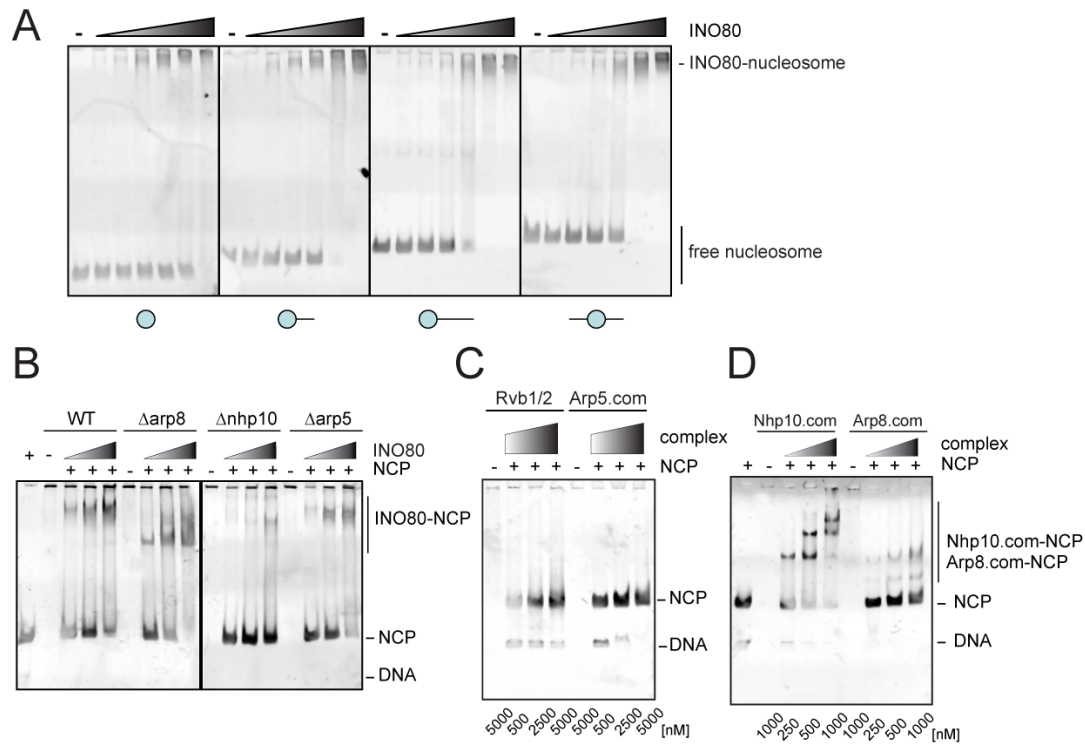


**Figure 34. EMSA analysis of nucleosome interaction of INO80 WT and mutants.** **A)** INO80(WT) interacted preferentially with nucleosomes containing longer linker DNA. 147 bp core nucleosomes, off-centered nucleosomes with 20 bp and 40 bp long linker DNA, as well as centered nucleosomes with 20 bp on each side were tested. **B)** Analysis of deletion mutants in nucleosome binding. Deletion of the Nhp10-module led to a substantial decrease of nucleosome binding. The affinity of INO80( $\Delta arp8$ ) was reduced, whereas nucleosome binding was only mildly affected upon deletion of the Arp5-module. **C-D)** Analysis of nucleosome binding of recombinantly expressed and purified sub-complexes. **C)** Purified Rvb1/2 sub-complex only marginally bound DNA and nucleosomes, Arp5-Ies6 bound DNA with low affinity. **D)** The Nhp10 and Arp8 sub-complexes bound nucleosome with high affinity and oligomerized on the substrate. (Figure adapted from (Tosi et al., 2013)).

In order to identify the role of the identified and localized modules in nucleosome recognition and remodeling, we analyzed INO80 from WT,  $\Delta arp8$ ,  $\Delta nhp10$  and  $\Delta arp5$  strains in their ability to bind DNA and nucleosomes, to slide nucleosomes and to hydrolysis ATP.

All deletion mutants were still capable to bind DNA and nucleosomes (see Fig. 34B; (Tosi et al., 2013)), which implies that all these modules are involved in substrate interaction and multiple contacts are required for optimal substrate recognition.

INO80( $\Delta arp5$ ) showed only a slightly reduced interaction with DNA (Shen et al., 2003; Tosi et al., 2013) and nucleosomes (see Fig. 34B; (Tosi et al., 2013)). In the reverse experiment, we confirmed that a recombinantly expressed and purified Arp5-module bound DNA with low affinity and was not able to shift nucleosomes (see Fig. 34C; Tosi et al., 2013).

Omission of the Arp8-module decreased DNA (Tosi et al., 2013) and nucleosome binding (see Fig. 34B), but did not lead to a complete loss of substrate binding as published earlier (Shen et al., 2003). In agreement, we observed moderate DNA and nucleosome binding (see Fig. 34D) by a recombinant Arp8 sub-complex consisting of Ino80<sup>HSA</sup>-Act1-Arp4-Arp8 (Tosi et al., 2013).

INO80( $\Delta nhp10$ ) showed substantially reduced affinity to DNA (Tosi et al., 2013) and nucleosomes (see Fig. 34B). Consistently, a recombinant sub-complex of Nhp10-Ies3-Ies5 was able to shift DNA (Tosi et al., 2013) and nucleosomes with high affinity (see Fig. 34D). Nhp10 was identified as a novel nucleosome binding element in INO80. The Nhp10-module is together with the Arp8-module mainly responsible for substrate binding and interaction.

To assess how the modules of INO80 contribute to nucleosome remodeling we performed nucleosome sliding and ATPase activity assays. Nucleosomes were assembled on a DNA sequence of the INO1 gene (bp +1 until +359), which has been shown to be a substrate for INO80 remodeling (Ford et al., 2007).

INO80(WT) was able to reposition nucleosomes on a part of the INO1 gene (bp +1 until +359) in an INO80 concentration and ATP hydrolysis depend manner (see Fig. 35A).

Although deletion of the Arp5-module did not significantly influence the affinity of INO80 towards DNA and nucleosomes, INO80( $\Delta arp5$ ) was not able to slide nucleosomes in our assay (see Fig. 35B; (Shen et al., 2003)). Lack of the Arp8 module negatively influenced binding of nucleosome and nucleosome remodeling (see Fig. 35B). Loss of the Nhp10 module led to a decrease of nucleosome affinity, but the remodeling activity of INO80( $\Delta nhp10$ ) was comparable to INO80(WT), suggesting that the Nhp10-module is required for targeting of INO80, but does not play an important role in the remodeling reaction itself (see Fig. 35B).

INO80(WT) had a low basal ATPase activity, which could be stimulated by the addition of DNA and stimulated even higher by nucleosome (see Fig. 35C). All mutants have similar intrinsic ATPase activity without a stimulus (see Fig. 35C). INO80( $\Delta arp5$ ) hydrolyzed ATP comparable to INO80(WT) upon DNA stimulation (see Fig. 35C), however unlike for INO80(WT), nucleosomes did not further increase the ATPase activity of INO80( $\Delta arp5$ ). Although, INO80( $\Delta arp5$ ) did not influence nucleosome interaction to a great extent. The ATPase activity of INO80( $\Delta arp8$ ) was not affected by DNA, and nucleosomes stimulated the hydrolysis rate equivalent to INO80(WT) upon

DNA stimulation. The Arp8-module has been suggested to be associated with extranucleosomal DNA (Kapoor et al., 2013) and histones (Gerhold et al., 2012; Harata et al., 1999; Saravanan et al., 2012; Shen et al., 2003) and may detect both in the remodeling reaction. Although the Nhp10-module was a high affinity DNA and nucleosome binder, the ATPase activity and its stimulation by DNA and nucleosomes were independent of the Nhp10-module (see Fig. 35C).

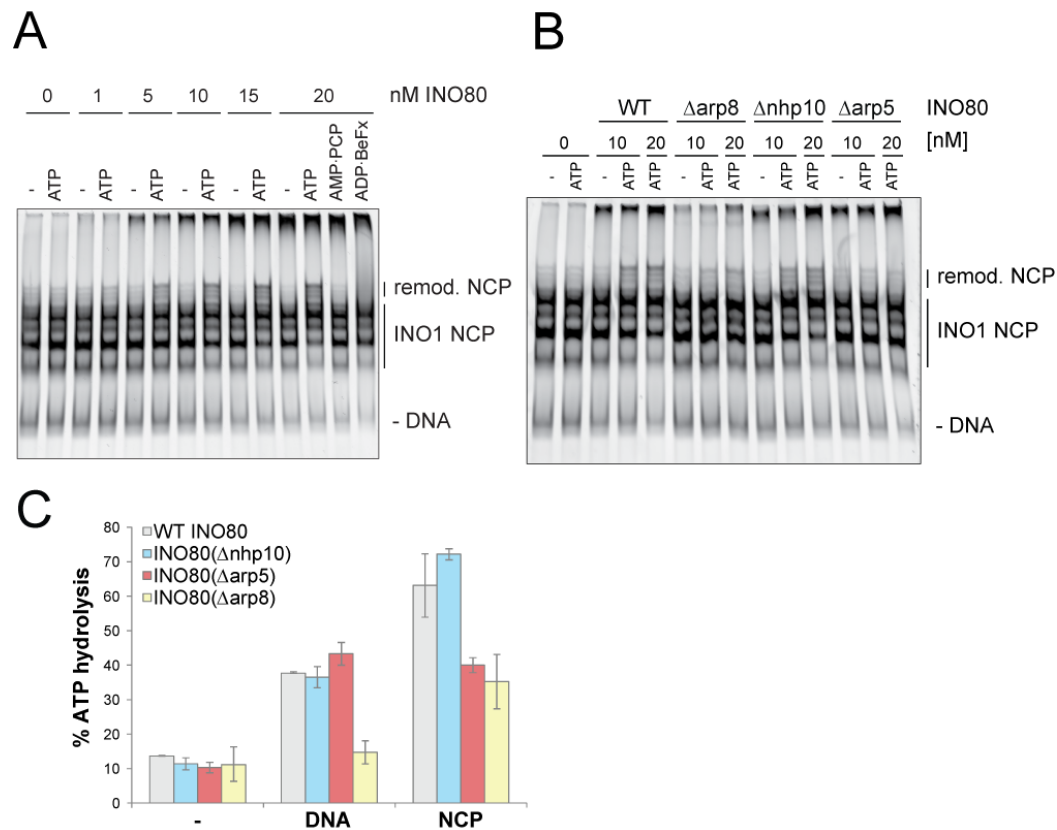


**Figure 35. Activity of INO80 deletion mutants.** **A)** Remodeling of INO1 nucleosomes by INO80 WT was dependent on the concentration of INO80 and the presence of hydrolysable ATP. **B)** Analysis of mutants in the remodeling reaction revealed that INO80(Δnhp10) was able to remodel equivalent to the WT. Remodeling of INO80(Δarp8) was reduced and INO80(Δarp5) was not able to remodel. **C)** ATP hydrolysis was measured either without a stimulus, or stimulated with 359bp long INO1 DNA or INO1 nucleosomes. The data was normalized to hydrolysis rates of calf intestinal alkaline phosphatase and is represented as mean  $\pm$  SEM). All mutants showed the same basal ATPase activity. Stimulation of DNA enhanced the hydrolysis rates expect for INO80(Δarp8). The addition of nucleosomes further enhanced the activity of INO80(WT) and INO80(Δnhp10), whereas INO80(Δarp5) was not stimulated further. INO80(Δarp8) was stimulated by nucleosomes, but not to the same extent as the WT. (Figures adapted from (Tosi et al., 2013)).

The Arp8- and Arp5-modules are responsible for the remodeling reaction, while the Nhp10-module contributes to high affinity nucleosome binding.

### 5.3.8 Interaction of INO80 with the nucleosome

To identify the interaction sites between INO80 and its substrate, we reconstituted and analyzed a complex of INO80 and nucleosomes by XL-MS (see Fig. 36A-B; see (Tosi et al., 2013) for details). 35 out of 52 inter-links were mapped to flexible histone tails, representing only loose constraints, whereas 17 inter-links were formed to structured parts of histones allowing us to approximately position the nucleosome in respect to the INO80 complex.

Remarkably, as suggested from the EMSA results, we found cross-links from all four modules of INO80 to all four histones, indicating a central position of the nucleosome within the INO80 structure. We detected 12 cross-links of the Rvb1/2 head, 14 of the Ino80 ATPase-Ies2-Arp5-Ies6 neck, 10 of the Ino80 N-term-Nhp10-Ies1-Ies3-Ies5 body and 16 of the foot containing the Ino80 HSA-Act1-Arp4-Arp8-Ies4-Taf14 (see Fig. 36A-B; see (Tosi et al., 2013) for details). One intriguing result was the interaction of H2A/H2B, which is the dimer pair that is exchanged by INO80 type remodeler (Morrison and Shen, 2009; Papamichos-Chronakis et al., 2011). The cross-links of subunits in the neck - RecA2, Arp5/Ies6, Ies2 and Rvb1/2 domains 2 - to H2A and H2B core secondary structures argued that the H2A/H2B dimer is located close to the neck of INO80. Interestingly, the position of the RecA2 cross-link to the loop insertion between  $\alpha 1$  and  $\alpha 2$  of H2A coincides with the binding site of the ATPase domain of the ISW2 remodeler (Dang and Bartholomew, 2007) implying a conserved mechanism in remodeling.

To confirm the inferred positioning of the nucleosome, we directly visualized the nucleosome on INO80 by negative staining. Stable reference-free class averages from ISAC (Yang et al., 2012) revealed additional density in the central groove between the head and the foot of INO80, which is not present in apo INO80 (see Fig. 36C). Indeed, this central location was in agreement with the prediction from XL-MS and the EMSA results. Robust 3D reconstruction of this heterogeneous complex is prohibited by the flexible nature of INO80, insufficient occupancy and possibly partial remodeling of the nucleosome so far.

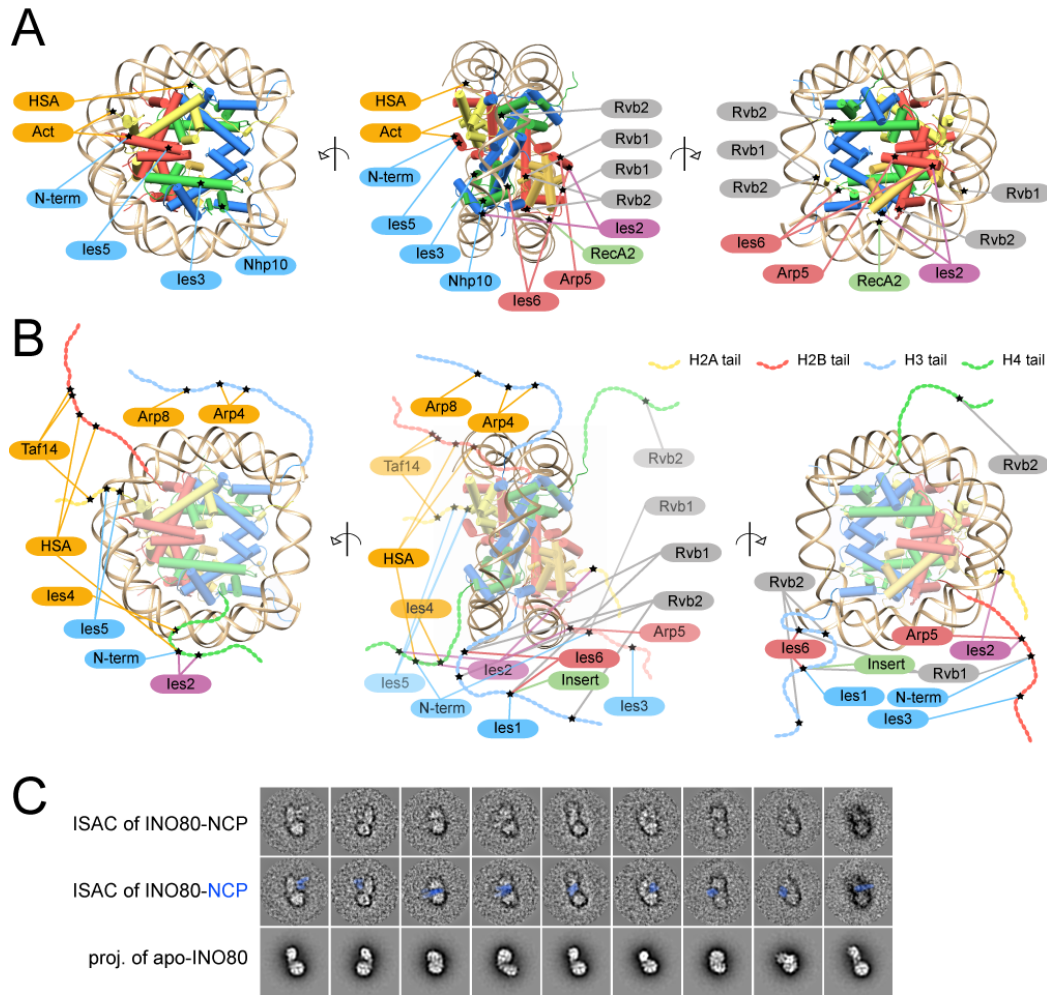


**Figure 36. Analysis of INO80-nucleosome complex. A-B)** XL-MS of INO80-nucleosome complexes. **B)** Cross-links to histone core folds impose tight distance constraints. The Arp8-module and Nhp10-module occupied one side of the nucleosome, whereas the other side was cross-linking to the Rvb1/2 head and the Ino80 ATPase, Ies2 and the Arp5-module situated in the neck. **B)** Reference free class averages (ISAC; (Yang et al., 2012)) from negatively stained INO80-nucleosome complexes in comparison to projections of the apo INO80 showed additional density (nucleosome marked in blue) bracketed between the head and foot). (Figure adapted from (Tosi et al., 2013)).

In summary, we could approximately position the nucleosome in the center of the INO80 complex with all modules involved in the interaction. A nucleosome sandwiched between the head and the foot is consistent with all data from biochemistry, XL-MS and EM analysis.



## 6 Discussion & Outlook

### 6.1 *Structural analysis of ISWI family remodeler*

ISWI remodeler are characterized by the fact that they are rather small and harbor only a few subunits. I studied the ISWI remodeler in order to gain information about the ATPase subunit of chromatin remodeler and their interaction with the nucleosome. Electron microscopy however is a method which is better applicable to larger complexes, and the drawback of studying small proteins is that they do not provide enough contrast for cryo-EM and enough details for accurate alignment and are thus limited in resolution. Nucleosomes bound to factors on the other hand, are apparently hard to crystallize given the small number of structures: crystal structure of the regulator of chromosome condensation RCC1 bound to a nucleosome (Makde et al., 2010), silencing involved Sir3 BAH domain on a nucleosome (Armache et al., 2011; Arnaudo et al., 2013; Wang et al., 2013; Yang et al., 2013). Thus, a combination of a low resolution EM structure with a high resolution crystallographic structure of the remodeler, at the best combined with cross-linking and mass spectrometry would allow a quasi atomic interpretation of the interaction.

Therefore, I started by aiming for an EM structure of ISWI in complex with the nucleosome. One premise to achieve this goal is the ability to homogeneously purify the components for structural biology. ISWI can be satisfactorily purified to near homogeneity at sufficient concentrations and yields. The purification procedure for ACF complex however has to be further optimized in order to increase the yield and to get rid of the aggregations problems. It might be that ACF is not a physiologically relevant complex and lacks the two histone fold CHRAC14/16 proteins for stability. Therefore, expression and purification of the complete CHRAC complex including, ISWI, Acf1 and CHRAC14, CHRAC16 from one baculovirus in insect cells should be tested. One further advantage of this approach would be that the CHRAC complex is approximately 2.5 fold larger compared to the single ISWI subunit and might thus be more suitable for analysis by EM. A structure of the human CHRAC complex has been published, however it was not bound to a nucleosome and the stoichiometric of the complex did not look satisfactorily (Hu et al., 2008).

The ISWI purifications yielded pure and homogenous protein, which is suitable for structural analysis. However, to gain a stable ISWI-nucleosome complex, which can ideally be purified further, should be the main focus for the future. The key problem



which arose during formation of the complex was aggregation upon mixing ISWI with nucleosomes. Optimization of conditions (such as detergents, various salts, salt concentrations, different DNA templates, pH), which would prevent aggregation, but preserve complex formation were so far not successful enough to entirely avoid aggregation. One possible solution would be to find a technique, which would allow separation of the ISWI-nucleosome complexes (monomeric from dimeric ISWI-nucleosome complexes, but also aggregation and single components). Gel filtration did not seem to be applicable due to aggregation issues, but GraFix and gel based techniques should be tested further.

Another issue that arose during analyzing the ISWI-nucleosome complexes was that the affinity of ISWI was overestimated when analyzed by gel retardation assays (EMSA) compared to in solution measurements (MST). One enormous problem for EM analysis, which derived from this finding, is that upon formation of sufficient ISWI-nucleosome complexes, the grid was over-crowded. For single particle analysis, the particles have to be distinguishable, but at those ISWI concentrations, nearly no complexes with the nucleosome were formed. Once the aggregation problematic is solved, one could try to shorten the incubation with the grid to prevent overcrowding. Instead, I focused on increasing the affinity of ISWI to the nucleosome by various ATP analogs and mutations in the ATPase domain. Among the ATP analogs I tested in MST, only one pre-transition state analog ADP·BeFx was able to increase the affinity of ISWI to the nucleosome. Unfortunately, exactly those conditions with an activated ATP mimetic were used to calculate a EM structure of the human ISWI homolog SNF2h (Racki et al., 2009). Another promising candidate is the Walker B mutant of ISWI (E257A), which in presence of ATP should also mimic an ATP bound state of ISWI and showed marginally higher affinity to the nucleosome compared to WT ISWI. Furthermore, the addition of other subunits such as Acfl and the two histone-fold CHRAC subunits could further increase the affinity and should be analyzed by MST. Finally, the binding affinity results from Thermophoresis measurements could be further complemented with ATPase assays of the various mutants.

MST seems to be a powerful method to deduce affinity values in solution without gel derived stabilization. Since this Thermophoresis technique is still rather novel, one could confirm the values for the affinities with an independent method, such as fluorescence anisotropy. This has been indirectly done by the Narlikar group, they found very similar values by studying the affinity of hSNF2h to nucleosomes with electron

paramagnetic resonance (EPR) (Racki et al., 2009). The thermophoresis technique is therefore suitable to study the interaction of nucleosome interacting factors such as chromatin remodeler.

A recent study from Timothy Richmond's group suggested that ISW1a( $\Delta$ ATPase) uses di-nucleosomes as a substrate (Yamada et al., 2011). It would be interesting to test, how di-nucleosomes interact with ISWI and if they prevent some of the aggregation problems. According to (Racki et al., 2009) two molecules of SNF2h bind one nucleosome, completely contrary to the results from the Richmond group. While in the Racki structure the HAND-SANT-SLIDE domain which interacts with the linker DNA binding is not visible, the (Yamada et al., 2011) complex does not contain the ATPase domain. It would therefore be very interesting, to analyze, how a complete ISWI including all domains (ATPase + HAND-SANT-SLIDE) binds to a mono- and dinucleosomal substrate.

Once the structure of the entire ISWI ATPase subunit in complex with the mono-nucleosome will be available, this can be used as a starting point to extend the substrate to nucleosomal and chromosomal arrays, which resemble a more physiological situation. This might also help to clarify the stoichiometry of ISIW-nucleosome complexes: dimeric remodeler or dimeric nucleosome. Furthermore, the reaction mechanism of remodeling could be visualized by solving structures of the complete ATP hydrolysis cycle. Finally, it will be very intriguing to be able to interpret the low resolution EM structures with complementary high resolution techniques such as crystallography and XL-MS to reveal quasi-atomic details of the enigmatic remodeling process.

## **6.2 Structural analysis of the INO80 chromatin remodeler**

We established a first complete structural framework of the 1.3 MDa INO80 chromatin remodeler and its interaction with a nucleosome. Using an integrative structural approach with a combination of structural, biochemical and mass spectrometric techniques we clarified the 3D EM structure, the complete subunit interaction topology and localized structural and functional modules within the INO80 structure.

So far, all chromatin remodeler visualized by EM did not exceed a resolution of 20Å. The overall resolution of the INO80 EM structure with 17Å is slightly better, but still rather limited, probably due the flexibility observed in the foot region. Sorting of elongated and bent conformations was difficult, presumably because there are no discrete intermediate bent conformations, but rather a continuum between various bent states. An improvement of the resolution might be achieved by stabilizing defined conformations. Another possibility would be to increase the contrast in cryo conditions to achieve a more accurate alignment, for example by recording longer exposed frames on a direct detector for alignment purposes, and taking the shorter exposed images without beam damage for back projection.

It is important to mention that native INO80 did not stay intact after freezing in liquid nitrogen or during preparation of grids for cryo-EM. The head of INO80 was separated from the remainder of INO80 and broke particles could be observed. After successful stabilization of INO80 with mild glutaraldehyde cross-linking, the complex stayed intact also after freezing and survived cryo-EM conditions.

An unexpected outcome of the EM analysis was that the overall elongated 3D structure of INO80 is markedly different from other large (>1 MDa) chromatin remodeler from the SWI/SNF family. In low resolution EM studies published so far, SWI/SNF remodeler are C-shaped with a rather globular structure exhibiting a central nucleosome-binding cavity (reviewed in (Leschziner, 2011)). In clear contrast INO80 does not contain an obvious nucleosome-binding pocket. Instead, based on XL-MS and 2D class averages of negatively stained INO80-nucleosomes complexes, we could position the nucleosome in the groove between the head, body and foot cone on the concave surface. This is in agreement with an involvement of all INO80 modules in substrate recognition as suggested by binding and activity assays. However, in order to satisfy all distance restraints from XL-MS analysis of the INO80-nucleosome complex, the flexible foot would have to fold back and grasp around the nucleosome. We indeed found this required

conformational flexibility in the foot region in both negative stain and cryo-EM. The described groove at the concave site of INO80 could form a flexible nucleosome binding pocket upon closure of the flexible foot region. Our results imply that INO80 has a distinct mechanism of interacting with the nucleosome by forming a flexible cradle that could partially embrace the nucleosome. RSC remodeler on the contrary are able to completely engulf nucleosomes (Chaban et al., 2008), whereas the binding site of SWI/SNF suggests an only partial envelopment (Dechassa et al., 2008). The notable structural divergence of INO80 and SWI/SNF type remodeler may reflect the catalysis of diverse actions by different chromatin remodeler families during chromatin remodeling and histone variant exchange.

Recently, the structure of the INO80 related SWR1 complex was solved by cryo-negative EM at 28Å resolution (Nguyen et al., 2013). INO80 and SWR1 share several subunits (Rvb1/2, Act1, Arp4), whereas others are homologous (the split ATPases Swr1 and Ino80 with the insertions and an HSA domain; Yaf9 and Taf14 both contain YEATS domains; Swc2 and Ies6 have YL-1 domains; Arp6 and Arp5; see Fig. 2C and 4). The 3D structure of SWR1 however differs from INO80: it is more compact, and globular, but also lacks an obvious nucleosome binding pocket. The nucleosome was shown to contact the SWR1 complex via the Swr1 ATPase domain and limited contacts by the C-module, which contains Swc2 that is known to interact with H2A.Z. Another clear difference between our INO80 structure and Leschziner's SWR1 structure is the assembly of the AAA+-ATPases Rvb1 and Rvb2: whereas EM and cross-linking analysis of our INO80 sample revealed that Rvb1/2 clearly adopt a double hetero-hexameric arrangement, the Rvb1/2 form only one hetero-hexameric ring in SWR1. It remains to be seen whether this discrepancy reflects a true difference between INO80 and SWR1 or results from different purification or data processing strategies. Without stabilization, we observed that the INO80 was prone to lose its Rvb1/2 head, and careful inspection of the SWR1 data indicates a similar behavior (Nguyen et al., 2013; Ranjan et al., 2013).

Within the INO80 structure, we localized functional modules in the elongated INO80 structure allowing us to speculate about implicated functions. A similar modular architecture with an N-module (Arp containing module) and a C-module (Swc2 containing module) has also been suggested for SWR1 (Nguyen et al., 2013), however the assignment of modules revealed a different arrangement in the compact SWR1 compared to the elongated INO80 complex. In INO80, the Ino80 ATPase domain is in close contact with the Rvb1/2 dodecamer, which explains the recruitment of the later by the ATPase

insertion (Tosi et al., 2013). In SWR1 on the other hand, the Swr1 ATPase is located on the other distal end in respect to the Rvb1/2 hexameric ring (Nguyen et al., 2013). In SWR1 the Arp4-containing module is located on one edge of the compact structure (Nguyen et al., 2013), whereas in INO80 the Arp4-containing module was mapped in the flexible and distal foot region (Tosi et al., 2013). Since assignment of subunits or modules in the density has not been reported for SWI/SNF type remodeler so far, a thorough structural comparison and correlation of structural features to different biochemical activities must await progress on architecture of SWI/SNF type remodeler (SWI/SNF and RSC). This is especially interesting because SWI/SNF and RSC like remodeler also have a Swi2/Snf2 or Sth1 subunit with an HSA domain and contain Arps, which are involved in histone binding. Both INO80 and SWI/SNF types of remodeler are suggested to exchange or remove H2A/H2B (or variant) dimers, albeit biochemical analysis also shows considerable differences in the remodeling reactions (Bruno et al., 2003; Mizuguchi et al., 2004; Papamichos-Chronakis et al., 2011). Given their small size, remodeler of the ISWI or Chd1 chromatin remodeler make only limited contacts to the nucleosome in comparison to INO80. ISWI remodeler for example have only a few contacts to the nucleosome core mediated by the Snf2 domain and engage extra-nucleosomal DNA with their characteristic HAND-SANT-SLIDE (HSS) domain and auxiliary subunits (Racki et al., 2009; Yamada et al., 2011). This is suggesting a yet different mode of interaction and probably remodeling mechanism compared to the large remodeler with their versatility of multiple subunits.

The head of the INO80 structure harbors the enigmatic AAA+-ATPases Rvb1 and Rvb2, which are essential for chromatin remodeling by INO80 (Jonsson et al., 2004) and have been implicated in cancer (Grigoletto et al., 2011; Huber et al., 2008; Menard et al., 2010). Rvb1/2 complexes have been intensely studied structurally with EM and crystallography. The functional role of Rvb1/2 in chromatin remodeler and other large complexes however was still elusive and needed to be addressed in future work. The assembly of Rvb1/2 into hexamers or dodecamers and the stacking arrangement within the dodecamer has been controversially discussed in the past. Our data allows the structural analysis of the Rvb1/2 complex within a native protein environment. Within the INO80 complex, we observed two hetero-hexameric Rvb1/2 rings stacked via their OB-fold containing domain 2. This arrangement is consistent with structural data on isolated Rvb1/2 complexes (Gorynia et al., 2011; Lopez-Perrote et al., 2012; Torreira et al., 2008). Interestingly, as mentioned already above the Rvb1/2 seem to adopt a hetero-hexameric

arrangement in the related SWR1 complex (Nguyen et al., 2013), which has also been described for isolated Rvb1/2 structures (Gribun et al., 2008). The authors argue that the hexameric Rvb1/2 is conserved also in INO80 by showing quantification of Coomassie-stained bands. However, in our hands a similar quantification of the highly purified and monodisperse intact INO80 showed a ratio of 1:5.4:5.5 for Ino80:Rvb1:Rvb2. More sophisticated methods for subunit stoichiometry determination, such as native mass spectrometry have to be applied on both the INO80 and SWR1 remodeler. What stoichiometry the Rvb1/2 adopts in other complexes and whether the difference observed in INO80 and SWR1 is biologically relevant remains to be analyzed. Recently it was demonstrated that conformational transitions of RuvBL1/2 dodecamers from elongated to more compact assemblies are driven by movements in domain 2, which might influence the DNA binding properties (Lopez-Perrote et al., 2012). The overall dimensions of Rvb1/2 dodecamers in the physiological context of INO80 are even smaller than the compact conformation observed for isolated RuvBL1/2 (Lopez-Perrote et al., 2012; Torreira et al., 2008). The variability in the length of isolated Rvb1/2 complexes might be restricted to the compact form within in the INO80 complex. We observed further structural differences between Rvb1/2 in the INO80 complex and isolated Rvb1/2. A more in depth examination reveals that the overall six-fold symmetry is not strict along the entire hexamer, but instead diverges at the site where the Rvb1/2 OB-folds are close to the neck of INO80. This deviation could be a result of the contact of the Snf2 ATPase of Ino80 and its insertion with the Rvb1/2 OB-folds. This also explains the recruitment of one Ino80 ATPase to one Rvb1/2 dodecamer mediated by the INO80 family specific insertion. The close structural vicinity of the Snf2 ATPase and the DNA binding OB-folds of Rvb1/2 suggests that conformational changes in Rvb1/2 could either directly cooperate with the Snf2 motor in nucleosome remodeling or histone variant exchange, or could help to modulate the interaction of INO80 with its substrate. Given the peripheral location of the Rvb1/2 complex, it is unlikely to be required during assembly or for the integrity of the INO80 complex, but rather contributes functionally to chromatin remodeling (Jonsson et al., 2004) and histone variant exchange.

The Rvb1/2 complex is responsible for the recruitment of Arp5 to INO80 (Jonsson et al., 2004). We localized the Arp5/Ies6-module in the neck at the back of the Snf2 Ino80 ATPase, in close proximity to the Rvb1/2 head. Interestingly, the Arp5-module is essential for remodeling and nucleosome stimulated ATPase activity, which might explain its localization close to the active catalytic center within the INO80 complex.

Human Arp5 has been shown to shuttle between the nucleus and cytoplasm (Kitayama et al., 2009) and yeast Arp5 is apparently also able to fulfill functions apart from the INO80 complex (Yen et al., 2012). The homologous subunit of Ies6 in SWR1, Swc2 has been proposed to act as a H2AZ/H2B chaperone (Mizuguchi et al., 2004; Wu et al., 2005). In INO80, Arp5-Ies6 could act as a histone chaperone and guide H2A/H2B or H2AZ-H2B dimers from or to INO80 during histone variant exchange. In agreement with this hypothesis, a recent study showed that upon deletion of Arp5, H2A.Z eviction is impaired and results in massively increased levels of H2A.Z at the +1 nucleosome (Yen et al., 2013). Another scenario could be that the Arp5-Ies6 module chaperones the histone octamer during the sliding process, stabilizing open or partially unwrapped nucleosome conformations.

The body of INO80 harbored the non-conserved, yeast specific Nhp10-module. Such a central location was rather unexpected, as there are no detectable sequence homologs of Nhp10 subunits (Nhp10, Ies1, Ies3, Ies5) in e.g. human or yeast. Structural conservation however must await analysis of the Nhp10 module and respective modules in other species. In agreement with the central location we identified the Nhp10-module as a high affinity nucleosome binding complex. Nhp10 belongs to the HMG2-box proteins, which are known interact with structurally distorted DNA (Ray and Grove, 2009, 2012), rendering Nhp10 a perfect candidate for binding to bent nucleosomal DNA. It is therefore reasonable that the DNA binding Nhp10-module is at this central location in close proximity to the Snf2 ATPase domain of Ino80. Despite being a high affinity nucleosome binding, the Nhp10-module is not required for proper ATPase hydrolysis stimulated or nucleosome sliding. This implies that the Nhp10-module might facilitate remodeling by stabilizing the nucleosome during the reaction by tight binding, but is not involved in direct catalysis of the reaction. This would also explain why the Nhp10 module is not conserved among species. It might also be possible that the Nhp10-module is required for or involved in substrate recognition and targeting of the INO80 complex.

The Arp8-module on the HSA domain of Ino80 is located in the distal foot region of Ino80. Subunits of the Arp8-module (Arp4, Arp8) have been implicated in histone binding (Gerhold et al., 2012; Harata et al., 1999; Shen et al., 2003), rendering this module suitable for interacting with the histone exposing side of the nucleosome. The structural arrangement of the HSA<sup>Ino80</sup>-Act-Arp4-Arp8 could partially be similar to the Arp7-Arp9 dimer described in the HSA<sup>Snf2</sup>-Arp7-Arp9-Rtt102 sub-complex of SWI/SNF (Schubert et al., 2013). Our XL-MS and EM data would be in accordance with an

elongated alpha-helical conformation of the HSA domain spanning the interface of actin-Arp4-Arp8 in INO80. However, the SWI/SNF HSA associated sub-complex contains only two Arps, whereas INO80 contains three and will therefore have to accommodate one additional Arp. Further interpretation of the Arp8-module of INO80 in the flexible foot region by high resolution methods will shed more light on its structural arrangement.

There is no obvious nucleosome binding site in INO80, but we could position the nucleosome in the central groove of the head-body-foot cone of INO80 using the XL-MS and negative stain EM analysis. At this location all modules of INO80 would be involved in nucleosome binding as suggested by our EMSA data. In order to satisfy all distance restraints from XL-MS, the flexible foot has to fold back in the direction of the head enclosing the bound nucleosome by forming a binding pocket. The observed conformational changes in INO80 could play a role in the remodeling reaction by assisting the formation or stabilizing of an "open" nucleosome conformations (Bohm et al., 2011) as reviewed in (Andrews and Luger, 2011). In "open" nucleosome conformations H2A-H2B dimers are partially dissociated from the H3-H4 tetramer, but remain bound to the neighboring DNA. INO80 could conceivably open the nucleosome like a book by binding to the intact nucleosome and stretching out to adopt the elongated conformation while staying bound to the nucleosome thereby dragging the H2A/H2B dimer away from the rest of the nucleosome. In this scenario, the "open" nucleosome formation would not only be formed by INO80, but could also be concomitantly stabilized. Within an intact nucleosome a few observed cross-links between Ies2 and helix  $\alpha 1$  of H3, Rvb2 to helix  $\alpha 2$  of H2B and Ies6 as well as Rvb2 to L1 of H4 are not surface exposed and thus only fulfilled, if or the nucleosome disk structure is opened up or the DNA at the entry/exit site of the nucleosome is already partially unwrapped. A partial unwrapping of DNA or an "open" nucleosome configuration would facilitate H2A/H2B dimer exchange by enhancing the accessibility. Interestingly, the Ino80 Snf2 cross-link site coincides with the binding site of the Snf2 fold of ISW2 on the nucleosome approximately at the SHL+2 (Dang and Bartholomew, 2007), implicating an analogy between both families of chromatin remodeler.



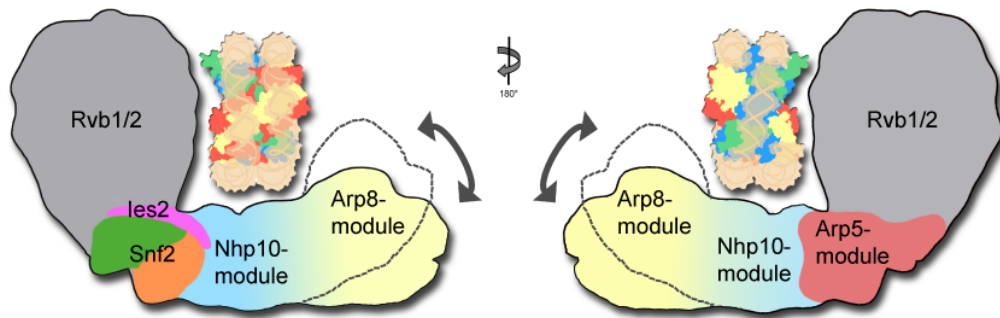


**Figure 37. Model of INO80 acting as a cradle to interact with the nucleosome.** The location of defined structural and functional modules was inferred from EM, XL-MS and DID-labeling. To bind the nucleosome, the flexible needs to fold back to bracket the nucleosome between the Rvb1/2 head and the Arp8-module in the foot.

The location of the structural and functional modules, the observed conformational flexibility in the foot region as well as the interaction of INO80 with the nucleosome implies that INO80 acts as a cradle (see Fig. 37). According to this model, the nucleosome is sandwiched between head and foot, with the nucleosomal DNA oriented towards the neck and body. The actin related Arps in Arp8- and Arp5-modules could help binding to histones at both sides of the nucleosome. This model is consistent with other studies according to which Arp4 and Arp8 (foot) bind histones (Gerhold et al., 2012; Harata et al., 1999; Shen et al., 2003), and Snf2 domains (neck) (Durr et al., 2005; Hauk et al., 2010; Thoma et al., 2005), Rvb1/2 OB-domains (head) (Matias et al., 2006), and Nhp10 (body) (Ray and Grove, 2009, 2012) bind DNA. The DNA close to the SHL+2 region could be spooled of the nucleosome surface by the Snf2 ATPase, generating a loop which then could be propagated as suggested over the octamer surface. Additionally, unwrapping of DNA in this region might facilitate access to the H2A/H2B dimer thereby promoting dimer exchange with the help of the Arp5-module.

Future work will focus on solving a 3D structure of the INO80 in complex with canonical and H2A.Z containing nucleosomes, preferably at different stages during the remodeling and variant exchange processes.

Our work has uncovered the structural and functional framework for the INO80 complex, providing now a basis for designing new experiments to mechanistically understand the involvement of INO80 in chromatin remodeling and histone variant exchange. Our hybrid approach is a considerable step forward in the understanding of the large and flexible macromolecular machines.

## 7 Materials and Methods

### 7.1 Materials

#### 7.1.1 Plasmids

**Table 3. Plasmids used in this study.**

Name	Gene	Promoter	Vector	Marker	Origin	Description	Source
pCH3	--	--	pUC18	Amp	pBR322	DNA amplification of 147bp of 601 sequence for mono-nucleosomes, use in DH5 $\alpha$ or XL1blue; Cut with SmaI	Widom/Müller-Planitz from P. Becker
pCH4	--	--	pUC18	Amp	pBR322	167bp long nucleosomes off-centered, 20bp overhang on left side, use in DH5 $\alpha$ or XL1blue; cut with SmaI	Widom/Müller-Planitz from P. Becker
pCH5	--	--	pUC18	Amp	pBR322	187bp long nucleosomes: off-centered with 40bp overhang on left side (SmaI) or centered with 20bp (EcoRV)	Widom/Müller-Planitz from P. Becker
pCH6	dH2A	T7	pET15b	Amp	pBR322	Expression of <i>D.m.</i> H2A in BL21(DE3); codon optimized	Müller-Planitz from P. Becker
pCH7	dH2B	T7	pET15b	Amp	pBR322	Expression of <i>D.m.</i> H2B in BL21(DE3); codon optimized	Müller-Planitz from P. Becker
pCH8	dH3	T7	pET3c	Amp	pBR322	Expression of <i>D.m.</i> H3 in BL21(DE3)	Nightingale from P. Becker
pCH9	dH4	T7	pET3c	Amp	pBR322	Expression of <i>D.m.</i> H4 in BL21(DE3)	Nightingale from Peter Becker
pFA6a KanMX6	Gentamicin	T7	pFA6a	Amp	pBR322	Kanamycin resistance marker, G418 selection	P. Wendler
pRS316	URA3 prom. and gene	T7	pBluescript	Amp	pBR322	URA3 auxotrophy marker for ura selection	K. Strässer
pCH13	GST-thrombin-CHRA14 & His <sub>8</sub> -TEV-CHRA16	Tac	pGEX2T	Amp	pBR322	Expression of bicistronic <i>D.m.</i> GST-CHRA14/ His <sub>8</sub> -CHRA16 in BL21(DE3) pLysS	Felix Hartlepp from P. Becker (pBCEXMaJo)
DID1-Nup120	DID1-Nup120	Trc	pProEx	Amp	pBR322	For DID tagging in yeast; fusion of DID1 to gene of interest	Flemming from E. Hurt
PrA-TEV-DID1	PrA-TEV-DID1	Trc	pProEx	Amp	pBR322	For DID tagging in yeast; fusion of DID1 to gene of interest	Flemming from E. Hurt
GST-FLAG-DID2	GST-FLAG-DID2	Trc	pProEx	Amp	pBR322	For DID tagging in yeast; DID2 is expressed in Rosetta(DE3)	Flemming from E. Hurt
His6-Dyn2	His6-Dyn2	T7	pET	Kan	pBR322	For DID tagging in yeast; Dynein2 (Dyn2) is expressed in Rosetta(DE3)	Flemming from E. Hurt
pCH10	His6-TEV-ISWI WT	Trc	pProEx HTb	Amp	pBR322	Expression of <i>D.m.</i> ISWI in BL21(DE3)	Müller-Planitz from P. Becker
ISWIK159R	His6-TEV-ISWI K159R	Trc	pProEx HTb	Amp	pBR322	Expression of <i>D.m.</i> ISWI Walker A mutant in BL21(DE3); t	This study
ISWI D256A	His6-TEV-ISWI D256A	Trc	pProEx HTb	Amp	pBR322	Expression of <i>D.m.</i> ISWI Walker B mutant in BL21(DE3)	This study
ISWI E257A	His6-TEV-ISWI E257A	Trc	pProEx HTb	Amp	pBR322	Expression of <i>D.m.</i> ISWI Walker B mutant in BL21(DE3)	This study

## 7.1.2 Primer

**Table 4. Oligonucleotides used in this study.** STOP codons are colored in red, URA3 homology is colored in orange, homology to the DID1-tag in pink and homology of gene of interest in green.

Primer	Sequence (5'→3')	T <sub>m</sub>	Template	Usage
1) 187cfor	ATCACCTATACGCGGAG	56°C	pCH5 187bp	for centered 187bp long nucleosomes
1)187Cy3for	Cy3-ATCACCTATACGCGGAG	56°C	pCH5 187bp	for centered 187bp long nucleosomes with a Cy3 label at 5' end
2) 187crev	ATCCATAACCCGAGTCGCC	56°C	pCH5 187bp	for centered 187bp long nucleosomes
3) 187offcfor	GGGCGACTCGGGTTATGG	56°C	pCH5 187bp	for off-centered 187bp long nucleosomes
4) 187offcrev	GGGGATGTATATATCTGACAC	56°C	Genomic yeast DNA	for off-centered 187bp long nucleosomes
INO1_+1-+359_fw	ATGACAGAAGATAATATTGCTCCAATC	55	Genomic yeast DNA	for INO1 nucleosomes
INO1_+1-+359_rv	TCGTAATCCCAAGTTTCAAGGTAG	55	Genomic yeast DNA	for INO1 nucleosomes
KanB rev	CTGCAGCGAGGAGCCGTAAT	69°C	pFA6a KanMX	check Geneticin G418 cassette in deletion strains
KanC for	TGATTTTGATGACGAGCGTAAT	64°C	pFA6a KanMX	check Geneticin G418 cassette in deletion strains
Arp8 up for	GAACAACTCTCGAACAAGG	58°C	Genomic yeast DNA from $\Delta$ arp8	amplify arp8 deletion box
Arp8 down rev	GCTACGGGGTATTGTCTC	58°C	Genomic yeast DNA from $\Delta$ arp8	amplify arp8 deletion box
Arp8 up check for	AGAGTGGTAAGTAACAAACAGAAC	58°C	Genomic yeast DNA from $\Delta$ arp8 candidates	check for right locus of deletion
Nhp10 up for	GTGATAGTCGGCAAAGG	57°C	Genomic yeast DNA from $\Delta$ nhp10	amplify nhp10 deletion box
Nhp10 down rev	GTGATATTAGGAATCGTCTG	54°C	Genomic yeast DNA from $\Delta$ nhp10	amplify nhp10 deletion box
Nhp10 up check for	GATCATCATTACTATCTACCATG	55°C	Genomic yeast DNA from $\Delta$ nhp10 candidate	check for right locus of deletion
Arp8 del L2 rev	GGGGATCCGTCGACCTGCAGCGTAC CATGTTAGGTGCGATTGTATCC	57°C	Genomic yeast DNA	deletion of ARP8 KanMX6, upstream of START rev
Arp8 del L3 for	AACGAGCTCGAATTCATCGATGATA TGAATATGCATATGGAAGTTTTG	58°C	Genomic yeast DNA	deletion of Arp8 by hand with KanMX6, downstream of STOP
L1 Arp5 up for	GAAGGTGACAATATAGAAGGG	57°C	pFA6a KanMX A	Amplification of deletion box
L4 Arp5 down rev	GGGTGTCAATCCAAAAG	57°C	pFA6a KanMX	Amplification of deletion box
Arp5 up check for	TACCAAAATGTGTGCAGG	59°C	Genomic yeast DNA from $\Delta$ arp5 candidate	check for right locus of deletion
L2 Arp5 del rev	GGGGATCCGTCGACCTGCAGCGTAC CATATACGTCTTATGTTTCAGAGTCC	57°C	Genomic yeast DNA	deletion by hand with KanMX6,

				upstream of START rev
<b>L3 Arp5 del for</b>	AACGAGCTCGAATTCATCGATGATA <b>TGA</b> AGGAGACAGCAAACTGAAAC	58°C	Genomic yeast DNA	deletion by hand with KanMX6, downstream of STOP
<b>L1 Ies1 up for</b>	AAAAGACCACTACTGTTATGACA	57°C	pFA6a KanMX	Amplification of deletion box
<b>L4 Ies1 down rev</b>	GGATAACGCTGAAGGTCA	59°C	pFA6a KanMX	Amplification of deletion box
<b>L1 Ies3 up for</b>	GAGAACTTGTTCCTTCGC	59°C	pFA6a KanMX	Amplification of deletion box
<b>L4 Ies3 down rev</b>	GGAGGTTGAGTTCGAGAAC	59°C	pFA6a KanMX	Amplification of deletion box
<b>L1 Ies5 up for</b>	CACGTTGCGGACTAAAC	58°C	pFA6a KanMX	Amplification of deletion box
<b>L4 Ies5 down rev</b>	ACGCAGTGAAGGAGATTAC	57°C	pFA6a KanMX	Amplification of deletion box
<b>L1 Dyn2 up for</b>	CCGACGAATGGATTATTATC	58°C	pFA6a KanMX	Amplification of deletion box
<b>L2 Dyn2 del rev</b>	GGGGATCCGTCGACCTGCAGCGTAC <b>CATTTTGGTTTTAATTGCTCTTC</b>	58°C	Genomic yeast DNA	deletion by hand with KanMX6, upstream of START rev
<b>L3 Dyn2 del for</b>	AACGAGCTCGAATTCATCGATGATA <b>TGA</b> ATAGTGTTCCTCAATAGTTAATCG	57°C	Genomic yeast DNA	deletion by hand with KanMX6, downstream of STOP
<b>L4 Dyn2 down rev</b>	CTACCCTCTCTGCAAACTC	58°C	pFA6a KanMX	Amplification of deletion box
<b>Dyn2 up check for</b>	GGCAAAGACGATGAAGAAG	60°C	Genomic yeast DNA from Δdyn2 candidate	check for right locus of deletion
<b>TagCxxx_1rev</b>	GAATAAAAAAAAAATGATGAATTGACT ACGTTCTCTTCCATATCG	60°C	DID1 plasmid	DID1 tagging with URA3 marker
<b>TagCxxx_2for</b>	CGATATGGAAGAAGGAACGTAGTCAATT CATCATTTTTTTTTTATTC	59°C	pRS316	DID1 tagging with URA3 marker
<b>TagCNhp10_1for_new</b>	CAAAAGTAGCTGATTCTAAAGGAGGTGAA GATGGAAGTTTAGTTTCCTCTAAC <b>ATGGCCAGGATCCAAAC</b>	58°C	DID1 plasmid	DID1 tagging with URA3 marker at Nhp10 C-terminus
<b>TagCNhp10_2rev_new</b>	CAATAAAGTTGAACAATTCTGGATAAAGCG CCTAGAACGTCTTACGATATCTTCCTA <b>GTTTTGCTGGCCGCATCTTC</b>	59°C	pRS316	DID1 tagging with URA3 marker at Nhp10 C-terminus
<b>TagCarp4_1for_new</b>	GGGAAAAAGGAATACGAAGAGGTGGGCGTCGAAA GATTGCTTAACGATAGGTTTAGA <b>ATGGCCAGGATCCAAAC</b>	60°C	DID1 plasmid	DID1 tagging with URA3 marker at Arp4 C- terminus
<b>TagCarp4_2rev_new</b>	GATCGAGTAGATGAATGGTCGCTCAAACCTG CTAAACTGAAAGGCGACTTGCTA <b>GTTTTGCTGGCCGCATCTTC</b>	60°C	pRS316	DID1 tagging with URA3 marker t Arp4 C- terminus
<b>TagC_Ies6_Did1_for</b>	GCGTCGATCAGGAGTACTTAAAATTGAGAG GGGCCAACTTCGTTCTAAAAA <b>ATGGCCAGGATCCAAAC</b>	62°C	DID1 plasmid	DID1 tagging with URA3 marker at Ies6 C- terminus
<b>TagC_Ies6_rev</b>	GTCGCACGTGACCAGCGACAAACTATGTAAG TGTGAAAGGTTGTCTACAAGCCTA <b>GTTTTGCTGGCCGCATCTTC</b>	69°C	pRS316	tagging with URA3 marker at Ies6 C-terminus
<b>TagC_Ies2_Did1_for</b>	GGGTATGACAAGAATTCTGCGGAGATATGAAG AAGACTTATTTGTACATTT <b>ATGGCCAGGATCCAAAC</b>	62°C	DID1 plasmid	DID1 tagging with URA3 marker of Ies2 C- terminus
<b>TagC_Ies2_rev</b>	GGTGTAAACAATAATACCGAGCCCAACCGATACC AACAGAAATAAAACAACGCTA <b>GTTTTGCTGGCCGCATCTTC</b>	69°C	pRS316	tagging with URA3 marker of Ies2 C-term
<b>Ies2 check for</b>	GCAAGATGCTGTTAGATTGT	58°C	DNA from Ies2-DID1 candidate	300bp before stop (1300bp pos, 300bp neg)

<b>ISWIK159Rforlong</b>	GAAATGGGTCTAGGACGTACCCTGCAGACCATATC	80°C	pCH10 ISWI WT	Site directed mutagenesis Walker A mutant
<b>ISWIK159Rrevlong</b>	GATATGGTCTGCAGGGTACGTCCTAGACCCATTTC	80°C	pCH10 ISWI WT	Site directed mutagenesis
<b>ISWI D256A for</b>	CGCTATTGGTCATCGCGGAGGCGCATCGTATCAAGAACG	87°C	pCH10 ISWI WT	Site directed mutagenesis Walker B mutant
<b>ISWI D256A rev</b>	CGTTCTTGATACGATGCGCCTCCGCGATGACCAAATAGCG	87°C	pCH10 ISWI WT	Site directed mutagenesis
<b>ISWI E257A for</b>	CGCTATTGGTCATCGACGCGGCGCATCGTATCAAGAACG	87°C	pCH10 ISWI WT	Site directed mutagenesis Walker B mutant
<b>ISWI E257A rev</b>	CGTTCTTGATACGATGCGCCGCGTCGATGACCAAATAGCG	87°C	pCH10 ISWI WT	Site directed mutagenesis

### 7.1.3 Yeast strains

**Table 5.** Yeast strains used in this study.

Strain	Genotype	Source
INO80-FLAG <sub>2</sub>	<i>MATa INO80-FLAG<sub>2</sub> his3Δ200 leu2Δ0 met15Δ0 trp1Δ63 ura3Δ0</i>	(Shen et al., 2000)
INO80Δarp5	<i>MATa INO80-FLAG his3Δ200 leu2Δ0 met15Δ0 trp1Δ63 ura3Δ0 arp5Δ::KanMX6</i>	Tosi et al., 2013
INO80Δarp8	<i>MATa INO80-FLAG his3Δ200 leu2Δ0 met15Δ0 trp1Δ63 ura3Δ0 arp8Δ::KanMX6</i>	Tosi et al., 2013
INO80Δnhp10	<i>MATa INO80-FLAG his3Δ200 leu2Δ0 met15Δ0 trp1Δ63 ura3Δ0 nhp10Δ::KanMX6</i>	Tosi et al., 2013
INO80Δdyn2	<i>MATa INO80-FLAG his3Δ200 leu2Δ0 met15Δ0 trp1Δ63 ura3Δ0 dyn2Δ::KanMX6</i>	Tosi et al., 2013
Arp4-DID1	<i>MATa INO80-FLAG his3Δ200 leu2Δ0 met15Δ0 trp1Δ63 dyn2Δ::KanMX6 Arp4-DID1::URA3</i>	Tosi et al., 2013
Nhp10-DID1	<i>MATa INO80-FLAG his3Δ200 leu2Δ0 met15Δ0 trp1Δ63 dyn2Δ::KanMX6 Nhp10-DID1::URA3</i>	Tosi et al., 2013
Ies6-DID1	<i>MATa INO80-FLAG his3Δ200 leu2Δ0 met15Δ0 trp1Δ63 dyn2Δ::KanMX6 Ies6-DID1::URA3</i>	Tosi et al., 2013
Ies2-DID1	<i>MATa INO80-FLAG his3Δ200 leu2Δ0 met15Δ0 trp1Δ63 dyn2Δ::KanMX6 Ies2-DID1::URA3</i>	Tosi et al., 2013

## **7.2 Methods**

### **7.2.1 General methods in molecular biology**

#### **7.2.1.1 Polymerase chain reaction**

The polymerase chain reaction (PCR) was used for the amplification of specific double stranded DNA fragments for cloning, yeast manipulation or as DNA template for nucleosome reconstitution. The Phusion Flash High Fidelity Master Mix (Finnzymes) was used according to the manufacturer's protocol. Self-made Taq polymerase (Charlotte Ungewickell, AG Beckmann) was used with a 10x Taq buffer (100 mM Tris pH 8.8, 500mM KCl, 0.8% Triton X-100, 15 mM MgCl<sub>2</sub>) and a dNTP mix (Roth). The concentrations of template and primers in the reactions are indicated in the respective sections. Cycling conditions were chosen depending on the fragment length and primer composition and are indicated in the respective sections. All primers were either synthesized by Metabion or BioTeZ (see Table 4 in section 7.1.2).

For cloning, primers were used that introduced a restriction site at the 5'- and 3'-end of the fragment. This allowed directional ligation into plasmids adding a tag for purification in frame. For site directed mutagenesis, primers containing the desired mutation were used to amplify the complete plasmid. The original plasmid was digested by addition of DpnI for 1 h at 37°C. The PCR amplified plasmid containing the specific alterations was then transformed into *E. coli*.

#### **7.2.1.2 Precipitation of proteins**

Proteins were concentrated for SDS PAGE by trichloroacetic acid (TCA). The sample was filled up to 1 ml with cold water. For precipitation of proteins, 100 µl of 15% sodiumdeoxycholate and 100 µl 72% TCA were added. The sample was vortexed and incubated on ice for 20 min. The precipitated proteins were collected by centrifugation (4°C, 20 min, 14.000 rpm). The supernatant was removed and the pellet was washed with 1 ml ice cold acetone. The pellet was air dried for 10 min at RT. The sample was resuspended in 10 µl 1x SB buffer, and neutralized if required with 1 M Tris Base.

### 7.2.1.3 SDS-polyacrylamide gel electrophoresis

Proteins were separated by size using denaturing discontinuous SDS-polyacrylamide gel electrophoresis (SDS-PAGE) (Laemmli, 1970). Samples were mixed with 4x sample buffer (200 mM Tris pH 6.8, 8% (w/v) SDS, 0.4% (w/v) bromphenol blue, 40% (v/v) glycerol, 400 mM DTT), heated for 5min at 95°C or 10min at 65°C and loaded on an 8-18% polyacrylamide gel. Electrophoresis was performed at 150-180 V for 30-60 min in Mini-Protean II electrophoresis cells (Bio-Rad) with a running buffer containing 25 mM Tris, 192 mM glycine and 0.1% SDS.

After electrophoresis, the gel was fixed and stained using Coomassie Blue staining solution (0.25% (w/v) Coomassie Blue R 250, 50% (v/v) ethanol, 10% (v/v) acetic acid) or SimplyBlue™ SafeStain (Invitrogen) according to the manufacturer's protocol. Excess staining was removed by repeated washing steps with de-staining solution (40% (v/v) ethanol, 10% (v/v) acetic acid) in case of Coomassie BlueR or with water in the case of SimplyBlue™. The gel was digitized using a standard flat bed scanner.

### 7.2.1.4 Silver staining of SDS gels

For silver staining, the gel was washed with water and incubated twice for 10 min in fixing solution (10% acidic acid, 45% methanol), twice for 10 min in 50% ethanol, once for 10 min with 30% ethanol. The gel was sensitized by shaking in 0.8 mM  $\text{Na}_2\text{S}_2\text{O}_3$  for 60 sec and washed off three times for 20 sec with water. The gels was shaken for 20 min in staining solution (2%  $\text{AgNO}_3$ , 0.026% formaldehyde), washed three times for 20 sec with water. Visualization was done by adding developer solution (6%  $\text{Na}_2\text{CO}_3$ , 0.0185% formaldehyde, 16  $\mu\text{M}$   $\text{Na}_2\text{S}_2\text{O}_3$ ). When the desired staining degree was reached, the developing process was stopped by adding 10% acidic acid. The gel was shaken for 1 hr at RT, and stored in water.

### 7.2.1.5 Native polyacrylamide gel electrophoresis

For native polyacrylamide electrophoresis, 4, 5 and 8 % gels were casted with acrylamide, TEMED and APS in 0.5 x TBE buffer. Gels were pre-run at 4°C for 90 min at 130 V to remove the APS and TEMED. Samples were loaded with 5% glycerol. The

gels were run at 4°C for 90-120 min at 100 V. For comparison between the gels, a 100 bp DNA ladder from NEB was used.

The gels were stained in 10 ml 0.5 x TBE with 1:500 SybrGreenI (Invitrogen) at RT for 30 min. After rinsing the gel with 0.5 x TBE, the gel was digitized at 300 nm using the Intas Gel Documentation System or using a Typhoon 9400 scanner (Amersham) at 488 nm excitation wavelength and 488 nm emission filter.

#### **7.2.1.6 Agarose gel electrophoresis**

DNA was analyzed by agarose gel electrophoresis. Gels were prepared with 1.0-1.2% agarose in 1x TAE buffer (40 mM Tris/HCl pH 8.0, 20 mM acetic acid, 1 mM EDTA) or 0.5 x TBE buffer (4.5 mM Tris, 45 mM boric acid, 0.1 mM EDTA pH 8.0). Before loading, the DNA samples were mixed with 6x Gel Loading Dye (NEB) and SybrGreenI (Invitrogen) according to the manufacturer's recommendations. The 100 bp and 1 kb DNA ladder Plus from NEB were used for size comparison. Gels were run at 100-120 V for 20-40 min using the PerfectBlue Gelsystem Mini (Peqlab). The gel was digitized at 300 nm using the Intas Gel Documentation System.

#### **7.2.2 GraFix**

GraFix was in principal performed as described (Kastner et al., 2008). ISWI (0.5-1 mM) was incubated with 187 bp long centered nucleosomes (200-600 nM) in presence of 2 mM ATP for 30 min at RT. Major aggregations were pelleted (4°C, 10 min, 10.000 rpm). The reaction mix was loaded onto a 5 - 25% sucrose gradient (50 mM Hepes pH 7.6, 100 mM KOAc, 1 mM EDTA, 2.5 mM Mg(OAc)<sub>2</sub>, 1 mM DTT) (Gradient Station, Biocomp). 0.1% glutaraldehyde (25% EM grade, agar) was added to 25% sucrose solution. The gradients were spun at 4°C with 35.000 rpm for 25 hrs 39 min in a SW60 Ti rotor (Beckman). The fractions were collected by hand, TCA precipitated and analyzed by SDS PAGE and silver staining.



### 7.2.3 General methods with *E. coli*

#### 7.2.3.1 Strains

For amplification of the plasmids the *E. coli* XL1-blue strain (genotype: *recA1 endA1 gyrA96 thi-1 hsdR17 supE44 relA1 lac* [F' *proAB lacIqZΔM15 Tn10* (Tet<sub>r</sub>)]; Stratagene) or DH5α (genotype: F<sup>−</sup> Φ80*lacZΔM15 Δ(lacZYA-argF)* U169 *recA1 endA1 hsdR17* (rK<sup>−</sup>, mK<sup>+</sup>) *phoA supE44 λ<sup>−</sup> thi-1 gyrA96 relA1*; Invitrogen<sup>TM</sup>) was used. For heterologous expression *E. coli* BL21(DE3) (genotype: *fhuA2 [lon] ompT gal (λ DE3) [dcm] ΔhsdS λ DE3 = λ sBamHI ΔEcoRI-B int::(lacI::PlacUV5::T7 gene1) i21 Δnin5*; Invitrogen<sup>TM</sup>), BL21(DE3)pLysS (as BL21(DE3) + pLysS, which carries the gene encoding T7 lysozyme to lower the background expression level of the target genes; Invitrogen<sup>TM</sup>) or Rosetta<sup>TM</sup>(DE3) (genotype: F<sup>−</sup> *ompT hsdSB(rB<sup>−</sup> mB<sup>−</sup>) gal dcm* (DE3), pRARE (Cam<sub>r</sub>, coding for rarely used tRNAs; Merck) were used.

#### 7.2.3.2 Chemically competent cells

For preparation of chemically competent *E. coli*, LB was inoculated 1:200 with an overnight culture of the strain of interest and grown at 37°C. At OD<sub>600</sub> = 0.6 the culture was cooled on ice for 15 min and the cells were harvested by centrifugation in sterile centrifuge beakers at 4°C with 4000 rpm for 10 min in a SLC6000 rotor (Sorvall). The pellet was suspended in cold 0.1 M CaCl<sub>2</sub> and incubated on ice for 30 min. After pelleting, the cells were resuspended in 0.1 M CaCl<sub>2</sub> and 15% glycerol. Aliquots of chemically competent cells were frozen in liquid nitrogen and stored at -80°C.

#### 7.2.3.3 Media

*E. coli* cells were grown in liquid LB medium or on LB plates. LB medium is prepared with 1% Bacto<sup>TM</sup> Peptone (BD Bionutrients), 1% NaCl, 0.5% Bacto<sup>TM</sup> Yeast Extract (BD Bionutrients) and for plates 15 g/l Bacto<sup>TM</sup> Agar (BD Bionutrients). The medium was autoclaved at 121°C for 20 min. To plates the required antibiotics were added when the media was hand-warm before pouring the plates. For liquid cultures, the appropriate antibiotic was added 1:1000 prior to use (ampicillin (100 mg/ml in H<sub>2</sub>O), kanamycine (50 mg/ml in H<sub>2</sub>O) and chloramphenicol (34 mg/ml in ethanol)).

### 7.2.3.4 Transformation

For transformation of chemically competent cells, 100 µl cells were thawed on ice and mixed with 40-100 ng purified plasmid DNA and incubated on ice for 10 min. After a heat shock at 42°C for 45 sec, the cells were kept on ice for additional 5 min. 1 ml LB was added and the cells were recovered at 37°C for 30-60 min in a Thermomixer comfort (Eppendorf) with 600 rpm. 100- 200 µl of the transformed cells were plated on LB plates containing the appropriate antibiotics and incubated at 37°C over night. Transformation plates were stored for a few weeks at 4°C.

### 7.2.3.5 Isolation of plasmids and sequencing

Single colonies were grown in 5 ml LB containing the appropriate antibiotic at 37°C over night. The plasmid DNA was isolated using the QIAprep®Spin Miniprep Kit (Qiagen) according to the manufacturer's protocol. After test-digestion, 1.5 µg purified plasmid, if required with the respective sequencing primers, was sent for sequencing to Eurofins MWG.

### 7.2.4 Expression and purification from *E. coli*

For *D.m.* core histone expression, a fresh colony of the respective plasmid in BL21(DE3) was used to inoculate 4 L of LB<sub>Amp</sub> and incubated at 200 rpm at 37°C and 200 rpm. Expression was induced by addition of 1 mM IPTG at OD<sub>600</sub> = 0.6 for 2 hrs. Cells were harvested at 4°C with 4000 rpm for 10 min in a SLC6000 rotor (Sorvall) and resuspended in 5-10 ml Sau-0 buffer (7 M urea, 20 mM NaOAc pH 5.2, 1 mM EDTA pH 8.0, 5 mM β-mercaptoethanol; prepared freshly), flash frozen in liquid nitrogen and stored at -80°C.

For expression of *D.m.* ISWI, a fresh colony of the respective plasmid in BL21(DE3) was used to inoculate 2 L LB<sub>Amp</sub>. Expression was induced with 0.2 mM IPTG at 16°C for 16 hrs. Cells were harvested as described above and resuspended in His buffer (50 mM Tris pH 7.4, 300 mM NaCl, 1 mM PMSF). The cell pellets were flash frozen in liquid nitrogen and stored at -80°C.

For expression of CHRAC14/16, plasmid pCH13 (see Table 3 in section 7.1.1) was transformed into BL21(DE3)pLysS and single colonies were used to inoculate LB<sub>AMP/CAM</sub>. AT OD<sub>600</sub> = 0.8, expression was induced with 0.3 mM IPTG at 30°C for

3 hrs. The cells were harvested and resuspended in 10 ml PBS with protease inhibitors per L culture, flash frozen in liquid nitrogen and stored at -80°C.

For DID labeling, Dyn2-His<sub>6</sub> (for plasmids see Table 3 in section 7.1.1) transformed into Rosetta(DE3). At OD<sub>600</sub> = 0.6-0.8 expression was induced with 0.5 mM IPTG at 23°C for 3-4 hrs. Cells were harvested and stored as described above. DID2 expression was performed equivalent to Dny2.

#### 7.2.4.1 Purification of *D.m* His<sub>6</sub>-TEV-ISWI

*D.m.* ISWI was over-expressed heterologously in *E. coli* with an N-terminal His<sub>6</sub> tag and a TEV protease cleavage site for removal of the tag (for primer see Table 4 in section 7.1.2, for plasmid see Table 3 in section 7.1.1).

Cell pellets were thawed and resuspended in 30 ml buffer His (50 mM Tris pH 7.4, 300 mM NaCl, 20 mM imidazole, 1 mM PMSF, 1 Complete Protease Inhibitor Cocktail tablet (Roche), 0.5 mM β-mercaptoethanol). The cells were lysed with three runs in a microfluidizer (Microfluidics) at a pressure of 1500 psi and sonicated (2 min effective sonication time, pulse 10'' on/10'' off, amplitude of 15%, Branson sonifier 250, Emerson). Benzonase® Nuclease (Novagen, 250 U/μl 8 μl per L culture) was added to digest the DNA and RNA; alternatively DNase was added. The lysate was cleared by spinning at 4°C with 19,000 rpm for 30 min in a SS34 rotor (Sorvall).

For affinity purification, the lysate was applied to a 5 ml HisTrap FF (GE Healthcare) with His-A buffer including 20 mM imidazole to minimize background binding. After washing for 10 CV with 5% buffer His-B (20 mM imidazole) (buffer His-A: 50 mM Tris pH 7.4, 300 mM NaCl; buffer His-B: 50 mM Tris pH 7.4, 300 mM NaCl, 400 mM imidazole). A second wash for 6 CV was performed at 10% buffer His-B (40 mM imidazole). Elution was performed with a gradient over 7 CV with a flow-rate of 2 ml/min from 20-100% buffer His-B (80-400 mM imidazole). 1.5 ml fractions were collected and analyzed by 8% SDS PAGE. Fractions were pooled according to the amount and purity of ISWI.

The His<sub>6</sub> tag was cleaved off by adding TEV protease (self-made, Heidi Sieber, AG Beckmann) and 4 mM β-mercaptoethanol. Concomitantly, the imidazole was removed by dialysis against 5% His-B buffer at 4°C over night. A second nickel affinity chromatography was used to separate cleaved from uncleaved ISWI.

DNA and other contaminations were removed by cation affinity purification. A 1 ml Mono S 5/50 GL column (GE Healthcare) was loaded with cleaved ISWI with 5% buffer B (100 mM NaCl) (buffer A (15 mM Tris pH 8.0, 1 mM  $\beta$ -mercaptoethanol) and buffer B (15 mM Tris pH 8.0, 2 M NaCl, 1 mM  $\beta$ -mercaptoethanol)). The flow through containing ISWI was collected. After washing for 5 CV with 5% buffer B (100 mM NaCl), the DNA and contaminations were eluted in two gradients from 5-30% B (100-600 mM NaCl) and 30-100% B (600-2000 mM NaCl). The fractions were analyzed by 8% SDS PAGE, pooled accordingly and concentrated using Amicon®Ultra Centrifugal Filters (Ultracel-30K, Milipore).

To remove aggregation and to achieve homogeneity, the purified ISWI sample was subjected to size exclusion chromatography (Superdex200 HR10/300 GL S200, GE Healthcare) with a gel filtration buffer (50 mM Hepes-KOH pH 7.6, 0.2 mM EDTA, 200 mM KOAc, 10 mM  $\beta$ -mercaptoethanol). The elution was pooled and concentrated using Amicon®Ultra Centrifugal Filters (Ultracel-30K, Milipore). The concentration was determined using a NanoDrop 1000 photospectrometer (Thermo Scientific) (extinction coefficient of ISWI  $\epsilon_{280}=119950$  cm/M). Small aliquots of pure and homogenous ISWI were flash frozen in liquid nitrogen and stored at -80°C.

#### **7.2.4.2 Purification of *D.m* Acf1**

##### ***7.2.4.2.1 Baculovirus expression system***

Expression of ACF and ISWI (ACF1-Flag virus was a kind of from James Kadona from Peter Becker's group, FLAG-ISWI Toshi Tsukiyama from Peter Becker's group) was done in Sf21 cells.  $1 \times 10^6$  Sf21 cells were grown in suspension with Sf-900II medium (Gibco) complemented with 9% foetal bovine serum (Sigma) were infected with both baculoviruses for 72 h at 27°C. The Cells were harvested and the supernatant containing the virus were sterile-filtered. Amounts of virus had to be titrated for optimal yield and the necessary 1:1 stoichiometry of ACF1 and ISWI to obtain functional ACF complexes. Protein expression was allowed for 72 h at 27°C.

##### ***7.2.4.2.2 Small scale purification***

In order to check expression and stoichiometry of the ACF complex (ISWI 120 kDa and Acf1 170 kDa), a small scale purification was performed. The infected Sf21 cells were

resuspended in 15 ml ACF crack buffer (100 mM Tris pH 7.8, 500 mM KOAc, 10% glycerol, 10 mM EDTA, 1 mM PMSF, protease inhibitor) per L culture and stored in 10 ml aliquots at -80°C. Cells were thawed and filled with 30 ml per L with ACF crack buffer with 1 Complete Protease Inhibitor Cocktail tablet (Roche). Cells were lysed by sonication for six rounds (2 min effective sonication time, pulse 10''on/10'' off, amplitude of 12%, Branson sonifier 250, Emerson). The lysate was cleared by centrifugation at 4°C with 19,000 rpm for 30 min in a SS34 rotor (Sorvall). The supernatant was incubated with pre-equilibrated FLAG beads (0.5 ml beads per L culture, ANTI-FLAG® M2 Magnetic Beads (Sigma-Aldrich)) at 4°C for 2 hrs on a rotation wheel. The beads were harvested by mild centrifugation (4°C, 2000 rpm, 1 min). The beads were washed five times with wash buffer (100 mM Tris pH 7.8, 500 mM KOAc, 10% glycerol, 1mM PMSF, 0.2 mM EDTA pH 8.0, 0.2% CHAPSO, protease inhibitors) and collected by centrifugation. After washing with ACF elution buffer without FLAG peptide (80 mM Tris pH 7.8, 400 mM KOAc, 8% glycerol, 1M urea, 1mM DTT), elution was performed twice with 2 CV elution buffer containing 0.5 mg/ml Flag peptide and for 60 min on a rotation wheel. The elutions were pooled, and centrifuged at 4°C with 14,000 rpm for 10 min to remove residual beads and aggregation. Finally, the expression and subunit stoichiometry was analyzed on a 8% SDS PAGE.

#### **7.2.4.2.3 Large scale purification**

Cells were harvested, resuspended in 15 ml ACF crack buffer per L culture, flash frozen in liquid nitrogen and stored at -80°C. Cells were thawed and filled up with 30 ml ACF crack buffer per L culture including protease inhibitors. Cells were cracked by sonication (2 min effective sonication time, pulse 10''on/10'' off, amplitude of 30%, Branson sonifier 250, Emerson). The lysate was twice cleared as described above (4°C, 19,000 rpm, 10 min, SS34 and 4°C, 19,000 rpm, 20 min, SS34). The supernatant was filtered through two layers of miracloth (Calbiochem). Additional protease inhibitors were added and FLAG affinity purification was performed equivalent to the small scale purification, except that the incubation period was expanded to 2 hrs. The elution fractions were pooled

The FLAG elution fractions were filtered with a syringe filter (Millex® Syringe-driven Filter Unit, 0.45 µm, Millipore) and then loaded on an anion exchange chromatography to remove residual DNA and other contaminations. The 1 ml MonoQ

column 5/50 GL (GE Healthcare) was equilibrated with 15% buffer B (240 mM NaCl; buffer A 12 mM Tris pH 8.0, 1 urea, 1 mM DTT, buffer B 12 mM Tris pH 8.0, 1.6 M NaCl, 1 M urea, 1 mM DTT), the sample was loaded with 1 ml/min, the flow through was collected. The column was washed for 10 CV with 15% buffer B and eluted with two gradients: over 6 CV from 15-55% (240 mM - 880 mM NaCl) at 1.5 ml/min, and over 2 CV from 55-100% B (880 mM – 1.6 M NaCl). ACF eluted at ~25% B (400 mM NaCl at 30-36mSi/cm). The fractions were analyzed by 8% SDS PAGE and fractions containing pure ACF were pooled, and precipitations were removed by centrifugation (4°C, 14.000 rpm, 10 min).

Finally, the ACF sample was applied to a size exclusion chromatography to ensure homogeneity of the purification. The sample was loaded onto Superose 6 (GE Healthcare), equilibrated with buffer GeFi (80 mM Tris pH 7.8, 400 mM KOAc, 1 M urea, 1.5 mM Mg(OAc)<sub>2</sub>, 10 mM DTT, 0.2% CHAPSO). 0.5 ml fractions were collected and concentrated using Amicon®Ultra Centrifugal Filters (Ultracel-30K, Milipore) to ~1-2 mg/ml according to the manufacturer's manual. The sample was centrifuged at 4°C with 14.000 rpm for 10 min, the concentration was measured using a NanoDrop 1000 photospetrometer (Thermo Scientific) (extinction coefficient of ACF  $\epsilon_{280}$ =244220 cm/M, 0.844 cm·L/g) and the purity was controlled on 8% SDS-PAGE. Aliquots of ACF were flash frozen in liquid nitrogen and stored at -80°C.

#### 7.2.4.3 Purification of *D.m.* CHRAC14/16

Purification of the two small histone fold proteins CHRAC14 and CHRAC16 was performed with a tandem affinity purification of the GST and His<sub>8</sub>-tag on CHRAC14 and CHRAC16, respectively (for plasmids see Table 3 in section 7.1.1).

Cells were lysed with three runs in a microfluidizer (Microfluidics) at a pressure of 1500 psi and sonicated (pulse 20'' on/20'' off, amplitude of 30%, Branson sonifier 250, Emerson). The cell lysate was cleared (4°C, 19.000 rpm, 30 min, SS34).

For the first affinity purification, the cell lysate was incubated with Ni-NTA agarose beads (2 ml per 1 L culture, Protino® Macherey and Nagel), pre-equilibrated with HEMG buffer (25 mM Hepes-KOH 7.6, 500 mM KCl, 1.5 mM MgCl<sub>2</sub>, 0.1 mM EDTA, 10% glycerol) at 4°C for 1 hr on a rotating wheel. The flow through was collected and the beads were washed with 1 CV HEMG, 2 CV HEMG-50 (50 mM imidazole) and 1 CV HEMG-100 (100 mM imidazole). The hetero-dimer of CHRAC14/16 was eluted

with steps of imidazole (150-500 mM imidazole). Over night at 4°C during dialysis against a HEMG buffer without imidazole, the His-tag was cleaved off CHRAC16 by addition of TEV protease.

For the second affinity purification step, Glutathione Sepharose™ 4 Fast Flow (2.5 ml per L culture, GE Healthcare) was pre-equilibrated with PSB pH 7.4 (137 mM NaCl, 2.7 mM KCl, 10 mM Na<sub>2</sub>HPO<sub>4</sub>, 2 mM KH<sub>2</sub>PO<sub>4</sub>) containing 0.05% NP-40 (IPEGAL® CA-630, Sigma-Aldrich) and collected at 4°C with 2000 rpm for 5 min. The pool from Ni-NTA elution was bound to the GST beads at 4°C for 3 hrs on a rotating wheel. Unbound sample was washed off by 1 CV PBS/0.05% NP-40, 2 CV PBS500/0.05% NP-40 (500 mM NaCl), 1 CV PBS/0.05% NP-40. Before cleavage, the beads were pre-equilibrated 1:1 with PBS/0.05% NP-40 with 1 mM CaCl<sub>2</sub> and the incubated with thrombin protease (GE Healthcare, 1 U/350 µg protein) for 3 hrs at room temperature on a rotating wheel. Alternatively, the complex was eluted with 100 mM Tris pH 8.0, 30 mM reduced L-Glutathione (Sigma-Aldrich) and cleaved afterwards. The elution was collected and pooled with a wash with 2 CV PBS/0.05% NP-40).

The purified complex was concentrated and flash frozen in liquid nitrogen and stored at -80°C.

#### **7.2.4.4 Purification of GST-TEV-FLAG-DID2**

For purification of GST-TEV-FLAG-DID2, cells were thawed in resuspended in modified H.02 buffer (25 mM HEPES pH 7.6, 200 mM KCl, 3% glycerol, 1 mM MgCl<sub>2</sub> and 1 mM DTT including protease inhibitors: 1 complete Protease Inhibitor Cocktail tablet (Roche), 1 mM PMSF; use 5-10 ml per L culture). The cells were lysed with three runs in a microfluidizer (Microfluidics) at a pressure of 1500 psi and sonicated six times (pulse 10'' on/10'' off, amplitude of 15%, Branson sonifier 250, Emerson). Cells were harvested by centrifugation (4°C, 19.000 rpm, 30 min, SS34).

For affinity purification, pre-equilibrated Glutathione Sepharose™ beads 4 Fast Flow (GE Healthcare; 1 ml per L culture) were incubated with the cleared cell lysate at 18°C for 1 hr on a rotating wheel. The flow through was collected by gravity flow and washed with 10 CV H0.2 buffer, 10 CV with H.05 (25 mM HEPES pH 7.6, 500 mM KCl, 3% glycerol, 1 mM MgCl<sub>2</sub> and 1 mM DTT, 1 mM PMSF) and again for 10 CV H0.2 buffer. For elution, H.02 was complemented with 10 mM reduced L-Glutathione (Sigma-Aldrich). Elution was performed three times with 1 CV at 4°C for 5 min. TEV cleavage

efficiency was also tested. Fractions were pooled according to 18% SDS PAGE, concentrated, flash frozen in liquid nitrogen and stored at -80°C.

#### **7.2.4.5 Purification of His<sub>6</sub>-Dyn2**

Cells from 6 L were thawed and resuspended in 30 ml buffer in a modified H.02 buffer (25 mM HEPES pH 7.6, 200 mM KCl, 3% glycerol, 1 mM MgCl<sub>2</sub> and 1 mM DTT including protease inhibitors: 1 complete Protease Inhibitor Cocktail tablet (Roche), 1 mM PMSF). The cells were lysed with three runs in a microfluidizer (Microfluidics) at a pressure of 1500 psi and sonicated six times (pulse 10''on/10'' off, amplitude of 15%, Branson sonifier 250, Emerson). Cells were harvested by centrifugation (4°C, 19.000 rpm, 30 min, SS34).

For affinity purification, 2.5 ml pre-equilibrated Ni-NTA agarose beads (Protino®, Macherey and Nagel) were incubated with the supernatant at 4°C for 60 min. The flow through was collected, and the beads were washed with 8 CV H0.2 buffer containing 10 mM imidazole, 8 CV H0.2 buffer containing 20 mM imidazole and eluted with 3x 3 CV H0.2 buffer containing 150 mM imidazole and 3x 3 CV H0.2 buffer containing 500 mM imidazole. Elution fractions were pooled according to 18% SDS PAGE and concentrated for gel filtration. The sample was finally purified over a size exclusion chromatography (S75 26/60, GE Healthcare) with H.02 buffer. Fractions containing pure and homogenous Dyn2-His<sub>6</sub> were pooled, concentrated and stored in small aliquots at -80°C after flash freezing the protein.

### **7.2.5 Reconstitution of nucleosomes**

#### **7.2.5.1 DNA preparation**

DNA for nucleosomes was prepared in two ways, either from a plasmid preparation with PEG followed by restriction enzyme digestion and acrylamide gel purification or via PCR followed by agarose gel purification.



### ***7.2.5.1.1 DNA large scale PEG precipitation***

For the plasmid preparation, a fresh colony of a 601 positioning sequence containing plasmid (see Table 3 in section 7.1.1 in DH5 $\alpha$  or XL1blue (a strain without recombinase) was used to inoculate 4L of terrific broth (TB) medium (for 1L mix 950ml medium with 50ml 20x TB salts; 950 ml TB medium: 12g bactotryptone, 24g yeast extract, 4ml glycerol; 20x TB salts: 0.17 M KH<sub>2</sub>PO<sub>4</sub>, 0.72 M KH<sub>2</sub>PO<sub>4</sub>). Cells were grown at 37°C to an OD<sub>600</sub> = 4-6 and harvested at 4°C with 4000 rpm for 15min in a SLC6000 rotor (Sorvall). Cells were washed with water flash-frozen in liquid nitrogen and stored at -80°C. The cells were thawed and resuspended in 300 ml P1 buffer (50 mM Tris-HCl pH 8.0, 10 mM EDTA pH 8.0) at RT and were lysed by adding 400 ml P2 buffer (0.2 M NaOH, 1% SDS) and incubating for 10 min at RT. DNA was precipitated by pouring 600 ml ice-cold P3 buffer (3M KOAc, 2M acetic acid) from the side of the bottle, immediate mixing. The bottle was then placed on ice and gently inverted intermittently over a period of 20-30 min. The cell debris was removed by centrifugation at 4°C with 9000 rpm for 20 min in a SLA3000 rotor (Sorvall). The supernatant was filtered through one layer of miracloth into a pre-weighted 400 ml bottle. 0.52 volumes of isopropanol were added and the suspension was mixed several times over 15min at 20°C. The nucleic acids were collected by spinning at 20°C with 10.000 rpm for 20 min in a SLA3000 rotor (Sorvall). The pellet was air dried at RT for 30 min and transferred to a SS43 tube, washed and dissolved in 24 ml TE/50 (10 mM Tris pH 8.0, 50 mM EDTA). 10  $\mu$ l RNase A (100mg/ml) were added and the DNA was incubated at 37°C over night. The DNA was purified three times by extracting with half the volume of buffered phenol (20°C, 19.000 rpm, 20 min) and finally with chloroform/isoamyl (24:1) (20°C, 10.000 rpm, 5min). The DNA was precipitated using 2/3 volume P4 buffer (20% PEG 8000, 1.8 M NaCl) and dissolved at 37°C with light shaking for 5min. After incubating on ice for 30min, the DNA was pelleted at 4°C with 3.500 rpm for 25 min and dissolved in 10 ml TE/0.1 buffer (10 mM Tris pH 8.0, 0.1 mM EDTA) at 37°C. The DNA was further purified by extracting 2x with chloroform/isoamyl (24:1) at RT and spun down with 3300 rpm for 5-10 min. 10% 3 M NaOAc pH 5.5-6 and 2.5 volumes ethanol were added and DNA precipitated over night at -20°C. The DNA was pelleted at 4°C with 18.000 rpm for 30 min and dissolved in 4 ml TE/0.1 at RT. The large scale plasmid preparation yielded 5-10 mg plasmid per L culture.

### ***7.2.5.1.2 Digestion and purification of DNA***

The purified plasmid was digested with SmaI or EcoRV (SmaI for or EcoRV for off-centered mono-nucleosomes). For 147 bp, 167 bp off-centered, 187 bp centered DNA, in 10 µl reaction volume 1-3 µg of plasmid DNA were digested with 1 µl of SmaI (NEB) with 1 µl buffer 4 (NEB) were incubated at 25°C for 1-24 hrs. For off-centered DNA 1-3 µg of plasmid DNA was digested with 1 µl EcoRV (NEB) with buffer 3 (NEB) and 1 µl 10x BSA (NEB) in 10 µl reaction volume at 37°C for 1-24 hrs. Digestion progress was monitored on 1.2% agarose gels.

After digestion was completed, the DNA samples were purified using a large native 8% acrylamide gel (8% acrylamide, 0.5x TBE buffer, pre-run at 40 W for 45 min) with 0.5x TBE as running buffer. Prior to loading the sample was mixed with 6x Gel Loading Dye (NEB). The gel was run at 17 W for ~2-4 hrs in fresh running buffer until the bromophenol blue dye reached the end of the gel. The DNA band was cut out using a UV lamp ( $\lambda=254$  nm) to visualize the DNA.

To elute the DNA from the acrylamide gel, an EluTrap Electroelution System (Whatman, GE Healthcare) was used according to the manufacturer's suggestion at 100 V for 3-14 hrs. Elution was monitored by measuring the DNA concentration at the NanoDrop 1000 photospetrometer (Thermo Scientific). The eluted DNA was precipitated with 2.5 volume ethanol and 1/10 3 M NaOAc pH 5.2 and pelleted at 4°C with 10,000 rpm for 30 min with a SLA1500 rotor (Sorvall). The DNA was dissolved in few µl of TE/0.1 at RT. The DNA concentration was determined on a NanoDrop 1000 photospetrometer (Thermo Scientific).

### ***7.2.5.1.3 PCR amplification of DNA***

For Cy3 labeled 187 bp centered mono-nucleosomes and INO1 nucleosomes, the DNA was amplified by PCR (for primer see Table 4 in section 7.1.2). 50 µl PCR contained ~2 ng of the respective DNA template, 5 µl 10x Taq buffer, 5 µl dNTPs (Roth), 2.5 µl 10 µM forward primer (Metabion for regular primer, BioTeZ for long primer), 2.5 µl 10 µM reverse primer, 1 µl Taq polymerase (self-made, Charlotte Ungewickell, AG Beckmann). The PCR was cycled on a MJMini<sup>TM</sup> Personal Thermal Cycler (BioRad) with the following program: 2 min at 94°C; 30 cycles with 15 sec 94°C, 15 sec 56°C,

30 sec 72°C; 5 min at 72°C, forever at 10°C. The amplified DNA was purified on a 1.2% agarose gel with a Gel Extraction Kit (QIAquick®) according to the manufacturer's protocol. The DNA was further purified with ethanol precipitation. 1/10 of volume NaOAc and 2.5 volume 100% ethanol were added and incubated at -20°C over night. The DNA was pelleted at 4°C with 14.000 rpm for 30 min, washed with 70% ethanol and pelleted again at 4°C with 14.000 rpm for 10-15 min. The purified DNA was dissolved in TE/0.1 to a final concentration of 5-7 µg/µl. The DNA concentration was determined on a NanoDrop 1000 photospectrometer (Thermo Scientific).

#### **7.2.5.2 *D.m.* core histones purification**

Expression of *D.m.* core histones was monitored by 18% SDS PAGE. The cells were mixed with urea sample buffer (9 M urea, 1% SDS, 25 mM Tris pH 6.6, 1 mM EDTA, 100 mM DTT) and heated for 15 min at 65°C prior to PAGE.

For *D.m.* core histones purification respective cell pellets were filled up to 30 ml Sau200 buffer (8 M urea, 40 mM NaOAc pH 5.2, 200 mM NaCl, 1mM EDTA, 10 mM lysine, 5 mM β-mercaptoethanol, 1 mM PMSF, 1 Complete Protease Inhibitor Cocktail tablet (Roche) and thawed. The cells disrupted with three runs in a microfluidizer (Microfluidics) at a pressure of 1500 psi and sonicated (2 min effective sonication time, pulse 15'' on/30'' off, amplitude of 30%, Branson sonifier 250, Emerson). Cell debris were removed by spinning at 4°C with 19.000 rpm for 20 min in a SS34 rotor (Sorvall).

Soluble histones were further purified on the Äkta system over a 5 ml SP Sepharose High Performance (GE Healthcare) after filtering through a 0.45 µm syringe filter. Buffer A was Sau-0 (8 M urea, 40 mM NaOAc pH 5.2, 1 mM EDTA, 10 mM lysine, 5 mM β-mercaptoethanol, prepare fresh), buffer B was Sau1000 (8 M urea, 40 mM NaOAc pH 5.2, 1000 mM NaCl, 1 mM EDTA, 10 mM lysine, 5 mM β-mercaptoethanol, prepare fresh). Loading was performed with 20% buffer B (Sau200 with 200 mM NaCl) with a flow rate of 1ml/min. The gradient profiles for the four core histones were: H2A wash 1 over 3 column volumes (CV) with 20% B (200 mM NaCl), wash 2 over 3CV with 36% B (360 mM NaCl), elution over 5 CV with 36-60% (360 - 600 mM NaCl), final wash over 3CV with 100% B (1000 mM NaCl); H2B and H3 wash 1 over 3 column volumes (CV) with 20% B (200 mM NaCl), wash 2 over 3 CV with 25% B (250 mM NaCl), elution over 5 CV with 25-60% (250 - 600 mM NaCl), final wash over 3 CV with 100% B (1000 mM NaCl); H4 wash 1 over 3 column volumes (CV) with

20% B (200 mM NaCl), wash 2 over 3 CV with 32% B (320 mM NaCl), elution over 5 CV with 32-60% (320 – 600 mM NaCl), final wash over 3 CV with 100% B (1000 mM NaCl). H2A eluted at ~24 mSi/cm, H2B at ~26 mSi/cm, H3 at ~24 Si/cm and H4 at ~25 mSi/cm. Elution fractions are pooled.

The sample was dialyzed three times against water (1h, O/N, 1h) using a SpectraPor® Dialysis Membrane (MWCO 6-8 kDa; Spectrumlabs). After dialysis, precipitation was removed by centrifugation at 4°C with 10.000 rpm for 30 min in a SS34 (Sorvall) and 15 mM Tris pH 8.0 was added to the supernatant.

For further purification and removal of DNA, the sample was loaded onto a 1 ml HiTrap Q HP (GE Healthcare) using buffer A (15 mM Tris-HCl pH 8.0) and buffer B (15 mM Tris-HCl pH 8.0, 2 M NaCl). The protein was collected in the flow through and the DNA was eluted from the column with a gradient over 10 CV from 0-100% B.

Concentration was measured on a NanoDrop 1000 photospectrometer (Thermo Scientific). Extinction coefficients of full-length *D.m.* histones: H2A has 13.362 kDa,  $\epsilon_{280}=4470$  cm/M or 0.335 cm·L/g, H2B has 13.696 kDa,  $\epsilon_{280}=7450$  cm/M or 0.544 cm·L/g, H3 has 15.388 kDa,  $\epsilon_{280}=4470$  cm/M or 0.290 cm·L/g, H4 has 11.381 kDa,  $\epsilon_{280}=5960$  cm/M or 0.524 cm·L/g. In addition 18% SDS PAGE with BSA standards were used to determine the concentration.

Aliquots of 1-3 mg protein were flash frozen in liquid nitrogen and stored at -80°C.

### 7.2.5.3 Octamer reconstitution

4 mg of each histone were lyophilized over night and stored at -80°C. Histones were dissolved in unfolding buffer (7 M Guanidinium-HCl, 20 mM Tris pH 7.5, 10 mM DTT) to a concentration of ~4 mg/ml for 0.5-3 hrs. In the meantime, the concentration was checked by 18% SDS PAGE in the and by  $A_{280}$  at the NanoDrop 1000 photospectrometer (Thermo Scientific). The four histones were mixed in equimolar ratios with excess of H2A/H2B (120-130% H2A and H2B, 100% H3 and H4). The mixed histones were dialyzed three times against 2 L refolding buffer (2 M NaCl, 10 mM Tris pH 7.5, 1 mM EDTA, 5 mM  $\beta$ -mercaptoethanol). Precipitation was removed by centrifugation at 4°C with 5.000 rpm for 10 min with a SS34 rotor (Sorvall). After concentration to a final volume of 2 ml with Amicon®Ultra Centrifugal Filters (Ultracel-30K, Milipore) the sample was loaded onto a HiLoad 16/600 Superdex 200 pg (GE Healthcare), equilibrated

with a refolding buffer. High molecular weight contaminations and aggregates elute at 45 ml, octamers eluted at ~65-68 ml, H2A/H2B dimers at ~ 84 ml. The purity and stoichiometry was assessed by 18% SDS PAGE. The concentration was determined  $A_{280}$  at the NanoDrop 1000 photospectrometer (Thermo Scientific) with an extinction coefficient of  $\epsilon_{280}=44700$  cm/M or 0.423 cm·L/g. For storage, the octamers were mixed with 50% glycerol (v/v) and frozen at -20°C.

#### **7.2.5.4 Salt gradient dialysis for nucleosome reconstitution**

Nucleosomes were reconstituted using a salt gradient dialysis. In order to estimate the correct octamer-nucleosome ratio, titrations were done with a constant concentration of octamers (0.1 mg/ml for titrations) and increasing amounts of DNA (from a mass ratio of octamers to DNA = 0.59, 0.84, 1.00, 1.16, 1.41). For large scale nucleosome preparations different octamers concentrations of 0.45-0.6 mg/ml were used with an optimal DNA concentration.

Octamers were mixed with 20 mM Tris pH 7.6, 2 M KCl, 1 mM DTT in siliconized Eppendorf tubes (Reaktionsgefäße 1.6 ml, farblos, Low Binding; Biozym Biotech Trading GmbH). Then this pre-mix was added to the respective amounts of purified DNA for the desired nucleosomes. Dialysis was performed in mini dialysis chambers (Slide-A-Lyzer® MINI Dialysis Units 7.000 MWCO; Thermo Scientific) at 4°C. The gradient was started with 100 ml buffer mono-2000 (20 mM Tris pH 7.6, 2 M KCl, 0.1 mM EDTA pH 8.0, 1 mM DTT); and 900 ml Buffer mono-0 (20 mM Tris pH 7.6, 0.1 mM EDTA pH 8.0, 1 mM DTT) were titrated in with a peristaltic pump (EconoPump, BioRad) for 7 hrs at 0.2 ml/min, 16 hrs at 0.4 ml/min and 7 hrs at 1 ml/min. Dialysis against the final buffer (20 mM Tris pH 7.6/50 mM Hepes pH 7.6, 50 mM KCl, 0.1 mM EDTA, 1 mM DTT) at 4°C. Precipitated octamers were removed by centrifugation at 4°C with 10.000 rpm for 10 min. The concentration of nucleosomes was estimated via the DNA concentration by absorption at 260 nm on the NanoDrop 1000 photospectrometer (Thermo Scientific). The quality of nucleosomes was checked by native 5% gel electrophoresis (see section 7.2.1.5).

### 7.2.6 MicroScale Thermophoresis (MST)

MicroScale Thermophoresis on a Monolith<sup>TM</sup> NT.015 (Nanotemper Technologies), (MST) was used to monitor binding of *D.m.* ISWI to DNA and nucleosomes in solution. Thermophoresis is the movement of molecules along a temperature gradient. Thermophoresis depends on the hydration shell, which changes upon binding of a partner. A change of thermophoretic properties of the formed complex can be observed as a change in fluorescence intensity and binding constants can be deduced.

In the beginning, conditions were optimized to avoid binding of ISWI to the capillaries. Therefore, ISWI was labeled with Monolith NT<sup>TM</sup> Protein Labeling Kit NT-494 blue (Nanotemper Technologies) according to the manufacturer's manual and binding to the capillaries was observed using the scanning mode.

For measuring binding affinities, indicated increasing amounts of purified *D.m.* ISWI (up to 16 serial dilutions from 0-10.000 nM) were mixed with constant amounts of the Cy3-labelled DNA (50-150 nM) or Cy3-labelled nucleosomes (75 nM) and incubated on ice for 10 min in a buffer containing 50 mM Hepes pH 7.6, 100 mM KOAc, 2.5 mM Mg(OAc)<sub>2</sub>, 1 mM DTT, 5% glycerol, 4% BSA, 0.01% Tween. The sample was centrifuged before transferring of 5-10 µl into K002 Monolith<sup>TM</sup> NT.015 Standard Treated Capillaries (Nanotemper Technologies) by capillary forces. Measurements were performed with the Green LED power set to 150, the IR-Laser was on for 20/30 sec with 0.6 V and off for 20 sec. Data analysis was performed with Data Analysis Software – NTAnalysis (Nanotemper Technologies)

### 7.2.7 General methods with yeast

All yeast strains used in this study were derived from a double FLAG tagged INO80 (Shen, 2004; Shen et al., 2000; Shen et al., 2003) (see Table 5 in section 7.1.3). Standard genetic techniques were used to manipulate yeast strains (Sherman, 2002). All media was prepared as described previously (Sherman, 2002).

#### 7.2.7.1 Gene deletion and tagging

Mutant strains (deletions and tagged subunits) were created with PCR based standard strategies (Reid et al., 2002): For deletion mutants the respective ORF was replaced by a KanMX6 resistance cassette (pFA6a KanMX6, Amp<sup>r</sup>, AG Wendler), DID1-tags

(Flemming et al., 2010) were C-terminally added in frame at the endogenous locus together with URA3 marker (pRS316, Amp<sup>r</sup>, AG Strässer) for selection. For deletions, either *xxΔ::KanMX* were transferred from the yeast genome gene disruption library strain *xx* by PCR-amplification of the marker *KanMX*, flanked by regions homologous to the upstream and downstream regions of the respective gene (Primers see Table 4 in section 7.1.2). Another strategy for creation of deletion mutants is amplification of the *KanMX6* cassette with primers flanking regions homologous to the upstream and downstream regions of the gene to be deleted. Via recombination, the integration of the G418 (Sigma<sup>®</sup>) resistance marker occurred after transformation of the purified PCR product into the INO80-FLAG<sub>2</sub> leading to a complete deletion of the respective ORF. For DID1-tagging, a PCR product was created such that the STOP codon of the gene of interest was removed, the DID1 tag was cloned in frame, followed by a STOP codon, the URA3 promoter and gene was inserted in the terminator of the gene of interest (see Fig. 38).

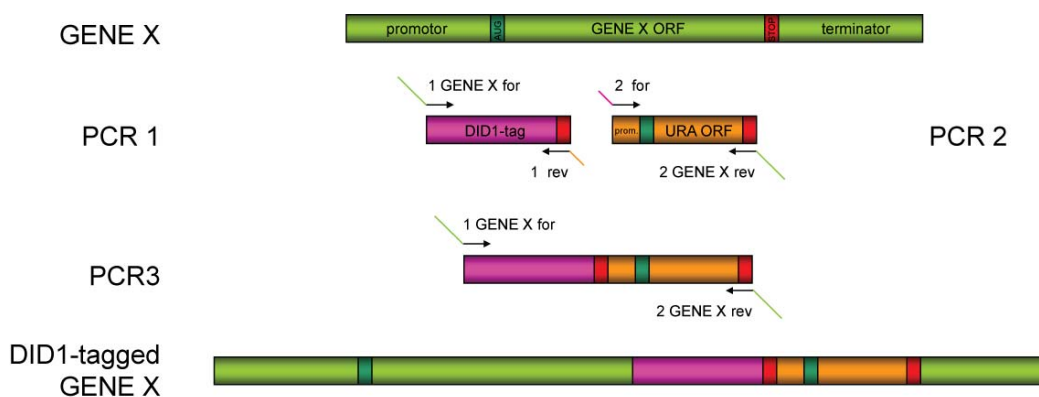


**Figure 38. PCR strategy for endogenous DID1 tagging.** For primers see Table 4 in section 7.1.2.

The PCR products were transformed into yeast cells using the LiAc method (Gietz et al., 1992). The reaction mix was incubated for 30 min at 30°C, and subjected to a heat shock for 20 min at 42°C. Cells were pelleted, resuspended with 200 µl ddH<sub>2</sub>O, plated on appropriate selective plates (G418 or –ura) and incubated at 30°C for 3–6 days. After LiOAc transformation and selection for the respective marker, the positive clones were confirmed by PCR on genomic DNA.

### 7.2.7.2 Preparation of yeast genomic DNA

For isolating total yeast DNA, a protocol modified from (Hoffman and Winston, 1987) was used. A single colony was used to inoculate a 5 ml YDP for overnight growth at

30°C. 1.5 ml of the culture was harvested by centrifugation. Cells were opened by vortexing at RT for 5 min with 0.2 ml lysis buffer (2% Triton X-100, 1% SDS, 100 mM NaCl, 10 mM Tris pH 8, 1 mM EDTA). 100 µl glass beads, 0.2 ml phenol and 0.3 ml TE/0.1 (10 mM Tris pH 8.0, 0.1 mM EDTA) were added. The sample was vortexed again for 2 min and centrifuged at RT with 14.000 rpm for 10 min. 400 µl of the aqueous top layer were transferred and the DNA was precipitated by adding 1 ml ethanol. The DNA was pelleted at RT with 14.000 rpm for 15 min and washed with 70% ethanol. The pellet was air-dried at RT for 10 min and resuspended in 50-100 µl TE with 100 µg/ml RNase. After the pellet was dissolved, DNases were inactivated by heating to 60°C for 5 min.

### **7.2.8 Purification of endogenous INO80 complex**

INO80 was purified endogenously from yeast with a C-terminal double FLAG-tag on Ino80. After affinity purification, homogeneity was achieved using ion exchange and size exclusion chromatography (for detail see (Tosi et al., 2013)). Deletion mutants were purified accordingly.

### **7.2.9 Cross-linking and mass spectrometry**

INO80 and INO80-nucleosome complexes were cross-linked with isotopically labeled disuccinimidyl suberate (DSS) and cross-linked peptides were identified using LC-MS/MS analysis (see (Tosi et al., 2013) for details).

### **7.2.10 Biochemical assays**

#### **7.2.10.1 Electrophoretic mobility shift assay**

For electromobility shift assays (EMSA) native gels were used (see section 7.2.1.5). EMSA were used to analyze complex formation of chromatin remodeler, purified sub-complex with DNA or nucleosomes. Indicated increasing amounts of the purified complex were incubated with 50 nM DNA or 50-100 nM nucleosomes (see section 7.2.5) on ice for 30 min. Complex formation was subsequently monitored by native PAGE.



### **7.2.10.2 Remodeling assay**

For remodeling assays, 50 nM nucleosomes reconstituted on a 359 bp long DNA (INO1 gene bp +1 until +359; see section 7.2.5, for primers see Table 4 in section 7.1.2) in a remodeling buffer (25 mM Hepes-KOH pH 7.6, 50 mM NaCl, 10% glycerol, 0.05% NP-40, 0.1 mM EDTA, 4 mM MgCl<sub>2</sub>, 1 mM DTT) were incubated with indicated amounts of INO80 WT or mutant complex and in absence or presence of ATP or ATP analogs AMP·PCP or ADP·BeF<sub>x</sub> at 30°C for 30 min. The nucleosomes and remodeling was then analyzed by native PAGE (see section 7.2.1.5).

### **7.2.10.3 ATPase assay**

ATPase activity of INO80 and mutant complexes was monitored without stimulus with DNA or INO1 nucleosomes as described in (Tosi et al., 2013).

## **7.2.11 Electron microscopy and single particle analysis**

For electron microscopy, ISWI and nucleosomes were used as indicated. For electron microscopy of INO80 samples were freshly purified and mildly stabilized by cross-linking, if not indicated otherwise. For stabilization of the head on the remainder of INO80, the samples had to be cross-linked with 0.05% glutaraldehyde (25% EM grade, agar) at 20°C for 30 min and quenched with a final concentration of 100 mM Tris. Integrity of fixed INO80 was monitored by purification over a second gel filtration and no aggregation or an overall change in the 3D structure could be observed.

### **7.2.11.1 Negative stain electron microscopy**

For negative staining, 3.5 µl of ISWI (200 nM), nucleosomes (50 nM) or freshly purified and mildly stabilized INO80 (0.03 mg/ml) were spotted onto glow discharged (45 sec;  $3 \cdot 10^{-1}$  mbar at 100 V) 2 nm Quantifoil holey grids (R3/3) pre-coated with a carbon layer and stained with 2% uranyl acetate (sample incubation 45 sec, staining 15 sec).

Micrographs of negatively stained images were recorded on a Tecnai G2 Spirit TEM at 120 keV under low-dose conditions ( $\sim 20$  e-/Å<sup>2</sup>) at a nominal magnification of

67.000 and a magnification of 90 600 at the plane of CCD (3.31 Å/pix) and defocus of -750 nm using an Eagle2048 x 2048 pixel CCD camera (FEI).

### 7.2.11.2 Cryo electron microscopy

For cryo-EM, the samples were flash frozen in liquid ethane to prevent formation of vitreous ice. To this end, freshly prepared and mildly fixed INO80 (2-3 mg/ml) was applied on 2 nm pre-coated Quantifoil R3/3 holey carbon supported grids and vitrified using a Vitrobot Mark IV (FEI Company). Cryo-EM micrographs were recorded either on a Tecnai G2 Spirit TEM at 120 keV principally as described above or on a Titan Krios TEM (FEI Company) at 200kV with an XFEG as electron source at 200 keV under low-dose conditions ( $\sim 20 \text{ e}^-/\text{\AA}^2$ ) with a magnification of  $\times 148,721$  at the plane of CCD (nominal magnification of  $\times 75.000$ ) using a TemCam-F416 CMOS camera (TVIPS GmbH,  $4,096 \times 4,096$  pixel,  $15.6 \mu\text{m}$  pixel, 1 s/full frame), resulting in an undecimated pixel size of  $1.048 \text{ \AA}$  on the object scale. For processing, the Titan data was used three-times decimated resulting in a pixel size of  $3.144 \text{ \AA}/\text{pix}$ . For the INO80 cryo-EM structure 14.874 micrographs were collected with help of the semi-automated acquisition software EM-TOOLS (TVIPS GmbH) (Becker et al., 2012) with nominal defoci between  $-2.0 \mu\text{m}$  and  $-4.5 \mu\text{m}$ .

### 7.2.11.3 Subunit localization in INO80 with DID-tagging

For localization of subunits, a dynein-light chain interaction domain 1 (DID1) tag (Flemming et al., 2010) was fused endogenously at the C-terminus of the respective INO80 subunits in a *dyn2Δ* INO80-FLAG<sub>2</sub> strain with a URA3 auxotrophy marker (for primers see Table 4 in section 7.1.2, for yeast manipulation see section 7.2.7.1; for sequence see appendix). The DID-tag was assembled on affinity purified INO80 (FLAG eluate) by incubation with purified GST-TEV-DID2 ( $\sim 5\times$  molar excess) and Dyn2 ( $\sim 50\times$  molar excess) at  $4^\circ\text{C}$  for 5 hrs. The complex was enriched for the assembled DID tag by affinity purification of GST-TEV-DID2 with pre-equilibrated Glutathione Sepharose<sup>TM</sup> beads 4 Fast Flow (GE Healthcare) at  $4^\circ\text{C}$  for 16 hrs. Unbound sample with not fully assembled DID-tags was washed off with H.02 buffer. For elution, the H.02 buffer was complemented with 0.5 mM EDTA and 20  $\mu\text{l}$  TEV protease (selfmade, Heidi Sieber, AG Beckmann) and the DID-tagged complexes were cut off the beads at  $18^\circ\text{C}$  for 1 hr. The

tagged INO80 complexes were subsequently purified by MonoQ and size exclusion chromatography as described (Tosi et al., 2013).

#### 7.2.11.4 Data Processing for INO80

For negative staining, 14,386 INO80 particles were selected by hand from negatively stained micrographs using `e2boxer.py` from the EMAN2 software package (Tang et al., 2007). Initial image processing, class averaging, calculation of initial models, as well as initial rounds of refinement were done with EMAN2 (Tang et al., 2007). The images were normalized and auto-high pass filtered to reduce the asymmetric appearance of the stain. Reference-free class averages of phase-flipped particles were calculated with ~20 particles per class. A low-resolution model was calculated with common lines and used as an initial model for projection matching in EMAN2. The correctness of this initial model was confirmed by using geometrical shapes, e.g. an ellipsoid or cylinder as initial model, which refined after few rounds to similar shapes. The low-resolution model, generated after several rounds of refinement in EMAN2, was subjected to SPIDER for iterative projection-matching and back-projection (Frank et al., 1996). After sorting, 10,982 particles were used for the final structure. The resolution of 22 Å was estimated based on the Fourier shell correlation (FSC) at 0.5. The handedness was chosen arbitrarily because of the intrinsic ambiguity generated by the EM reconstruction procedure. Reference-free class averaging was repeated with iterative and stable alignment and clustering (ISAC) (Yang et al., 2012) and ISAC classes were correlated to projections of INO80 structure using the `AP SH` command from SPIDER to demonstrate the structural flexibility.

For cryo-EM, 9012 micrographs were selected on the basis of power spectra and ice quality. 415,155 particles were selected automatically with Signature (Chen and Grigorieff, 2007) with the negative stain INO80 as a template. Data processing was performed with the negative stain volume filtered at 30-35 Å as reference using the SPIDER software package (Frank et al., 1996). Cryo-EM data was then further processed with the SPIDER software package in principal as described (Becker et al., 2012). The dataset was sorted for elongated INO80 and inverted (closed) volumes. The final data set contained 395,988 particles and the final resolution was at 17.5 Å (FSC = 0.5).

Visualization was done using the UCSF Chimera package (Pettersen et al., 2004). The threshold of surface representations was adjusted to enclose a volume accounting for the calculated mass of INO80 (1.3 MDa).

## 8 References

- Albert, I., Mavrich, T.N., Tomsho, L.P., Qi, J., Zanton, S.J., Schuster, S.C., and Pugh, B.F. (2007). Translational and rotational settings of H2A.Z nucleosomes across the *Saccharomyces cerevisiae* genome. *Nature* **446**, 572-576.
- Allard, S., Utley, R.T., Savard, J., Clarke, A., Grant, P., Brandl, C.J., Pillus, L., Workman, J.L., and Cote, J. (1999). NuA4, an essential transcription adaptor/histone H4 acetyltransferase complex containing Esa1p and the ATM-related cofactor Tra1p. *EMBO J* **18**, 5108-5119.
- Andrews, A.J., and Luger, K. (2011). Nucleosome structure(s) and stability: variations on a theme. *Annu Rev Biophys* **40**, 99-117.
- Armache, K.J., Garlick, J.D., Canzio, D., Narlikar, G.J., and Kingston, R.E. (2011). Structural basis of silencing: Sir3 BAH domain in complex with a nucleosome at 3.0 Å resolution. *Science* **334**, 977-982.
- Arnaudo, N., Fernandez, I.S., McLaughlin, S.H., Peak-Chew, S.Y., Rhodes, D., and Martino, F. (2013). The N-terminal acetylation of Sir3 stabilizes its binding to the nucleosome core particle. *Nat Struct Mol Biol* **20**, 1119-1121.
- Asturias, F.J., Chung, W.H., Kornberg, R.D., and Lorch, Y. (2002). Structural analysis of the RSC chromatin-remodeling complex. *Proc Natl Acad Sci U S A* **99**, 13477-13480.
- Babiarz, J.E., Halley, J.E., and Rine, J. (2006). Telomeric heterochromatin boundaries require NuA4-dependent acetylation of histone variant H2A.Z in *Saccharomyces cerevisiae*. *Genes Dev* **20**, 700-710.
- Badis, G., Chan, E.T., van Bakel, H., Pena-Castillo, L., Tillo, D., Tsui, K., Carlson, C.D., Gossett, A.J., Hasinoff, M.J., Warren, C.L., *et al.* (2008). A library of yeast transcription factor motifs reveals a widespread function for Rsc3 in targeting nucleosome exclusion at promoters. *Mol Cell* **32**, 878-887.
- Bao, Y., and Shen, X. (2007). INO80 subfamily of chromatin remodeling complexes. *Mutat Res* **618**, 18-29.
- Bargaje, R., Alam, M.P., Patowary, A., Sarkar, M., Ali, T., Gupta, S., Garg, M., Singh, M., Purkanti, R., Scaria, V., *et al.* (2012). Proximity of H2A.Z containing nucleosome to the transcription start site influences gene expression levels in the mammalian liver and brain. *Nucleic Acids Res* **40**, 8965-8978.
- Bauer, A., Chauvet, S., Huber, O., Usseglio, F., Rothbacher, U., Aragnol, D., Kemler, R., and Pradel, J. (2000). Pontin52 and reptin52 function as antagonistic regulators of beta-catenin signalling activity. *EMBO J* **19**, 6121-6130.
- Becker, T., Franckenberg, S., Wickles, S., Shoemaker, C.J., Anger, A.M., Armache, J.P., Sieber, H., Ungewickell, C., Berninghausen, O., Daberkow, I., *et al.* (2012). Structural basis of highly conserved ribosome recycling in eukaryotes and archaea. *Nature* **482**, 501-506.
- Bender, C.M., Gonzalgo, M.L., Gonzales, F.A., Nguyen, C.T., Robertson, K.D., and Jones, P.A. (1999). Roles of cell division and gene transcription in the methylation of CpG islands. *Mol Cell Biol* **19**, 6690-6698.
- Billon, P., and Cote, J. (2012). Precise deposition of histone H2A.Z in chromatin for genome expression and maintenance. *Biochim Biophys Acta* **1819**, 290-302.
- Blosser, T.R., Yang, J.G., Stone, M.D., Narlikar, G.J., and Zhuang, X. (2009). Dynamics of nucleosome remodelling by individual ACF complexes. *Nature* **462**, 1022-1027.
- Bohm, V., Hieb, A.R., Andrews, A.J., Gansen, A., Rocker, A., Toth, K., Luger, K., and Langowski, J. (2011). Nucleosome accessibility governed by the dimer/tetramer interface. *Nucleic Acids Res* **39**, 3093-3102.
- Bouazoune, K., and Kingston, R.E. (2012). Chromatin remodeling by the CHD7 protein is impaired by mutations that cause human developmental disorders. *Proc Natl Acad Sci U S A* **109**, 19238-19243.
- Bowman, G.D. (2010). Mechanisms of ATP-dependent nucleosome sliding. *Curr Opin Struct Biol* **20**, 73-81.
- Brehm, A., Langst, G., Kehle, J., Clapier, C.R., Imhof, A., Eberharter, A., Muller, J., and Becker, P.B. (2000). dMi-2 and ISWI chromatin remodelling factors have distinct nucleosome binding and mobilization properties. *EMBO J* **19**, 4332-4341.
- Bruno, M., Flaus, A., Stockdale, C., Rencurel, C., Ferreira, H., and Owen-Hughes, T. (2003). Histone H2A/H2B dimer exchange by ATP-dependent chromatin remodeling activities. *Mol Cell* **12**, 1599-1606.
- Cai, Y., Jin, J., Yao, T., Gottschalk, A.J., Swanson, S.K., Wu, S., Shi, Y., Washburn, M.P., Florens, L., Conaway, R.C., *et al.* (2007). YY1 functions with INO80 to activate transcription. *Nat Struct Mol Biol* **14**, 872-874.

- Caiafa, P., and Zampieri, M. (2005). DNA methylation and chromatin structure: the puzzling CpG islands. *J Cell Biochem* 94, 257-265.
- Cairns, B.R. (2007). Chromatin remodeling: insights and intrigue from single-molecule studies. *Nat Struct Mol Biol* 14, 989-996.
- Carlson, M.L., Wilson, E.T., and Prescott, S.M. (2003). Regulation of COX-2 transcription in a colon cancer cell line by Pontin52/TIP49a. *Mol Cancer* 2, 42.
- Chaban, Y., Ezeokonkwo, C., Chung, W.H., Zhang, F., Kornberg, R.D., Maier-Davis, B., Lorch, Y., and Asturias, F.J. (2008). Structure of a RSC-nucleosome complex and insights into chromatin remodeling. *Nat Struct Mol Biol* 15, 1272-1277.
- Chambers, A.L., Ormerod, G., Durley, S.C., Sing, T.L., Brown, G.W., Kent, N.A., and Downs, J.A. (2012). The INO80 chromatin remodeling complex prevents polyploidy and maintains normal chromatin structure at centromeres. *Genes Dev* 26, 2590-2603.
- Chen, J.Z., and Grigorieff, N. (2007). SIGNATURE: a single-particle selection system for molecular electron microscopy. *J Struct Biol* 157, 168-173.
- Chen, L., Cai, Y., Jin, J., Florens, L., Swanson, S.K., Washburn, M.P., Conaway, J.W., and Conaway, R.C. (2011). Subunit organization of the human INO80 chromatin remodeling complex: an evolutionarily conserved core complex catalyzes ATP-dependent nucleosome remodeling. *J Biol Chem* 286, 11283-11289.
- Cheung, K.L., Huen, J., Kakihara, Y., Houry, W.A., and Ortega, J. (2010). Alternative oligomeric states of the yeast Rvb1/Rvb2 complex induced by histidine tags. *J Mol Biol* 404, 478-492.
- Ciferri, C., Lander, G.C., Maiolica, A., Herzog, F., Aebersold, R., and Nogales, E. (2012). Molecular architecture of human polycomb repressive complex 2. *eLife* 1, e00005.
- Clapier, C.R., and Cairns, B.R. (2009). The biology of chromatin remodeling complexes. *Annu Rev Biochem* 78, 273-304.
- Clapier, C.R., and Cairns, B.R. (2012). Regulation of ISWI involves inhibitory modules antagonized by nucleosomal epitopes. *Nature* 492, 280-284.
- Clapier, C.R., Chakravarthy, S., Petosa, C., Fernandez-Tornero, C., Luger, K., and Muller, C.W. (2008). Structure of the Drosophila nucleosome core particle highlights evolutionary constraints on the H2A-H2B histone dimer. *Proteins* 71, 1-7.
- Clapier, C.R., Langst, G., Corona, D.F., Becker, P.B., and Nightingale, K.P. (2001). Critical role for the histone H4 N terminus in nucleosome remodeling by ISWI. *Mol Cell Biol* 21, 875-883.
- Clapier, C.R., Nightingale, K.P., and Becker, P.B. (2002). A critical epitope for substrate recognition by the nucleosome remodeling ATPase ISWI. *Nucleic Acids Res* 30, 649-655.
- Collins, N., Poot, R.A., Kukimoto, I., Garcia-Jimenez, C., Dellaire, G., and Varga-Weisz, P.D. (2002). An ACF1-ISWI chromatin-remodeling complex is required for DNA replication through heterochromatin. *Nat Genet* 32, 627-632.
- Corona, D.F., Clapier, C.R., Becker, P.B., and Tamkun, J.W. (2002). Modulation of ISWI function by site-specific histone acetylation. *EMBO Rep* 3, 242-247.
- Corona, D.F., Eberharter, A., Budde, A., Deuring, R., Ferrari, S., Varga-Weisz, P., Wilm, M., Tamkun, J., and Becker, P.B. (2000). Two histone fold proteins, CHRAC-14 and CHRAC-16, are developmentally regulated subunits of chromatin accessibility complex (CHRAC). *EMBO J* 19, 3049-3059.
- Corona, D.F., Langst, G., Clapier, C.R., Bonte, E.J., Ferrari, S., Tamkun, J.W., and Becker, P.B. (1999). ISWI is an ATP-dependent nucleosome remodeling factor. *Mol Cell* 3, 239-245.
- Cote, J., Quinn, J., Workman, J.L., and Peterson, C.L. (1994). Stimulation of GAL4 derivative binding to nucleosomal DNA by the yeast SWI/SNF complex. *Science* 265, 53-60.
- Dang, W., and Bartholomew, B. (2007). Domain architecture of the catalytic subunit in the ISW2-nucleosome complex. *Mol Cell Biol* 27, 8306-8317.
- Dechassa, M.L., Zhang, B., Horowitz-Scherer, R., Persinger, J., Woodcock, C.L., Peterson, C.L., and Bartholomew, B. (2008). Architecture of the SWI/SNF-nucleosome complex. *Mol Cell Biol* 28, 6010-6021.
- Deindl, S., Hwang, W.L., Hota, S.K., Blosser, T.R., Prasad, P., Bartholomew, B., and Zhuang, X. (2013). ISWI remodeler slide nucleosomes with coordinated multi-base-pair entry steps and single-base-pair exit steps. *Cell* 152, 442-452.
- Denslow, S.A., and Wade, P.A. (2007). The human Mi-2/NuRD complex and gene regulation. *Oncogene* 26, 5433-5438.
- Deuring, R., Fanti, L., Armstrong, J.A., Sarte, M., Papoulas, O., Prestel, M., Daubresse, G., Verardo, M., Moseley, S.L., Berloco, M., *et al.* (2000). The ISWI chromatin-remodeling protein is required for gene expression and the maintenance of higher order chromatin structure in vivo. *Mol Cell* 5, 355-365.

- Downs, J.A., Allard, S., Jobin-Robitaille, O., Javaheri, A., Auger, A., Bouchard, N., Kron, S.J., Jackson, S.P., and Cote, J. (2004). Binding of chromatin-modifying activities to phosphorylated histone H2A at DNA damage sites. *Mol Cell* 16, 979-990.
- Doyon, Y., Selleck, W., Lane, W.S., Tan, S., and Cote, J. (2004). Structural and functional conservation of the NuA4 histone acetyltransferase complex from yeast to humans. *Mol Cell Biol* 24, 1884-1896.
- Duhr, S., and Braun, D. (2006). Why molecules move along a temperature gradient. *Proc Natl Acad Sci U S A* 103, 19678-19682.
- Durr, H., Korner, C., Muller, M., Hickmann, V., and Hopfner, K.P. (2005). X-ray structures of the *Sulfolobus solfataricus* SWI2/SNF2 ATPase core and its complex with DNA. *Cell* 121, 363-373.
- Eberharter, A., Ferrari, S., Langst, G., Straub, T., Imhof, A., Varga-Weisz, P., Wilm, M., and Becker, P.B. (2001). Acf1, the largest subunit of CHRAC, regulates ISWI-induced nucleosome remodelling. *EMBO J* 20, 3781-3788.
- Eberharter, A., Vetter, I., Ferreira, R., and Becker, P.B. (2004). ACF1 improves the effectiveness of nucleosome mobilization by ISWI through PHD-histone contacts. *EMBO J* 23, 4029-4039.
- Erdel, F., and Rippe, K. (2011). Binding kinetics of human ISWI chromatin-remodeler to DNA repair sites elucidate their target location mechanism. *Nucleus* 2, 105-112.
- Fan, J.Y., Gordon, F., Luger, K., Hansen, J.C., and Tremethick, D.J. (2002). The essential histone variant H2A.Z regulates the equilibrium between different chromatin conformational states. *Nat Struct Biol* 9, 172-176.
- Fan, J.Y., Rangasamy, D., Luger, K., and Tremethick, D.J. (2004). H2A.Z alters the nucleosome surface to promote HP1 $\alpha$ -mediated chromatin fiber folding. *Mol Cell* 16, 655-661.
- Fenn, S., Breitsprecher, D., Gerhold, C.B., Witte, G., Faix, J., and Hopfner, K.P. (2011). Structural biochemistry of nuclear actin-related proteins 4 and 8 reveals their interaction with actin. *EMBO J* 30, 2153-2166.
- Ferreira, R., Eberharter, A., Bonaldi, T., Chioda, M., Imhof, A., and Becker, P.B. (2007). Site-specific acetylation of ISWI by GCN5. *BMC Mol Biol* 8, 73.
- Flanagan, J.F., Mi, L.Z., Chruszcz, M., Cymborowski, M., Clines, K.L., Kim, Y., Minor, W., Rastinejad, F., and Khorasanizadeh, S. (2005). Double chromodomains cooperate to recognize the methylated histone H3 tail. *Nature* 438, 1181-1185.
- Flemming, D., Thierbach, K., Stelter, P., Bottcher, B., and Hurt, E. (2010). Precise mapping of subunits in multiprotein complexes by a versatile electron microscopy label. *Nat Struct Mol Biol* 17, 775-778.
- Ford, J., Odeyale, O., Eskandar, A., Kouba, N., and Shen, C.H. (2007). A SWI/SNF- and INO80-dependent nucleosome movement at the INO1 promoter. *Biochem Biophys Res Commun* 361, 974-979.
- Frank, J., Radermacher, M., Penczek, P., Zhu, J., Li, Y., Ladjadj, M., and Leith, A. (1996). SPIDER and WEB: processing and visualization of images in 3D electron microscopy and related fields. *J Struct Biol* 116, 190-199.
- Fyodorov, D.V., Blower, M.D., Karpen, G.H., and Kadonaga, J.T. (2004). Acf1 confers unique activities to ACF/CHRAC and promotes the formation rather than disruption of chromatin in vivo. *Genes Dev* 18, 170-183.
- Gadad, S.S., Shandilya, J., Swaminathan, V., and Kundu, T.K. (2009). Histone chaperone as coactivator of chromatin transcription: role of acetylation. *Methods Mol Biol* 523, 263-278.
- Gerhold, C.B., Winkler, D.D., Lakomek, K., Seifert, F.U., Fenn, S., Kessler, B., Witte, G., Luger, K., and Hopfner, K.P. (2012). Structure of Actin-related protein 8 and its contribution to nucleosome binding. *Nucleic Acids Res* 40, 11036-11046.
- Gietz, D., St Jean, A., Woods, R.A., and Schiestl, R.H. (1992). Improved method for high efficiency transformation of intact yeast cells. *Nucleic Acids Res* 20, 1425.
- Gkikopoulos, T., Schofield, P., Singh, V., Pinskaya, M., Mellor, J., Smolle, M., Workman, J.L., Barton, G.J., and Owen-Hughes, T. (2011). A role for Snf2-related nucleosome-spacing enzymes in genome-wide nucleosome organization. *Science* 333, 1758-1760.
- Gorynia, S., Bandejas, T.M., Pinho, F.G., McVey, C.E., Vornrhein, C., Round, A., Svergun, D.I., Donner, P., Matias, P.M., and Carrondo, M.A. (2011). Structural and functional insights into a dodecameric molecular machine - the RuvBL1/RuvBL2 complex. *J Struct Biol* 176, 279-291.
- Goto, D.B., and Nakayama, J. (2012). RNA and epigenetic silencing: insight from fission yeast. *Dev Growth Differ* 54, 129-141.
- Gribun, A., Cheung, K.L., Huen, J., Ortega, J., and Houry, W.A. (2008). Yeast Rvb1 and Rvb2 are ATP-dependent DNA helicases that form a heterohexameric complex. *Journal of molecular biology* 376, 1320-1333.
- Grigoletto, A., Lestienne, P., and Rosenbaum, J. (2011). The multifaceted proteins Reptin and Pontin as major players in cancer. *Biochim Biophys Acta* 1815, 147-157.

- Grune, T., Brzeski, J., Eberharter, A., Clapier, C.R., Corona, D.F., Becker, P.B., and Muller, C.W. (2003). Crystal structure and functional analysis of a nucleosome recognition module of the remodeling factor ISWI. *Mol Cell* 12, 449-460.
- Hall, M.A., Shundrovsky, A., Bai, L., Fulbright, R.M., Lis, J.T., and Wang, M.D. (2009). High-resolution dynamic mapping of histone-DNA interactions in a nucleosome. *Nat Struct Mol Biol* 16, 124-129.
- Harata, M., Oma, Y., Mizuno, S., Jiang, Y.W., Stillman, D.J., and Wintersberger, U. (1999). The nuclear actin-related protein of *Saccharomyces cerevisiae*, Act3p/Arp4, interacts with core histones. *Mol Biol Cell* 10, 2595-2605.
- Hartlepp, K.F., Fernandez-Tornero, C., Eberharter, A., Grune, T., Muller, C.W., and Becker, P.B. (2005). The histone fold subunits of *Drosophila* CHRAC facilitate nucleosome sliding through dynamic DNA interactions. *Mol Cell Biol* 25, 9886-9896.
- Hauk, G., McKnight, J.N., Nodelman, I.M., and Bowman, G.D. (2010). The chromodomains of the Chd1 chromatin remodeler regulate DNA access to the ATPase motor. *Mol Cell* 39, 711-723.
- Heard, E., Rougeulle, C., Arnaud, D., Avner, P., Allis, C.D., and Spector, D.L. (2001). Methylation of histone H3 at Lys-9 is an early mark on the X chromosome during X inactivation. *Cell* 107, 727-738.
- Herzog, F., Kahraman, A., Boehringer, D., Mak, R., Bracher, A., Walzthoeni, T., Leitner, A., Beck, M., Hartl, F.U., Ban, N., *et al.* (2012). Structural probing of a protein phosphatase 2A network by chemical cross-linking and mass spectrometry. *Science* 337, 1348-1352.
- Hoffman, C.S., and Winston, F. (1987). A ten-minute DNA preparation from yeast efficiently releases autonomous plasmids for transformation of *Escherichia coli*. *Gene* 57, 267-272.
- Hu, M., Zhang, Y.B., Qian, L., Brinas, R.P., Kuznetsova, L., and Hainfeld, J.F. (2008). Three-dimensional structure of human chromatin accessibility complex hCHRAC by electron microscopy. *J Struct Biol* 164, 263-269.
- Huber, O., Menard, L., Haurie, V., Nicou, A., Taras, D., and Rosenbaum, J. (2008). Pontin and reptin, two related ATPases with multiple roles in cancer. *Cancer Res* 68, 6873-6876.
- Hughes, R.M., Bolger, S., Tapadia, H., and Tucker, C.L. (2012). Light-mediated control of DNA transcription in yeast. *Methods* 58, 385-391.
- Hur, S.K., Park, E.J., Han, J.E., Kim, Y.A., Kim, J.D., Kang, D., and Kwon, J. (2010). Roles of human INO80 chromatin remodeling enzyme in DNA replication and chromosome segregation suppress genome instability. *Cell Mol Life Sci* 67, 2283-2296.
- Jaskelioff, M., Gavin, I.M., Peterson, C.L., and Logie, C. (2000). SWI-SNF-mediated nucleosome remodeling: role of histone octamer mobility in the persistence of the remodeled state. *Mol Cell Biol* 20, 3058-3068.
- Jha, S., and Dutta, A. (2009). RVB1/RVB2: running rings around molecular biology. *Mol Cell* 34, 521-533.
- Jonsson, Z.O., Dhar, S.K., Narlikar, G.J., Auty, R., Wagle, N., Pellman, D., Pratt, R.E., Kingston, R., and Dutta, A. (2001). Rvb1p and Rvb2p are essential components of a chromatin remodeling complex that regulates transcription of over 5% of yeast genes. *J Biol Chem* 276, 16279-16288.
- Jonsson, Z.O., Jha, S., Wohlschlegel, J.A., and Dutta, A. (2004). Rvb1p/Rvb2p recruit Arp5p and assemble a functional Ino80 chromatin remodeling complex. *Mol Cell* 16, 465-477.
- Kapoor, P., Chen, M., Winkler, D.D., Luger, K., and Shen, X. (2013). Evidence for monomeric actin function in INO80 chromatin remodeling. *Nat Struct Mol Biol* 20, 426-432.
- Kasten, M., Szerlong, H., Erdjument-Bromage, H., Tempst, P., Werner, M., and Cairns, B.R. (2004). Tandem bromodomains in the chromatin remodeler RSC recognize acetylated histone H3 Lys14. *EMBO J* 23, 1348-1359.
- Kasten, M.M., Clapier, C.R., and Cairns, B.R. (2011). SnapShot: Chromatin remodeling: SWI/SNF. *Cell* 144, 310 e311.
- Kastner, B., Fischer, N., Golas, M.M., Sander, B., Dube, P., Boehringer, D., Hartmuth, K., Deckert, J., Hauer, F., Wolf, E., *et al.* (2008). GraFix: sample preparation for single-particle electron cryomicroscopy. *Nat Methods* 5, 53-55.
- Keogh, M.C., Mennella, T.A., Sawa, C., Berthelet, S., Krogan, N.J., Wolek, A., Podolny, V., Carpenter, L.R., Greenblatt, J.F., Baetz, K., *et al.* (2006). The *Saccharomyces cerevisiae* histone H2A variant Htz1 is acetylated by NuA4. *Genes Dev* 20, 660-665.
- Kitayama, K., Kamo, M., Oma, Y., Matsuda, R., Uchida, T., Ikura, T., Tashiro, S., Ohyama, T., Winsor, B., and Harata, M. (2009). The human actin-related protein hArp5: nucleo-cytoplasmic shuttling and involvement in DNA repair. *Exp Cell Res* 315, 206-217.
- Krogan, N.J., Baetz, K., Keogh, M.C., Datta, N., Sawa, C., Kwok, T.C., Thompson, N.J., Davey, M.G., Pootoolal, J., Hughes, T.R., *et al.* (2004). Regulation of chromosome stability by the histone H2A variant Htz1, the Swr1 chromatin remodeling complex, and the histone acetyltransferase NuA4. *Proc Natl Acad Sci U S A* 101, 13513-13518.

- Kurdistani, S.K., and Grunstein, M. (2003). Histone acetylation and deacetylation in yeast. *Nat Rev Mol Cell Biol* 4, 276-284.
- Kuroda, T.S., Maita, H., Tabata, T., Taira, T., Kitaura, H., Ariga, H., and Iguchi-Ariga, S.M. (2004). A novel nucleolar protein, PAPA-1, induces growth arrest as a result of cell cycle arrest at the G1 phase. *Gene* 340, 83-98.
- Laemmli, U.K. (1970). Cleavage of structural proteins during the assembly of the head of bacteriophage T4. *Nature* 227, 680-685.
- Lander, G.C., Saibil, H.R., and Nogales, E. (2012). Go hybrid: EM, crystallography, and beyond. *Curr Opin Struct Biol* 22, 627-635.
- Lantermann, A.B., Straub, T., Stralfors, A., Yuan, G.C., Ekwall, K., and Korber, P. (2010). *Schizosaccharomyces pombe* genome-wide nucleosome mapping reveals positioning mechanisms distinct from those of *Saccharomyces cerevisiae*. *Nat Struct Mol Biol* 17, 251-257.
- Lau, W.C., and Rubinstein, J.L. (2012). Subnanometre-resolution structure of the intact *Thermus thermophilus* H<sup>+</sup>-driven ATP synthase. *Nature* 481, 214-218.
- Leitner, A., Reischl, R., Walzthoeni, T., Herzog, F., Bohn, S., Forster, F., and Aebersold, R. (2012). Expanding the chemical cross-linking toolbox by the use of multiple proteases and enrichment by size exclusion chromatography. *Mol Cell Proteomics* 11, M111 014126.
- Leschziner, A.E. (2011). Electron microscopy studies of nucleosome remodeler. *Curr Opin Struct Biol* 21, 709-718.
- Leschziner, A.E., Lemon, B., Tjian, R., and Nogales, E. (2005). Structural studies of the human PBAF chromatin-remodeling complex. *Structure* 13, 267-275.
- Leschziner, A.E., Saha, A., Wittmeyer, J., Zhang, Y., Bustamante, C., Cairns, B.R., and Nogales, E. (2007). Conformational flexibility in the chromatin remodeler RSC observed by electron microscopy and the orthogonal tilt reconstruction method. *Proc Natl Acad Sci U S A* 104, 4913-4918.
- Lopez-Perrote, A., Munoz-Hernandez, H., Gil, D., and Llorca, O. (2012). Conformational transitions regulate the exposure of a DNA-binding domain in the RuvBL1-RuvBL2 complex. *Nucleic Acids Res* 40, 11086-11099.
- Lowary, P.T., and Widom, J. (1998). New DNA sequence rules for high affinity binding to histone octamer and sequence-directed nucleosome positioning. *J Mol Biol* 276, 19-42.
- Luger, K., Mader, A.W., Richmond, R.K., Sargent, D.F., and Richmond, T.J. (1997). Crystal structure of the nucleosome core particle at 2.8 Å resolution. *Nature* 389, 251-260.
- Makde, R.D., England, J.R., Yennawar, H.P., and Tan, S. (2010). Structure of RCC1 chromatin factor bound to the nucleosome core particle. *Nature* 467, 562-566.
- Masse, J.E., Wong, B., Yen, Y.M., Allain, F.H., Johnson, R.C., and Feigon, J. (2002). The *S. cerevisiae* architectural HMGB protein NHP6A complexed with DNA: DNA and protein conformational changes upon binding. *J Mol Biol* 323, 263-284.
- Matias, P.M., Gorynia, S., Donner, P., and Carrondo, M.A. (2006). Crystal structure of the human AAA+ protein RuvBL1. *J Biol Chem* 281, 38918-38929.
- Mavrich, T.N., Ioshikhes, I.P., Venters, B.J., Jiang, C., Tomsho, L.P., Qi, J., Schuster, S.C., Albert, I., and Pugh, B.F. (2008). A barrier nucleosome model for statistical positioning of nucleosomes throughout the yeast genome. *Genome Res* 18, 1073-1083.
- Meadsday, V., Baetz, K., Guzzo, J., Yuen, K., Kwok, T., Sheikh, B., Ding, H., Ueta, R., Hoac, T., Cheng, B., et al. (2005). Systematic yeast synthetic lethal and synthetic dosage lethal screens identify genes required for chromosome segregation. *Proc Natl Acad Sci U S A* 102, 13956-13961.
- Menard, L., Taras, D., Grigoletto, A., Haurie, V., Nicou, A., Dugot-Senart, N., Costet, P., Rousseau, B., and Rosenbaum, J. (2010). In vivo silencing of Reptin blocks the progression of human hepatocellular carcinoma in xenografts and is associated with replicative senescence. *J Hepatol* 52, 681-689.
- Min, J.N., Tian, Y., Xiao, Y., Wu, L., Li, L., and Chang, S. (2013). The mINO80 chromatin remodeling complex is required for efficient telomere replication and maintenance of genome stability. *Cell Res*.
- Mitchell, L., Lambert, J.P., Gerdes, M., Al-Madhoun, A.S., Skerjanc, I.S., Figeys, D., and Baetz, K. (2008). Functional dissection of the NuA4 histone acetyltransferase reveals its role as a genetic hub and that Eaf1 is essential for complex integrity. *Mol Cell Biol* 28, 2244-2256.
- Miyagi, A., Ando, T., and Lyubchenko, Y.L. (2011). Dynamics of nucleosomes assessed with time-lapse high-speed atomic force microscopy. *Biochemistry* 50, 7901-7908.
- Mizuguchi, G., Shen, X., Landry, J., Wu, W.H., Sen, S., and Wu, C. (2004). ATP-driven exchange of histone H2AZ variant catalyzed by SWR1 chromatin remodeling complex. *Science* 303, 343-348.
- Mizuguchi, G., Tsukiyama, T., Wisniewski, J., and Wu, C. (1997). Role of nucleosome remodeling factor NURF in transcriptional activation of chromatin. *Mol Cell* 1, 141-150.



- Morrison, A.J., Highland, J., Krogan, N.J., Arbel-Eden, A., Greenblatt, J.F., Haber, J.E., and Shen, X. (2004). INO80 and gamma-H2AX interaction links ATP-dependent chromatin remodeling to DNA damage repair. *Cell* 119, 767-775.
- Morrison, A.J., Kim, J.A., Person, M.D., Highland, J., Xiao, J., Wehr, T.S., Hensley, S., Bao, Y., Shen, J., Collins, S.R., *et al.* (2007). Mec1/Tel1 phosphorylation of the INO80 chromatin remodeling complex influences DNA damage checkpoint responses. *Cell* 130, 499-511.
- Morrison, A.J., and Shen, X. (2009). Chromatin remodelling beyond transcription: the INO80 and SWR1 complexes. *Nat Rev Mol Cell Biol* 10, 373-384.
- Mueller-Planitz, F., Klinker, H., Ludwigsen, J., and Becker, P.B. (2013). The ATPase domain of ISWI is an autonomous nucleosome remodeling machine. *Nat Struct Mol Biol* 20, 82-89.
- Mujtaba, S., Zeng, L., and Zhou, M.M. (2007). Structure and acetyl-lysine recognition of the bromodomain. *Oncogene* 26, 5521-5527.
- Neumann, F.R., Dion, V., Gehlen, L.R., Tsai-Pflugfelder, M., Schmid, R., Taddei, A., and Gasser, S.M. (2012). Targeted INO80 enhances subnuclear chromatin movement and ectopic homologous recombination. *Genes Dev* 26, 369-383.
- Newman, D.R., Kuhn, J.F., Shanab, G.M., and Maxwell, E.S. (2000). Box C/D snoRNA-associated proteins: two pairs of evolutionarily ancient proteins and possible links to replication and transcription. *RNA* 6, 861-879.
- Nguyen, V.Q., Ranjan, A., Stengel, F., Wei, D., Aebersold, R., Wu, C., and Leschziner, A.E. (2013). Molecular Architecture of the ATP-Dependent Chromatin-Remodeling Complex SWR1. *Cell* 154, 1220-1231.
- Ong, M.S., Richmond, T.J., and Davey, C.A. (2007). DNA stretching and extreme kinking in the nucleosome core. *J Mol Biol* 368, 1067-1074.
- Papamichos-Chronakis, M., and Peterson, C.L. (2008). The Ino80 chromatin-remodeling enzyme regulates replisome function and stability. *Nat Struct Mol Biol* 15, 338-345.
- Papamichos-Chronakis, M., Watanabe, S., Rando, O.J., and Peterson, C.L. (2011). Global Regulation of H2A.Z Localization by the INO80 Chromatin-Remodeling Enzyme Is Essential for Genome Integrity. *Cell* 144, 200-213.
- Pettersen, E.F., Goddard, T.D., Huang, C.C., Couch, G.S., Greenblatt, D.M., Meng, E.C., and Ferrin, T.E. (2004). UCSF Chimera--a visualization system for exploratory research and analysis. *J Comput Chem* 25, 1605-1612.
- Petukhov, M., Dagkessamanskaja, A., Bommer, M., Barrett, T., Tsaneva, I., Yakimov, A., Queval, R., Shvetsov, A., Khodorkovskiy, M., Kas, E., *et al.* (2012). Large-scale conformational flexibility determines the properties of AAA+ TIP49 ATPases. *Structure* 20, 1321-1331.
- Pointner, J., Persson, J., Prasad, P., Norman-Axelsson, U., Stralfors, A., Khorosjutina, O., Krietenstein, N., Svensson, J.P., Ekwall, K., and Korber, P. (2012). CHD1 remodeler regulate nucleosome spacing in vitro and align nucleosomal arrays over gene coding regions in *S. pombe*. *EMBO J* 31, 4388-4403.
- Polach, K.J., and Widom, J. (1995). Mechanism of protein access to specific DNA sequences in chromatin: a dynamic equilibrium model for gene regulation. *J Mol Biol* 254, 130-149.
- Puri, T., Wendler, P., Sigala, B., Saibil, H., and Tsaneva, I.R. (2007). Dodecameric structure and ATPase activity of the human TIP48/TIP49 complex. *Journal of molecular biology* 366, 179-192.
- Racki, L.R., Yang, J.G., Naber, N., Partensky, P.D., Acevedo, A., Purcell, T.J., Cooke, R., Cheng, Y., and Narlikar, G.J. (2009). The chromatin remodeler ACF acts as a dimeric motor to space nucleosomes. *Nature* 462, 1016-1021.
- Raisner, R.M., Hartley, P.D., Meneghini, M.D., Bao, M.Z., Liu, C.L., Schreiber, S.L., Rando, O.J., and Madhani, H.D. (2005). Histone variant H2A.Z marks the 5' ends of both active and inactive genes in euchromatin. *Cell* 123, 233-248.
- Ranjan, A., Mizuguchi, G., Fitzgerald, P.C., Wei, D., Wang, F., Huang, Y., Luk, E., Woodcock, C.L., and Wu, C. (2013). Nucleosome-free Region Dominates Histone Acetylation in Targeting SWR1 to Promoters for H2A.Z Replacement. *Cell* 154, 1232-1245.
- Ray, S., and Grove, A. (2009). The yeast high mobility group protein HMO2, a subunit of the chromatin-remodeling complex INO80, binds DNA ends. *Nucleic Acids Res* 37, 6389-6399.
- Ray, S., and Grove, A. (2012). Interaction of *Saccharomyces cerevisiae* HMO2 domains with distorted DNA. *Biochemistry* 51, 1825-1835.
- Reid, R.J., Sunjevaric, I., Keddache, M., and Rothstein, R. (2002). Efficient PCR-based gene disruption in *Saccharomyces* strains using intergenic primers. *Yeast* 19, 319-328.
- Reynolds, N., Salmon-Divon, M., Dvinge, H., Hynes-Allen, A., Balasooriya, G., Leaford, D., Behrens, A., Bertone, P., and Hendrich, B. (2012). NuRD-mediated deacetylation of H3K27 facilitates recruitment of Polycomb Repressive Complex 2 to direct gene repression. *EMBO J* 31, 593-605.

- Richmond, T.J., and Davey, C.A. (2003). The structure of DNA in the nucleosome core. *Nature* **423**, 145-150.
- Robinson, P.J., and Rhodes, D. (2006). Structure of the '30 nm' chromatin fibre: a key role for the linker histone. *Curr Opin Struct Biol* **16**, 336-343.
- Rogakou, E.P., Pilch, D.R., Orr, A.H., Ivanova, V.S., and Bonner, W.M. (1998). DNA double-stranded breaks induce histone H2AX phosphorylation on serine 139. *J Biol Chem* **273**, 5858-5868.
- Rougeulle, C., Navarro, P., and Avner, P. (2003). Promoter-restricted H3 Lys 4 di-methylation is an epigenetic mark for monoallelic expression. *Hum Mol Genet* **12**, 3343-3348.
- Ryan, D.P., Sundaramoorthy, R., Martin, D., Singh, V., and Owen-Hughes, T. (2011). The DNA-binding domain of the Chd1 chromatin-remodelling enzyme contains SANT and SLIDE domains. *EMBO J* **30**, 2596-2609.
- Saha, A., Wittmeyer, J., and Cairns, B.R. (2006). Chromatin remodelling: the industrial revolution of DNA around histones. *Nat Rev Mol Cell Biol* **7**, 437-447.
- Santisteban, M.S., Hang, M., and Smith, M.M. (2011). Histone variant H2A.Z and RNA polymerase II transcription elongation. *Mol Cell Biol* **31**, 1848-1860.
- Santisteban, M.S., Kalashnikova, T., and Smith, M.M. (2000). Histone H2A.Z regulates transcription and is partially redundant with nucleosome remodeling complexes. *Cell* **103**, 411-422.
- Saravanan, M., Wuerges, J., Bose, D., McCormack, E.A., Cook, N.J., Zhang, X., and Wigley, D.B. (2012). Interactions between the nucleosome histone core and Arp8 in the INO80 chromatin remodeling complex. *Proc Natl Acad Sci U S A* **109**, 20883-20888.
- Schubert, H.L., Wittmeyer, J., Kasten, M.M., Hinata, K., Rawling, D.C., Heroux, A., Cairns, B.R., and Hill, C.P. (2013). Structure of an actin-related subcomplex of the SWI/SNF chromatin remodeler. *Proc Natl Acad Sci U S A*.
- Schwanbeck, R., Xiao, H., and Wu, C. (2004). Spatial contacts and nucleosome step movements induced by the NURF chromatin remodeling complex. *J Biol Chem* **279**, 39933-39941.
- Shen, X. (2004). Preparation and analysis of the INO80 complex. *Methods Enzymol* **377**, 401-412.
- Shen, X., Mizuguchi, G., Hamiche, A., and Wu, C. (2000). A chromatin remodelling complex involved in transcription and DNA processing. *Nature* **406**, 541-544.
- Shen, X., Ranallo, R., Choi, E., and Wu, C. (2003). Involvement of actin-related proteins in ATP-dependent chromatin remodeling. *Mol Cell* **12**, 147-155.
- Sherman, F. (2002). Getting started with yeast. *Methods Enzymol* **350**, 3-41.
- Shimada, K., Oma, Y., Schleker, T., Kugou, K., Ohta, K., Harata, M., and Gasser, S.M. (2008). Ino80 chromatin remodeling complex promotes recovery of stalled replication forks. *Curr Biol* **18**, 566-575.
- Shivaswamy, S., Bhinge, A., Zhao, Y., Jones, S., Hirst, M., and Iyer, V.R. (2008). Dynamic remodeling of individual nucleosomes across a eukaryotic genome in response to transcriptional perturbation. *PLoS Biol* **6**, e65.
- Sims, J.K., and Wade, P.A. (2011). SnapShot: Chromatin remodeling: CHD. *Cell* **144**, 626-626 e621.
- Singleton, M.R., Dillingham, M.S., and Wigley, D.B. (2007). Structure and mechanism of helicases and nucleic acid translocases. *Annu Rev Biochem* **76**, 23-50.
- Skiniotis, G., Moazed, D., and Walz, T. (2007). Acetylated histone tail peptides induce structural rearrangements in the RSC chromatin remodeling complex. *J Biol Chem* **282**, 20804-20808.
- Smeenk, G., and van Attikum, H. (2013). The chromatin response to DNA breaks: leaving a mark on genome integrity. *Annu Rev Biochem* **82**, 55-80.
- Smith, C.L., Horowitz-Scherer, R., Flanagan, J.F., Woodcock, C.L., and Peterson, C.L. (2003). Structural analysis of the yeast SWI/SNF chromatin remodeling complex. *Nat Struct Biol* **10**, 141-145.
- Stargell, L.A., and Gorovsky, M.A. (1994). TATA-binding protein and nuclear differentiation in *Tetrahymena thermophila*. *Mol Cell Biol* **14**, 723-734.
- Stopka, T., and Skoultchi, A.I. (2003). The ISWI ATPase Snf2h is required for early mouse development. *Proc Natl Acad Sci U S A* **100**, 14097-14102.
- Suto, R.K., Clarkson, M.J., Tremethick, D.J., and Luger, K. (2000). Crystal structure of a nucleosome core particle containing the variant histone H2A.Z. *Nat Struct Biol* **7**, 1121-1124.
- Suto, R.K., Edayathumangalam, R.S., White, C.L., Melander, C., Gottesfeld, J.M., Dervan, P.B., and Luger, K. (2003). Crystal structures of nucleosome core particles in complex with minor groove DNA-binding ligands. *J Mol Biol* **326**, 371-380.
- Szerlong, H., Hinata, K., Viswanathan, R., Erdjument-Bromage, H., Tempst, P., and Cairns, B.R. (2008). The HSA domain binds nuclear actin-related proteins to regulate chromatin-remodeling ATPases. *Nat Struct Mol Biol* **15**, 469-476.
- Talbert, P.B., and Henikoff, S. (2010). Histone variants--ancient wrap artists of the epigenome. *Nat Rev Mol Cell Biol* **11**, 264-275.

- Tang, G., Peng, L., Baldwin, P.R., Mann, D.S., Jiang, W., Rees, I., and Ludtke, S.J. (2007). EMAN2: an extensible image processing suite for electron microscopy. *J Struct Biol* 157, 38-46.
- Thoma, N.H., Czyzewski, B.K., Alexeev, A.A., Mazin, A.V., Kowalczykowski, S.C., and Pavletich, N.P. (2005). Structure of the SWI2/SNF2 chromatin-remodeling domain of eukaryotic Rad54. *Nat Struct Mol Biol* 12, 350-356.
- Tillo, D., and Hughes, T.R. (2009). G+C content dominates intrinsic nucleosome occupancy. *BMC Bioinformatics* 10, 442.
- Torreira, E., Jha, S., Lopez-Blanco, J.R., Arias-Palomo, E., Chacon, P., Canas, C., Ayora, S., Dutta, A., and Llorca, O. (2008). Architecture of the pontin/reptin complex, essential in the assembly of several macromolecular complexes. *Structure* 16, 1511-1520.
- Tosi, A., Haas, C., Herzog, F., Gilmozzi, A., Berninghausen, O., Ungewickell, C., Gerhold, C.B., Lakomek, K., Aebersold, R., Beckmann, R., *et al.* (2013). Structure and Subunit Topology of the INO80 Chromatin Remodeler and Its Nucleosome Complex. *Cell* 154, 1207-1219.
- Tsukuda, T., Fleming, A.B., Nickoloff, J.A., and Osley, M.A. (2005). Chromatin remodelling at a DNA double-strand break site in *Saccharomyces cerevisiae*. *Nature* 438, 379-383.
- Udugama, M., Sabri, A., and Bartholomew, B. (2011). The INO80 ATP-dependent chromatin remodeling complex is a nucleosome spacing factor. *Molecular and cellular biology* 31, 662-673.
- Valouev, A., Johnson, S.M., Boyd, S.D., Smith, C.L., Fire, A.Z., and Sidow, A. (2011). Determinants of nucleosome organization in primary human cells. *Nature* 474, 516-520.
- van Attikum, H., Fritsch, O., Hohn, B., and Gasser, S.M. (2004). Recruitment of the INO80 complex by H2A phosphorylation links ATP-dependent chromatin remodeling with DNA double-strand break repair. *Cell* 119, 777-788.
- van Heel, M., Harauz, G., Orlova, E.V., Schmidt, R., and Schatz, M. (1996). A new generation of the IMAGIC image processing system. *J Struct Biol* 116, 17-24.
- Vincent, J.A., Kwong, T.J., and Tsukiyama, T. (2008). ATP-dependent chromatin remodeling shapes the DNA replication landscape. *Nat Struct Mol Biol* 15, 477-484.
- Volpe, T., and Martienssen, R.A. (2011). RNA interference and heterochromatin assembly. *Cold Spring Harbor perspectives in biology* 3, a003731.
- Vorobiev, S., Strokopytov, B., Drubin, D.G., Frieden, C., Ono, S., Condeelis, J., Rubenstein, P.A., and Almo, S.C. (2003). The structure of nonvertebrate actin: implications for the ATP hydrolytic mechanism. *Proc Natl Acad Sci U S A* 100, 5760-5765.
- Walzthoeni, T., Claassen, M., Leitner, A., Herzog, F., Bohn, S., Forster, F., Beck, M., and Aebersold, R. (2012). False discovery rate estimation for cross-linked peptides identified by mass spectrometry. *Nat Methods* 9, 901-903.
- Wang, A.Y., Aristizabal, M.J., Ryan, C., Krogan, N.J., and Kobor, M.S. (2011). Key functional regions in the histone variant H2A.Z C-terminal docking domain. *Mol Cell Biol* 31, 3871-3884.
- Wang, A.Y., Schulze, J.M., Skordalakes, E., Gin, J.W., Berger, J.M., Rine, J., and Kobor, M.S. (2009). Asf1-like structure of the conserved Yaf9 YEATS domain and role in H2A.Z deposition and acetylation. *Proc Natl Acad Sci U S A* 106, 21573-21578.
- Wang, F., Li, G., Altaf, M., Lu, C., Currie, M.A., Johnson, A., and Moazed, D. (2013). Heterochromatin protein Sir3 induces contacts between the amino terminus of histone H4 and nucleosomal DNA. *Proc Natl Acad Sci U S A* 110, 8495-8500.
- Watkins, N.J., Dickmanns, A., and Luhrmann, R. (2002). Conserved stem II of the box C/D motif is essential for nucleolar localization and is required, along with the 15.5K protein, for the hierarchical assembly of the box C/D snoRNP. *Mol Cell Biol* 22, 8342-8352.
- Watkins, N.J., Lemm, I., Ingelfinger, D., Schneider, C., Hossbach, M., Urlaub, H., and Luhrmann, R. (2004). Assembly and maturation of the U3 snoRNP in the nucleoplasm in a large dynamic multiprotein complex. *Mol Cell* 16, 789-798.
- Wood, M.A., McMahon, S.B., and Cole, M.D. (2000). An ATPase/helicase complex is an essential cofactor for oncogenic transformation by c-Myc. *Mol Cell* 5, 321-330.
- Wu, W.H., Alami, S., Luk, E., Wu, C.H., Sen, S., Mizuguchi, G., Wei, D., and Wu, C. (2005). Swc2 is a widely conserved H2AZ-binding module essential for ATP-dependent histone exchange. *Nat Struct Mol Biol* 12, 1064-1071.
- Yadon, A.N., and Tsukiyama, T. (2011). SnapShot: Chromatin remodeling: ISWI. *Cell* 144, 453-453 e451.
- Yamada, K., Frouws, T.D., Angst, B., Fitzgerald, D.J., DeLuca, C., Schimmele, K., Sargent, D.F., and Richmond, T.J. (2011). Structure and mechanism of the chromatin remodelling factor ISW1a. *Nature* 472, 448-453.
- Yang, D., Fang, Q., Wang, M., Ren, R., Wang, H., He, M., Sun, Y., Yang, N., and Xu, R.M. (2013). Nalpha-acetylated Sir3 stabilizes the conformation of a nucleosome-binding loop in the BAH domain. *Nat Struct Mol Biol* 20, 1116-1118.

- Yang, Z., Fang, J., Chittuluru, J., Asturias, F.J., and Penczek, P.A. (2012). Iterative stable alignment and clustering of 2D transmission electron microscope images. *Structure* 20, 237-247.
- Yen, K., Vinayachandran, V., Batta, K., Koerber, R.T., and Pugh, B.F. (2012). Genome-wide nucleosome specificity and directionality of chromatin remodeler. *Cell* 149, 1461-1473.
- Yen, K., Vinayachandran, V., and Pugh, B.F. (2013). SWR-C and INO80 Chromatin Remodeler Recognize Nucleosome-free Regions Near +1 Nucleosomes. *Cell* 154, 1246-1256.
- Yu, E.Y., Steinberg-Neifach, O., Dandjinou, A.T., Kang, F., Morrison, A.J., Shen, X., and Lue, N.F. (2007). Regulation of telomere structure and functions by subunits of the INO80 chromatin remodeling complex. *Mol Cell Biol* 27, 5639-5649.
- Zhang, W., Zhang, J., Zhang, X., Xu, C., and Tu, X. (2011). Solution structure of the Taf14 YEATS domain and its roles in cell growth of *Saccharomyces cerevisiae*. *Biochem J* 436, 83-90.
- Zhang, Y., LeRoy, G., Seelig, H.P., Lane, W.S., and Reinberg, D. (1998). The dermatomyositis-specific autoantigen Mi2 is a component of a complex containing histone deacetylase and nucleosome remodeling activities. *Cell* 95, 279-289.
- Zofall, M., Persinger, J., Kassabov, S.R., and Bartholomew, B. (2006). Chromatin remodeling by ISW2 and SWI/SNF requires DNA translocation inside the nucleosome. *Nat Struct Mol Biol* 13, 339-346.

## 9 Appendix

### 9.1 Genetic information

#### 9.1.1 601 positioning sequences for nucleosomes

147bp long core nucleosomes with 601 positioning sequence

```
GGGGGAGAATCCCGGTGCCGAGGCCGCTCAATTGGTCGTAGCAAGCTCTAGCACCGCTTAAACGCACGTACGCGCTGTC
CCCCGCGTTTTAACGCCAAGGGGATTACTCCCTAGTCTCCAGGCACGTGTCAGATATATACATCCCC
```

Off-centered 167bp long core nucleosomes with 601 positioning sequence, 20bp linker on left side

```
ATCACCTATACGCGGCAGTACTGGAGAATCCCGGTGCCGAGGCCGCTCAATTGGTCGTAGCAAGCTCTAGCACCGCTT
AAACGCACGTACGCGCTGTCCCCGCGTTTTAACGCCAAGGGGATTACTCCCTAGTCTCCAGGCACGTGTCAGATATA
TACATCCCC
```

Centered 167bp long core nucleosomes with 601 positioning sequence, 20bp linker on each side

```
ATCACCTATACGCGGCAGTACTGGAGAATCCCGGTGCCGAGGCCGCTCAATTGGTCGTAGCAAGCTCTAGCACCGCTT
AAACGCACGTACGCGCTGTCCCCGCGTTTTAACGCCAAGGGGATTACTCCCTAGTCTCCAGGCACGTGTCAGATATA
TACATCCCCGGGCGACTCGGGTTATGGAT
```

Off-centered 187bp long core nucleosomes with 601 positioning sequence, 40bp linker on left side

```
GGGCGACTCGGGTTATGGATATCACCTATACGCGGCAGTACTGGAGAATCCCGGTGCCGAGGCCGCTCAATTGGTCGT
AGCAAGCTCTAGCACCGCTTAAACGCACGTACGCGCTGTCCCCGCGTTTTAACGCCAAGGGGATTACTCCCTAGTCT
CCAGGCACGTGTCAGATATATACATCCCC
```

#### 9.1.2 Part of INO1 gene for nucleosome reconstitution

```
atgacagaagataatattgctccaatcacctccgttaaagtagttaccgacaagtgcacgtacaaggacaacgagctgctcaccaagtacagctacgaaaat
gctgtagttacgaagacagctagtgccgcttcgatgtaacgccactgttcaagactacgtgttcaaaacttgacttgaaaaagccggaaaaactaggaatta
tgctcattgggttagtggaacaatggctccacttagtgccctcggtattggcgaaataagcacaatgtggagtttcaactaaggaaggcgtaagcaacc
aaactacttcggctccatgactcaatgttctaccttgaaactgggtatcga
```

#### 9.1.3 INO80-FLAG2

The ATG is marked in blue, the INO80 gene in black, the FLAG2-tag in green and the STOP codon in red.

```
ATG.....GTCAGGCATTATCCGATATTCCAGCAATAACGCAATATAACATGCACGTTAAAGACAGGACTATTCCCTGAAC
CACTAAATAAAAAATTTTCATCCAACATATCAATGCCATCTATGGATAGGTTTCATTACCGAATCAGCGAAATTAAGAAA
ATTGGATGAATTGTTGGTAAAGTTGAAATCAGAAGGCCACAGAGTTTTGATATATTCCAAATGACCAAGATGATGGAT
CTTATGGAAGAATACTTGACCTATAGACAATATAATCATATTAGACTGGATGGTTCTCAAAGTTGGAGGACCGTCGAG
ATTTGGTCCATGATTGGCAGACTAATCCAGAAATCTTTGTTTTCTCCTAAGTACAAGAGCAGGTGGTCTAGGTATCAAC
CTGACCGCAGCTGACACTGTTATATTCTATGATTGAGATTGGAACCCTACTATTGATTACAGGCTATGGATAGGGCAC
ATAGGTTGGGCCAAACGAGGCAAGTACAGTGTACAGATTACTTGTTCGTGGTACCATCGAAGAAAGAATGAGGGGATA
```

GAGCAAAGCAAAAAGAGCAAGTTCAACAAGTCGTCATGGAAGGTAAGACTCAGGAAAAAACATTAAACCATTGAA  
GTGGGTGAAAATGATTCCGAAGTCACTCGTGAAGGTAGCAAAAGCATAAGTCAAGATGGAATTAAGGAAGCGGCAAGT  
GCATTGGCAGACTACAAGGACGACGATGACAAGGGTACCGATTACAAGGATGATGACGACAAGTGA

#### 9.1.4 URA3 marker: promoter and ORF

The URA3 primers is marked in orange, the ATG in blue, the STOP codon in red.

TCAATTCATCATTTTTTTTTATTC TTTTTTTGATTTCCGTTTCTTTGAAATTTTTTGATTCCGTAATCTCCGAACAGAA  
GGAAGAACGAAGGAAGGAGCACAGACTTAGATTGGTATATATACGCATATGTAGTGTTGAAGAAACATGAAATTGCC  
AGTATTCTTAACCCAATGCACAGAACAAAAACCTGCAGGAAACGAAGATAAATC ATGTCGAAAGCTACATATAAGGA  
ACGTGCTGCTACTCATCTAGTCTGTTGCTGCCAAGCTATTTAATATCATGCACGAAAAGCAAACTTGTGTGCTT  
CATTGGATGTTCTGACCAAGGAATTACTGGAGTTAGTTGAAGCATTAGGTCCCAAAATTTGTTTACTAAAAACACA  
TGTGGATATCTTGACTGATTTTTCCATGGAGGGCACAGTTAAGCCGCTAAAGGCATTATCCGCCAAGTACAATTTTTAC  
TCTTCGAAGACAGAAAATTTGCTGACATTGGTAATACAGTCAAATTGCAGTACTCTGCGGGTGTATACAGAATAGCAGA  
ATGGGCAGACATTACGAATGCACACGGTGTGGTGGGCCAGGTATTGTTAGCGGTTTGAAGCAGCGGGCAGAAGAAGT  
AACAAAGGAACCTAGAGGCCTTTGATGTTAGCAGAATTGTCATGCAAGGGCTCCCTATCTACTGGAGAATATACTAAG  
GGTACTGTTGACATTGCGAAGAGCGACAAAGATTTTGTATCGGCTTTATTGCTCAAAGAGACATGGGTGGAAGAGATG  
AAGGTTACGATTGGTTGATTATGACACCCGGTGTGGGTTTAGATGACAAGGGAGACGATTGGGTCAACAGTATAGAA  
CCGTGGATGATGTGGTCTCTACAGGATCTGACATTATTATTGTTGGAAGAGGACTATTTGCAAAGGGAAGGGATGCTAA  
GGTAGAGGGTGAACGTTACAGAAAAGCAGGCTGGGAAGCATATTTGAGAAGATGCGGCCAGCAAACTAG

#### 9.1.5 DID1 sequence

The DID1 primer is marked in pink, the STOP codon in red. The sequence was adapted from (Flemming et al., 2010).

ATGGCCAGGATCCAA CATACGACAAAGGCATTCAAACAGATCAAATTGAGGGGATGGTCAGCGTTTCAGTGCAGAC  
CGACATGGAGGAAGGTACTTACGATAAAGGTATTTCAGACAGACCAAAATCGAGGGAATGGTGAGCGTATCAGTTCAGAC  
GGACATGGAAGAGGGTACGTATGACAAGGGCATACAAACCGATCAGATTGAAGGTATGGTAAGTGTTTCGGTGCAAAAC  
CGATATGGAAGAAGGAACGTAG

## 10 Curriculum Vitae Caroline Haas

Education	
Since 03/2009	<b>PhD Thesis in Roland Beckmann's Group at the Gene Center in Munich, Germany</b>
10/2003 - 12/2008	<b>Ludwig-Maximilians-University in Munich, Germany</b>
10/2006 - 12/2008	<b>Master in Biochemistry (ø 1.0)</b>
10/2003 - 10/2006	<b>Bachelor in Chemistry and Biochemistry (ø 1.7)</b>
09/1994 - 05/2003	<b>Secondary School: Louise-Schroeder-Gymnasium in Munich, Germany</b> Diploma qualifying for General University Admission (ø 1.2)
Experience	
Since 03/2009	<b>PhD Thesis in Roland Beckmann's group at the Gene Center in Munich</b> In collaboration with Karl-Peter Hopfner's group at the Gene Center and Ruedi Aebersold's group, ETH, Zurich, Switzerland Topic: "Structural analysis of chromatin remodeler by electron microscopy."
05/2008 - 12/2008	<b>Master Thesis in Michael Lisby's group at the University of Copenhagen in Copenhagen, Denmark</b> Topic: "Regulation of chromatin structure during recombinational DNA repair"
11/2007	<b>Internship in Klaus Foerstemann's group Gene at the Center in Munich</b>
03/2007 - 05/2007	<b>Internship in Stefan Jentsch's group at the Max-Planck-Institute in Munich</b>
11/2006 - 12/2007	<b>Internship in Roland Beckmann's group at the Gene Center in Munich</b>
06/2006 - 10/2006	<b>Bachelor Thesis in Ralf-Peter Jansen's group at the Gene Center in Munich</b> Topic: "Reinvestigating the function of the nuclear protein Loc1p"
05/2006 - 12/2007	<b>Student Assistant</b> in Roland Beckmann's & Ralf-Peter Jansen's group at the Gene Center in Munich
10/2005 -06/2006	<b>Student Assistant</b> for the Practical Course I & II in Inorganic Chemistry at the LMU in Munich
Publications	
09/2013	Tosi A*, <b>Haas C*</b> , Herzog F*, Gilmozzi A, Berninghausen O, Ungewickell C, Gerhold CB, Lakomek K, Aebersold R, Beckmann R and Hopfner KP (2013): Structure and subunit topology of the INO80 chromatin remodeler and its nucleosome complex. <i>Cell</i> , Volume 154, Issue 6, 1207-1219, 12 September 2013. *contributed equally
02/2011	Germann SM, Oestergaard VH, <b>Haas C</b> , Salis P, Motegi A, Lisby M (2011): Dpb11/TopBP1 plays distinct roles in DNA replication, checkpoint response and homologous recombination. <i>DNA Repair</i> 10, 210-24.
Conferences and Presentations	
05/2013	<b>Poster presentation and poster prize talk</b> at the EMBO Conference "Chromatin and Epigenetics" at the EMBL Heidelberg, Germany
03/2013	<b>Poster presentation</b> at the Conference "Epigenetics & Chromatin: Interactions and processes" at Harvard Medical School in Boston, USA
05/2012	<b>Poster and oral presentation</b> at the "Gene Center Retreat" in Wildbad-Kreuth

04/2011	<b>Poster presentation</b> at the EMBO workshop “Chromatin structure, organization and dynamics” in Prague, Czech Republic
03/2011	<b>NCMI Workshop</b> on Single Particle Reconstruction, Validation and Analysis in Houston, Texas, USA
10/2010	<b>Poster presentation</b> at the 3rd SFB TR5 Symposium “Chromatin Assembly and Inheritance of Functional States” in Munich, Germany

### Awards and Scholarships

Since 02/2013	<b>Scholarship from e-fellows.net</b>
05/2013	<b>Poster Prize including a talk</b> at the EMBO Conference “Chromatin and Epigenetics” at the EMBL Heidelberg, Germany
05/2012	<b>Poster Prize</b> at the Gene Center Retreat in Wildbad-Kreuth, Germany
10/2009 - 09/2011	<b>Doctoral Fellowship from the Ernst-Schering-Foundation</b>
05/2008 - 09/2008	<b>Scholarship for Master Thesis</b> in Denmark given by “Deutscher Akademischer Austauschdienst” DAAD
06/2003	<b>Prize for excellent Performance in the Subject Biology</b> on the occasion of the “Abitur“ 2003, given by the “Verband Deutscher Biologen und biowissenschaftlicher Fachgesellschaften e.V.”

### Research Skills

Structural Biology	Electron microscopy, single particle analysis and 3D reconstruction <i>ab initio</i> , processing with the software packages EMAN2 and Spider
Molecular Biology	Molecular cloning by DNA techniques including PCR, site-directed mutagenesis
Yeast Manipulation	Gene deletion, gene tagging, Yeast two hybrid
Protein Purification	Standard purification techniques including affinity purification, ion exchange and size exclusion chromatography on Äkta systems, membrane protein purification, Co-IP
Protein Analysis & Characterization	SDS-PAGE, native PAGE, Western Blotting, Far Western Blotting, Electrophoretic mobility shift assays (EMSA), nucleosome remodeling, MicroScale Thermophoresis for binding constants
Protein Expression	Bacteria, yeast, insect cell culture
Nucleic Acids	Southern Blotting, MNase assay, quantitative PCR

### Special Skills and Interests

Since 11/2012	Courses at the “ <b>Center for Leadership and People Management</b> ” at the LMU
05/2011 - 07/2011	Course for <b>Business Economics</b> from “Student und Arbeitsmarkt” at the LMU
IT Skills	MS office, Adobe Creative Suite (Photoshop, Illustrator), Linux, EMAN, Spider, Chimera
Language Skills	<b>German</b> native language, <b>English</b> proficient, <b>French</b> school knowledge, <b>Danish and Italian</b> basic competence
Hobbies	Cooking, cultural traveling, piano, yoga, ballet, hiking, skiing



## 11 Acknowledgements

First of all, I would like to thank Prof. Dr. Roland Beckmann for offering me the possibility to perform my PhD Thesis in his laboratory and for giving me the opportunity to work on the challenging project of chromatin remodeler, which are so far away from ribosomes. After my Master Thesis I was curious how chromatin remodeler may function, and this project offered me the possibility to tackle this question with the structural technique of electron microscopy, which I was always fascinated by. Roland offered me professional advice, stimulating support and suggestions in all the time of this thesis. He was always helping me out with his razor-sharp mind, his texting skills and visual brilliance. Thank you so much for your excellent guidance, you are a great mentor!

I also wish to thank Prof. Dr. Karl-Peter Hopfner for his support and help on the INO80 project. Supported by the fruitful discussions, our story made it into *Cell*, this success speaks for itself. Thank you so much for your help and encouragement!

I also would like to thank Prof. Peter Becker from the Adolf-Butenandt-Institute and especially Felix-Müller Planitz and Henrike Klinker for introducing me to nucleosome preparation and ISWI purifications.

Furthermore, I want to thank all members of Beckmann group for their help, support and for providing a stimulating and fun environment to work in. special thanks goes to Andrea Gilmozzi: thanks for your help and support with your charming personality; without you, the workload would have been just too much! I wish to thank Charlotte Ungewickell for relieving jogging sessions and mutual discussion of problems in daily life. And of course, I would like to thank Charlotte and Otto Berninghausen for analyzing so many EM conditions and grids and for collecting gazillions of data. Sarah Matheisl, I want to thank you for your always full drawer and for the fun we had sitting next to each other. I want to thank Stefan Wickles, Sibylle Frankenberg, Julian Deeng, Alex Jarasch, Jean-Paul Armache and Thomas Becker for their support during processing and whenever I had computer related problems. And I would like to thank the whole Beckmann group for always being there with support, protocols, advice, open ears, a lot of fun and some gin tonics.

Of course, I also have to mention a lot of people at the gene center: I thank Franz Herzog for a really nice and successful collaboration. I want to thank the members of the group of Karl-Peter Hopfner and especially the INO80 subgroup for support. I am grateful to Andi Hauser for answering all my naïve cluster-related problems. I thank Petra

Wendler for Imagic support and Rvb1/2 discussions. Members of the Strässer group helped me with their protocols, plates and other materials to handle yeast. From the AG Förstemann I want to thank Milijana Mirkovic-Hösle for her friendship and Romy Böttcher for always funny lunch time discussions about food and other stuff.

Of course, I also would like to especially thank the Ernst Schering foundation for their financial support in form of two years doctoral fellow scholarship. I had a lot of fun at the two Schering meetings I visited. They were an inspiring combination of science and art and I am already looking forward to the next meeting.

This work would not have been possible without the support and encouragement of my friends. I enjoyed all evenings full of food and joy, although they were very scarce during the high time of the project. I also want to thank my family, especially my parents and my sister who supported me in every way and situation.

Last, but not least, I want to thank Alessandro for being him. I am looking forward to our future, wherever it takes us.